ABSTRACT

GAWDI, YASH JAGDISHLAL. Underwater Free Space Optics. (Under the direction of Dr. John F. Muth and Dr. Leda M. Lunardi.)

Radio waves propagate poorly in water and acoustics have been the dominant method for undersea communications, but its data rates are bandwidth limited. Free Space Optics potentially provides an alternative solution to acoustical communications with wider bandwidth and wireless flexibility that would benefit many undersea applications over short ranges.

Compared to atmospheric propagation, ocean waters are a more complex medium for light propagation presenting a very high attenuation, depending on a variety of different parameters and conditions. In this work, a model is investigated to that estimates the total attenuation of the light propagation in natural waters in the context of optical communications. Using a one parameter model of absorption and scattering, a general framework has been structured in MathCAD, where the absorption and scattering coefficients are iteratively calculated for a variable vertical chlorophyll profile. The beam spread function is implemented to estimate the total beam attenuation. Link budget simulations are also computed to address the feasibility of the underwater free space optical links. Laboratory experiments of light attenuation in sea water with red (633nm) and green (532nm) wavelengths corroborate simulated results obtained with the beam spread function within 25% error margin. Particulate scattering experiments with polystyrene latex spheres of sizes 500nm and 6μm were carried out to confirm its dependence on wavelength and particle size. These phase function of the measured experimental results are in agreement with the previously published data.

UNDERWATER FREE SPACE OPTICS

by

YASH JAGDISHLAL GAWDI

A thesis submitted to the
Graduate Faculty of North Carolina State University
in partial fulfillment of the requirements for the
Degree of Master of Science

ELECTRICAL AND COMPUTER ENGINEERING

Raleigh, North Carolina

2006

APPROVED BY:

Dr. John F. Muth	**Dr. Leda M. Lunardi**
(Chair of Advisory Committee)	**(Co-Chair of Advisory Committee)**

Dr. Kevin G. Gard
(Member of Advisory Committee)

I would like to dedicate my Thesis to

my parents (Mr. Jagdish and Pushpa Gawdi),

my sister & brother-in-law (Dr. Meghna and Dr. Divyagynan Sarvaiya),

my fiancé (Vijeta Sinha) and my friend (Mrunal Shah)

BIOGRAPHY

The author was born in Bombay, India on the 10th of August 1982. He earned his Bachelors degree in Electronics Engineering from Mumbai University, India in May 2004. He had the privilege of working with Global Telesystems Ltd., India for his final year project, where he assisted as a link engineer to design and commission a point to point Microwave link. He has been a Masters student at North Carolina State University, USA in the department of Electrical and Computer Engineering since August 2004. He was honored with the position of a Research Assistant under Dr. John Muth and Dr. Leda Lunardi. He has held the position as a Teachers Assistant for Dr. John Muth and Dr. Michael Escuti in Photonics and Optical communication. His interests lie in RF & Microwave circuit design and optical communication.

ACKNOWLEDGEMENTS

Foremost, I would like to thank Dr. John Muth for giving me an opportunity to work under him and be a part of his research group. This research is a result of his vision and guidance. I would like to convey my sincere gratitude to Dr. Leda Lunardi for her continuous encouragement and help through out my research. She has been very patient and instrumental during the preparation of this thesis. I would like to acknowledge Dr Kevin Gard for establishing my foundations in subjects like analog circuits and being a part of my advisory committee.

Special thanks to Dr. Dan Kamykowski (Marine, Earth & Atmospheric Sciences), Geoffrey Sinclair and Blake Schaeffer for sharing their facility and information which was very helpful in my research. I would like to acknowledge National Science Foundation for providing the funds to carry out this research.

I would like to show my appreciation to all the students of my research group, especially Khalid Alhamadi, Anuj Dhawan and Praveen Golakotta for all their help during the past year.

I am thankful to Harnish, Siddharth for being great friends and for supporting me selflessly through my two years at NC State. I appreciate the good time that I have spent with my friends Arin, Ullas, Mitul, Aditya, Ira, Viraj, Manan and Harshwardhan. I am thankful to my friend Mrunal, my sister Meghna and my fiancé Vijeta for being the pillars of support throughout my life.

My mother has been the biggest driving force in my life; it’s because of her upbringing and unconditional love that I have been successful in my endeavors. I dedicate this work to her.

TABLE OF CONTENTS

LIST OF TABLES

LIST OF FIGURES

LIST OF ABBREVIATIONS

Abbreviation	Full Description
APD	Avalanche Photodiode
CDOM	Color Dissolved Organic Material
FSO	Free Space Optics
Gbps	Giga bits per second
kbps	Kilo bits per second
LED	Light Emitting Diode
LOS	Line of Sight
nm	Nano meters
pW	Pico-Watts
RF	Radio Frequency
UUV	Unmanned Underwater Vehicle

LIST OF SYMBOLS

Symbol	Unit	Description
α	radians	Angle of the path length from the vertical
$a(\lambda)$	m^{-1}	Total spectral absorption coefficient
$a_w(\lambda)$	m^{-1}	Absorption coefficient for pure seawater
$a_{cl}(\lambda)$	m^{-1}	Absorption coefficient for chlorophyll
$a_c^o(\lambda)$	m^{-1}	Specific absorption coefficient of chlorophyll
$a_f(\lambda)$	m^{-1}	Absorption coefficient for fulvic acid
$a_f^o(\lambda)$	m^{-1}	Specific absorption coefficient of fulvic acid
$a_h(\lambda)$	m^{-1}	Absorption coefficient for humic acid
$a_h^o(\lambda)$	m^{-1}	Specific absorption coefficient of humic acid
C_c	mg/m^3	Total concentration of chlorophyll
C_f	g/m^3	Concentration of fulvic acid
C_h	g/m^3	Concentration of humic acid
$b(\lambda)$	m^{-1}	Total spectral scattering coefficient
$b_o(\lambda)$	m^{-1}	Scattering coefficient of pure seawater
$b_s^o(\lambda)$	m^{-1}	Scattering coefficient of small particles
$b_l^o(\lambda)$	m^{-1}	Scattering coefficient of large particles
C_s	g/m^3	Concentration of small particles
C_l	g/m^3	Concentration of large particles
$Chl_{depth}(z)$	mg/m^3	Chlorophyll concentration as function of depth
B_o	mg/m^3	Background chlorophyll concentration
S	$mg/m^3/m$	Vertical chlorophyll concentration gradient
z	m	Depth
h	mg/m^2	Total chlorophyll above the background
σ	unit less	Standard deviation of Gaussian distribution
τ	seconds	Multipath time delay
θ_{mean}	radians	Mean of the scattering angle

Symbol	Unit	Description
$z_{\max}$	m	Depth of chlorophyll maximum
P_r	W	Optical power received
Pt	W	Initial optical power from transmitter
D_r	m	Diameter of receiving aperture
D_t	m	Diameter of transmitting aperture
Div	radians	Divergence of the optical beam
Lm	m	Distance of optical link
K	m^{-1}	Total attenuation coefficient

CHAPTER 1 INTRODUCTION

Communication underwater is very challenging. Unlike terrestrial communication links, radio frequencies and microwaves do not propagate through water. Acoustics communication links have been of keen interest for underwater applications in the past few decades, but provide limited bandwidth [1]. Optical communication satisfies the requisites of high bandwidth, efficient and reliable links, but numerous undersea applications would benefit from the flexibility of wireless links. We investigate the application and feasibility of Free Space Optical links to serve the purpose of underwater communications. Free Space Optical modules can be potentially deployed on Unmanned Underwater Vehicles (UUV) that would provide an extra degree of freedom to communicate with fixed bases or other UUV's. As seen in Figure 1-1, the blue-green region of the visible spectrum has the least attenuation. Communicating with floor sensors for data collection or adhoc networks would significantly enhance ocean laboratories. Remote inspection of oil rigs, real-time video transmission and communications between underwater platforms are other examples of underwater applications.

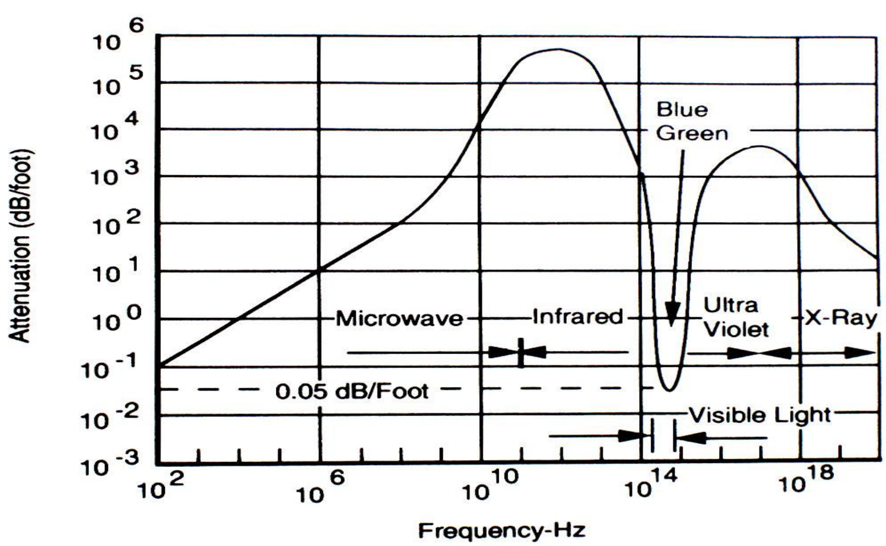

Figure 1-1 Spectral attenuation coefficient of ocean waters [2].

Terrestrial Free Space Optical links have demonstrated operational success for short links and can be used as a model for underwater communication links. However ocean waters offer high attenuation which is at least two orders higher than the worst atmospheric conditions. To better understand the problem, it is important to survey the system performance over wide spectrum of ocean waters types and sea state conditions.

The overview of the problem can begin with drawing parallels between optical fiber communication and free space optical communication. The basic difference between the two is the absence of a fiber channel in free space optics. For underwater applications the medium for free space optics is water. Ocean waters are a new medium for optical communication and hence it is important to understand the nature of light propagation through these waters; qualitatively and quantitatively. Ocean waters contain organic and inorganic materials that influence the absorption and scattering of light. The complexity of the problem increases as, the concentration of organic and inorganic not uniform and varies with the place and time. There needs to be a general model that takes into consideration these variations and to estimate the total light attenuation for different ocean conditions, since its essential to know the signal losses in the medium before designing a communication link. Separate models are present in oceanography that deal with individual parts of these sub-problems like, determining the concentration of organic particles in water, specific absorption and scattering coefficients of pure seawater and its constituents etc. But there is an absence of a general attenuation model that can be applied to most water types. This research investigates this problem from an optical communication point of view, estimating the unknown factor of signal attenuation.

Objectives:

- Provide systematic approach to the problem of light propagation in natural waters, in the context of optical communications.
- Develop a general model that estimates the total attenuation in sea water that can be made applicable to a variety of ocean conditions.
- Conduct experiments to enhance the understanding of the phenomena of scattering in water media and how scattering influences optical communications.

Chapter II introduces the optical properties of water and establishes the foundations of absorption and scattering by natural waters. The effects of absorption and scattering are distributed among the various constituents of water [3, 4].

Chapter III presents a one-parameter bio-optical model that defines the absorption coefficient and scattering coefficient of water. Based on empirical work, the constituents of ocean water can be correlated to the chlorophyll concentration [5]. Various methods to estimate the chlorophyll concentration are discussed. A model is developed in MathCAD that computes the total chlorophyll concentration in water and estimates the absorption and scattering coefficients.

Chapter IV examines the scattering phenomena. An empirical particulate scattering is carried out to qualitative understand the influence of scattering on the beam attenuation. A model is developed that calculates the total beam attenuation which is based on the multipath time delay caused due to scattering [6]. Being a different approach, this beam attenuation model is compared to Beer's Law, which supported by an experiment of light transfer in seawater containing chlorophyll. MathCAD simulations are included that compute the total beam attenuation for different water types.

Chapter V provides a system approach to the underwater free space optical link. Beginning with a detailed discussion on link budget analysis, all the gains and losses of an optical link have been explained [2, 7]. Geometric loss factor and transmitter-receiver topologies are discussed [8, 9].

1.1 References

[1] I. F. Akyildiz, D. Pompili and T. Melodia, "Underwater acoustic sensor networks: research challenges," *Ad Hoc Networks,* vol. 3, pp. 257–279, 2005.

[2] M. E. Katzman, *Laser Satellite Communications.* New Jersey: Prentice Hall Inc., 1987, pp. 1-30.

[3] C. D. Mobley, *Light and Water- Radiative Transfer in Natural Waters.* California: Academic Press Inc., 1994, pp. 60-144;300-303;487-488.

[4] R. E. Walker, *Marine Light Field Statistics.* New York: John Wiley & Sons Inc., 1994, pp. 142-162;168-172.

[5] V. I. Haltrin, "Chlorophyll-based model of seawater optical properties," *Applied Optics,* vol. 38, 1999.

[6] J. W. McLean, J. D. Freeman and R. E. Walker, "Beam spread function with time dispersion," *Applied Optics,* vol. 37, 1998.

[7] S. G. Lambert and W. Casey, *Laser Communication in Space.* MA: Artech House Inc., 1995, pp. 94-119.

[8] S. Bloom, E. Korevaar, J. Schuster and H. Willebrand, "Understanding the performance of free-space optics," *Journal of Optical Networking,* vol. 2, 2003.

[9] N. Farr, A. Chave, L. Freitag, J. Preisig, S. White and D. Yoerger, "Optical modem technology for seafloor observatories," *IEEE,* 2005.

CHAPTER 2 OPTICAL PROPERTIES OF WATER

2.1 Introduction:

In order to estimate the attenuation of light, we need to understand the nature of the optical properties of the medium. Optical properties of natural waters are very different as compared to pure water.

Optical Properties of natural waters are broadly classified into Inherent Optical Properties (IOP) and Apparent Optical Properties (AOP) [1-3]. Inherent properties are those that are dependent only on the medium, while Apparent Optical properties depend on both the medium as well as the ambient light [1]. The two main Inherent Optical Properties are spectral absorption coefficient a(λ) and spectral scattering coefficient b(λ). Beam attenuation coefficient and single-scattering albedo are other IOPs. Apparent Optical Properties find use in radiometric studies. These are often used to derive the inherent optical properties or other water constituent concentrations. Remote sensing reflectance (Rrs), downward irradiance (Ed) and upward irradiance (Eu) are a few common Apparent Optical Properties.

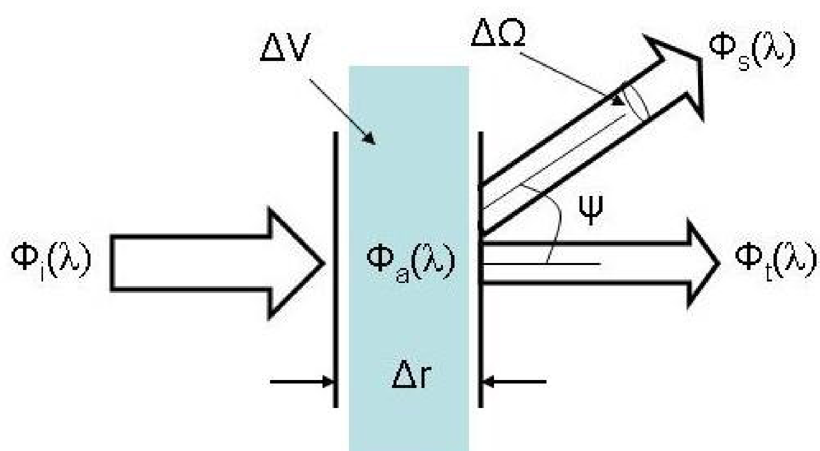

Figure 2-1 Geometry used to define inherent optical properties.[1]

Our interest revolves around the spectral absorption coefficient a(λ) and spectral scattering coefficient b(λ), since these are the main sources responsible for attenuation of light. The illustration in Figure 2-1 will give a good start to our approach.

This case is considered under the assumption that the inelastic scattering occurs for monochromatic light. The spectral absorptance A(λ) is the fraction of the incident power that is absorbed within the water volume [1].

$$\mathrm{A}(\lambda) = \frac{\Phi_a}{\Phi_\mathrm{i}} \qquad \text{Eq. 2.1}$$

Likewise the spectral scatterance B(λ) is the fraction of the incident power that is scattered.

$$\mathrm{B}(\lambda) = \frac{\Phi_s}{\Phi_\mathrm{i}} \qquad \text{Eq. 2.2}$$

The volume of water considered is of thickness Δr, hence the spectral absorption coefficient a(λ) is defined as

$$a(\lambda) = \lim_{\Delta r \to 0} \frac{\mathrm{A}(\lambda)}{\Delta \mathrm{r}} \qquad \text{Eq. 2.3}$$

and the spectral scattering coefficient b(λ) is

$$b(\lambda) = \lim_{\Delta r \to 0} \frac{\mathrm{B}(\lambda)}{\Delta \mathrm{r}} \qquad \text{Eq. 2.4}$$

Inherent properties of water like scattering and absorption are motivated by the water and its constituents. Natural waters contain particles with sizes ranging from water molecules of size ~0.1nm to small organic molecules ~1 nm, large organic molecules of size ~10nm to viruses of size ~100nm, bacteria of size ~1µm, phytoplankton size range between 1µ to 200µm etc. Traditionally natural waters are divided into dissolved and particulate matter which is either has organic or inorganic origins. Every particle in water contributes in some way to it optical properties.

2.2 Absorption

The absorption coefficient of natural water is the fundamental IOP. It is important to understand and quantify the value of the absorption coefficient that would enable us to estimate the light absorbed by the medium. Inherent properties including absorption and scattering have been measured and modeled since the past few decades. Extensive *in situ* measurements have been conducted and generalized models have been proposed to calculate the absorption coefficient for a given medium of water.

The absorption by water itself is known, however the absorption due to various dissolved particles need to found. The concentration of these dissolved particles is variable. The spectral absorption of water is a combination of the absorption by pure sea water, phytoplankton, detritus and Colored Dissolved Organic Matter (CDOM).

$$a(\lambda)=a_w(\lambda)+a_{chl}(\lambda)+a_{CDOM}(\lambda)+a_{detritus}(\lambda) \qquad \text{Eq. 2.5}$$

2.2.1 Absorption by pure sea water

Pure Sea water consists of pure water with dissolved salts, which average about 35 parts per thousand (35‰) by weight. Absorption by these salts has been assumed negligible over the visible region of operation. Indirect method have been adopted to find the upper bound of the spectral absorption coefficient of pure sea water, $a_w(\lambda)$ in the wavelength of oceanographic interest, 200nm<λ<800nm [2].

$$a_w(\lambda)< K_d(\lambda)-1/2\ b_w(\lambda) \qquad \text{Eq. 2.6}$$

where $b_w(\lambda)$ is the spectral scattering coefficient for pure sea water and $K_d(\lambda)$ is the spectral diffuse attenuation coefficient function. Scattering of pure sea water is attributed to the scattering by the water molecules and dissolved salts. The results from the model have been included in the MathCAD model.

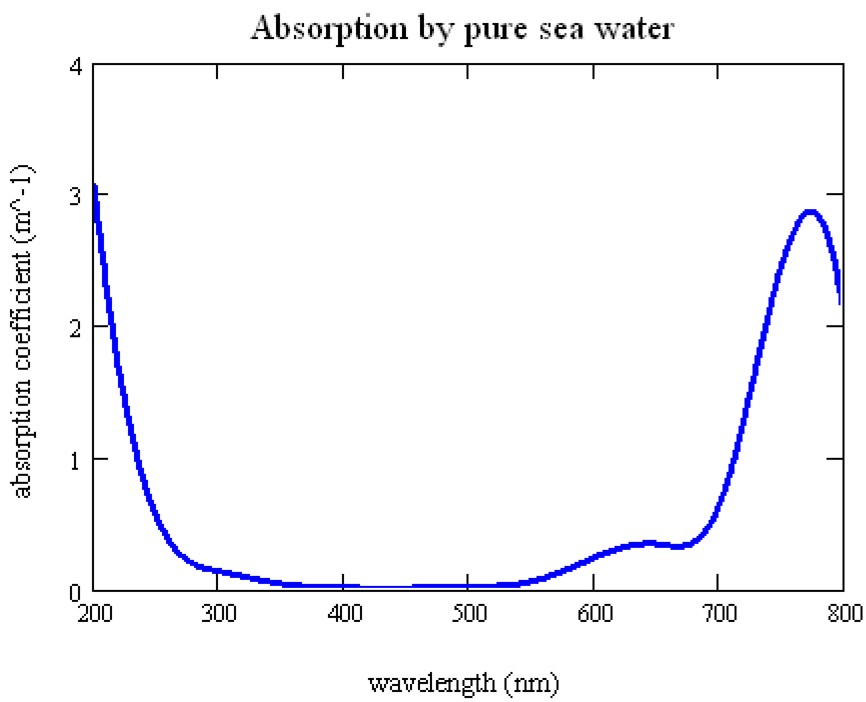

Figure 2-2 The Absorption coefficient of pure sea water [2].

2.2.2 Absorption by phytoplankton

Particulate matter is the primary source of absorption in natural waters. Phytoplankton are the ubiquitous microscopic plants that are found with variable size, shape and concentration. The cell size of phytoplankton range from 1µm to over 200µm [1]. Since phytoplankton cells are strong absorbers of visible light, they play a major role in determining the absorption coefficient. Absorption by phytoplankton occurs in various photosynthetic pigments, chlorophyll-*a* is the main photosynthetic pigment and has been commonly used as an indicator of biomass in ocean sphere. The absorption by chlorophyll-*a* can be considered similar to the absorption from phytoplankton. The qualitative feel for the nature of phytoplankton absorption can be obtained from the Figure 2-3.

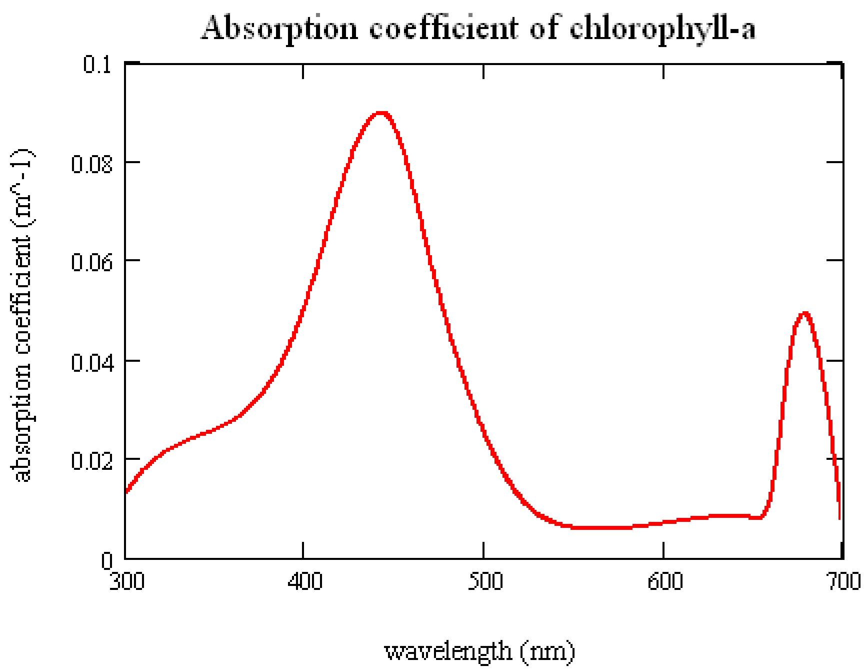

Figure 2-3 Cubic spline curve fitting for spectral absorption coefficient of chlorophyll-*a* [4].

The specific absorption coefficient is interpolated using data from Haltrin and Kattawar [4]. It can be seen from above that the absorption peaks occur at 440nm and 675nm. Absorption from other photosynthetic pigments such as chlorophyll-*b*, chlorophyll-*c*, photosynthetic carotenoids and photo-protecting carotenoids are certainly present, but are not considered due to uncertainty of their concentration in phytoplankton. The specific absorption coefficients of these pigments are shown in Figure 2-4 [5]. From this figure we see that the spectrum is generally similar to that of chlorophyll-*a*. Potentially in future work more precise data would be available and be included in the absorption model.

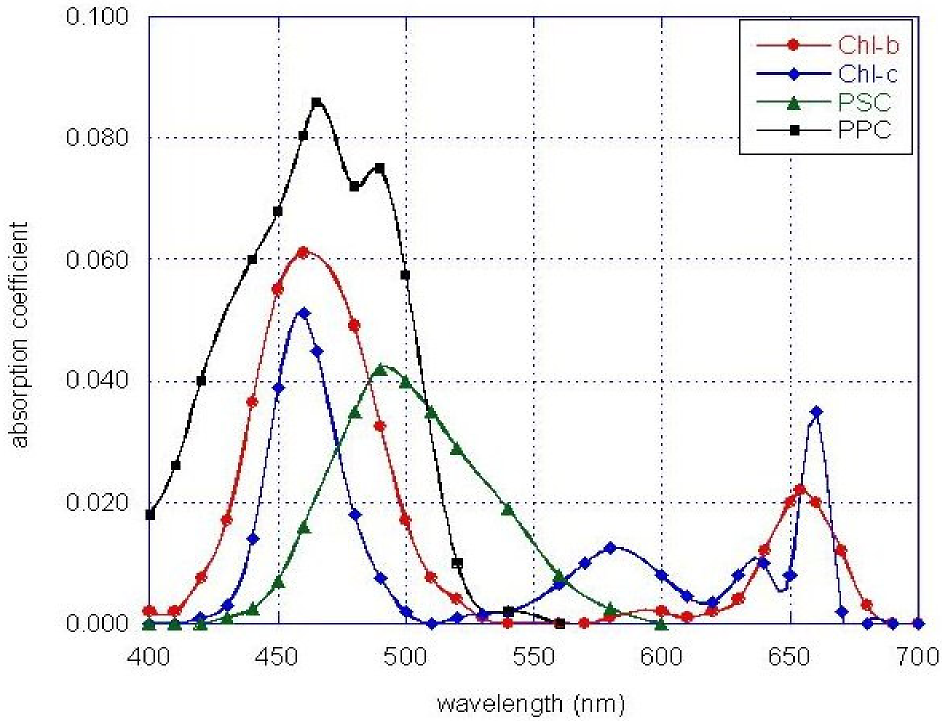

Figure 2-4 Cubic spline curve fitting for the specific absorption coefficients of chlorophyll-*b[* ● *]*, chlorophyll-*c [*◆*]*, photosynthetic carotenoids [▲]and photo-protective carotenoids [■] [5].

2.2.3 Absorption by CDOM:

Colored dissolved organic matter (CDOM) is a mixture of organic compounds that are present in both fresh and saline waters. These compounds are a product of decaying plants and primarily contain humic and fulvic acid. Due to its brown coloration, it gives a yellowish shade to water and are called as Gelbstoff (yellow substance). CDOM absorbs very little Red and its absorption decreases exponentially with wavelength.

A direct empirical relation to the phytoplankton concentration has been investigated [6,7]. Both constituents, humic and fulvic acid are derivative of the decomposition of chlorophyll-a. The specific absorption coefficient of fulvic acid is known to be a_f^0=35.959 m^2/mg and that for humic acid is known to be a_h^0=18.828 m^2/mg [7].

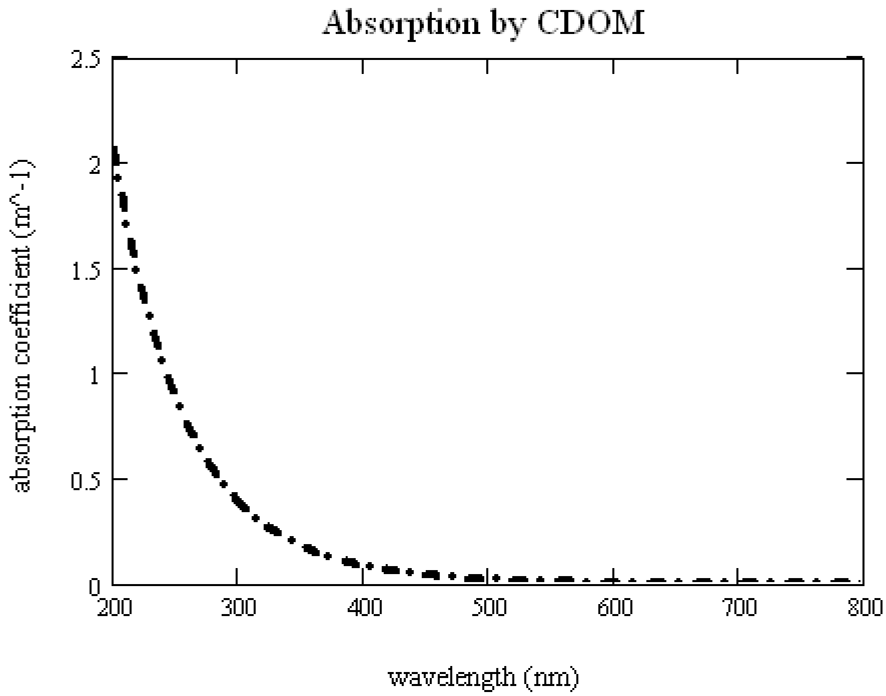

Figure 2-5 Spectral absorption by CDOM (chlorophyll concentration=1mg/m^3) [2].

2.2.4 Absorption by Organic Detritus

Detritus is organic waste formed due to dead plants and animals. Having particles of different sizes, detritus absorbs light in the blue region of the visible spectrum. It exhibits negative exponential decline, similar to CDOM [3].

Some studies apply Beer's Law to express the specific absorption coefficient of detritus.

$$a_{det}(\lambda) = a_{det}(\lambda_o)\exp[-\alpha_{det}(\lambda - \lambda_o)] \qquad \text{Eq. 2.7}$$

where the $\alpha_{det} = 0.014$ per nm^{-1} and $a_{det}^0 = 0.153$ [8].

However many studies produce different constants for α_{det}. The above equation is stated for unit concentration of the detritus. A general model to determine the concentration of detritus or its absorption is not available.

Inorganic matter has been given least attention due to their restricted presence in turbid coastal water and unknown concentration. Though optically important no empirical relation for their concentration is found, but if the concentration and particle size are known then Mie theory can be applied. Inorganic matter generally consists of finely ground quartz san, clay minerals or metal oxides.

2.3 Scattering

Scattering of light is fundamentally seen as the deviation of photons from its straight trajectory by non-uniformities in the medium through which they propagate. All scattering in water arise from interaction of photons and molecules or atoms. In order to develop a framework of scattering theory, we can physically divide each scattering event to be caused by small scale density fluctuations ($<<\lambda$), large organic or inorganic particles ($>\lambda$) and from turbulence induced fluctuations in real index of refraction ($>>\lambda$). For wavelengths in the visible region, photons would experience Rayleigh scattering from small density fluctuations, while large organic particles would result in Mie scattering. Turbulence induced fluctuations lead to geometric refractions of the light beam. Unlike Rayleigh scattering which scatters uniformly in all directions, Mie scattering is forward peaked.

2.3.1 Scattering by pure seawater

Physically small scale density fluctuation scattering are associated with scattering from pure seawater [1,3]. Random fluctuations in the concentration of various salt ions (Cl^-, Na^+, etc) attributed to variations in temperature and pressure are of the order much less than the wavelength of light and are the prime reasons for scattering in pure seawater.

$$b_w(\lambda) = 0.005826 * \left(400\text{nm}/\lambda\right)^{4.322} \qquad \text{Eq. 2.8}$$

The total scattering coefficient of pure sea water expressed in Equation 2.8 is reminiscent to Rayleigh scattering which has a wavelength dependence of the power of 4.322 [1,3,7]. Scattering by pure sea water is more effective at shorter wavelengths.

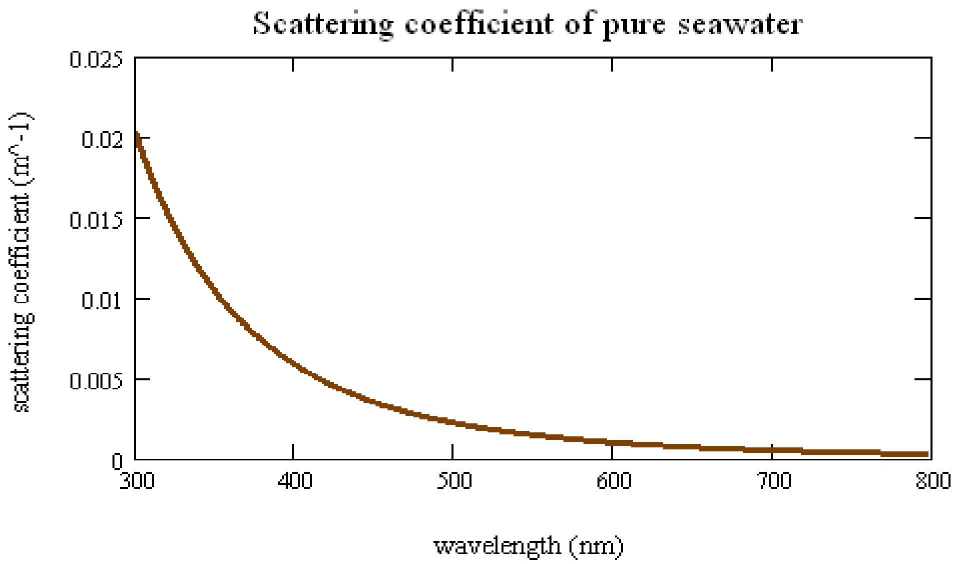

Figure 2-6 Scattering coefficient of Pure Seawater [7].

2.3.2 Scattering by particles

Often difficult to directly measure, efforts have been made to estimate the scattering by particles in natural waters. Highly peaked forward scattering dominates particle scattering suggesting application of Mie scattering theory [1, 9].

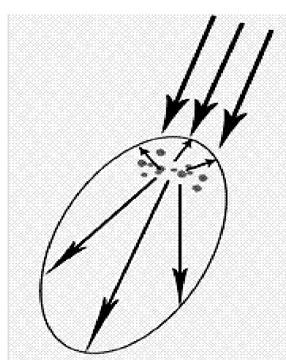

Figure 2-7 Scattering peaked in forward direction

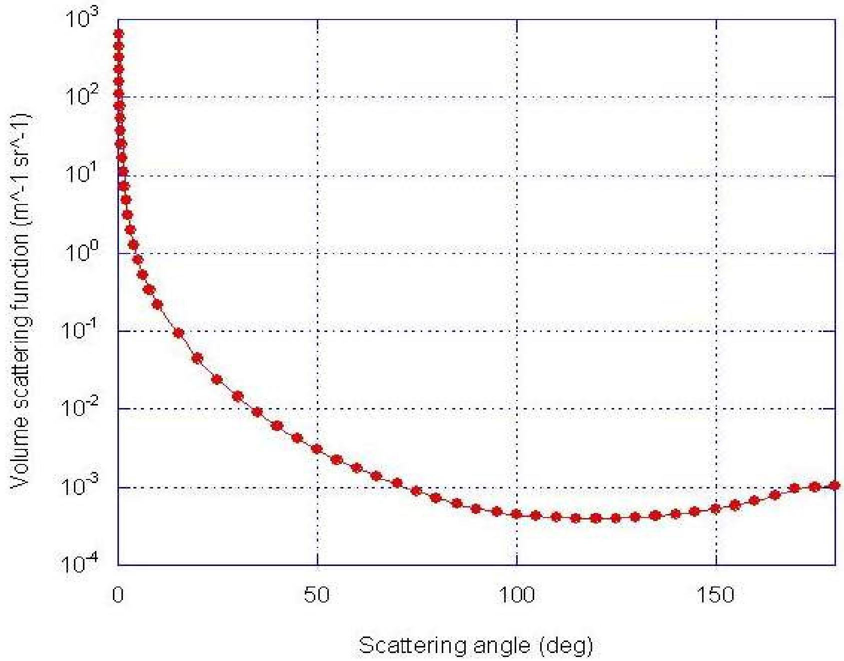

Figure 2-8 Volume scattering function measured for coastal ocean at λ=514nm [1].

The parameters needed to apply Mie scattering theory are particle size, shape, composition, distribution and complex refractive index [3]. Some models separate the contributions of particle scattering into small and large particle scatterings. Small particles are defined as having size less than 1μm with a refractive index(relative to water) of 1.15, while large particles have size larger than 1μm with a refractive index of 1.03 [1, 10]. The scattering coefficients of the small and large particles are wavelength dependent and their relation can be defined as follows [7, 10]:

$$b_s^0(\lambda) = 1.151302 * (400\text{nm}/\lambda)^{1.17} \quad \text{m}^2/\text{g} \qquad \text{Eq. 2.9}$$

$$b_l^0(\lambda) = 0.341074 * (400\text{nm}/\lambda)^{0.3} \quad \text{m}^2/\text{g} \qquad \text{Eq. 2.10}$$

Small particle scattering is found to influence the total particle scattering component as compared to large particle scattering.

Most bio-optical models restrict the scattering model to pure seawater scattering and particle scattering, excluding the scattering caused from turbulence induced fluctuations in index of refraction. This spectral scattering coefficient is presented as in Equation 2.11.

$$b(\lambda) = b_w(\lambda) + b_{small}(\lambda) + b_{large}(\lambda) \qquad \text{Equation 2.11}$$

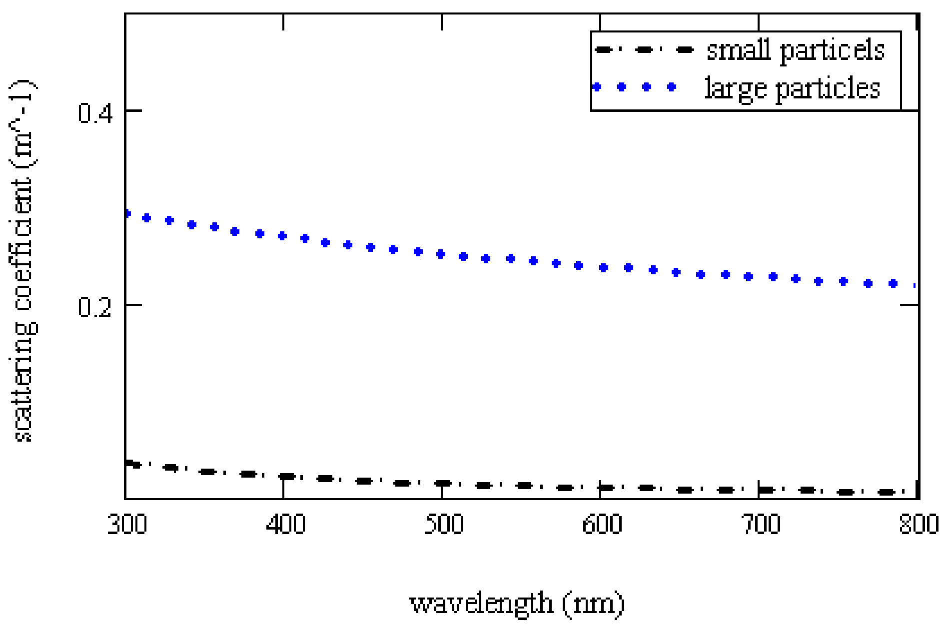

Figure 2-9 Spectral scattering coefficients of large and small particles for seawater with 1mg/m^3 of chlorophyll concentration [7].

2.3.3 Turbulence

The importance of turbulence induced scintillation has been well studied for terrestrial free space optical links. Scintillation is caused almost exclusively by small temperature variations in the random medium, resulting in index of refraction fluctuation.

This leads to deviation of the light beam and greatly influences stability of the optical link. The magnitude of the scintillation effect is proportional to the length scales of turbulence and strengths of the turbulence regimes [11]. The turbulence models revolve around the normalized variance of irradiance:

$$\sigma_I^2 = \frac{\langle I^2 \rangle - \langle I \rangle^2}{\langle I \rangle^2} \qquad \text{Eq. 2.12}$$

The irradiance (intensity) of the optical wave and the angle brackets < > denote a time average. In weak-fluctuation regimes, derived expressions for the scintillation index show that it is proportional to the Rytov variance [11, 12].

$$\sigma_1^2 = 1.23 C_n^2 \left(\frac{2\pi}{\lambda} \right)^{\frac{7}{11}} L^{\frac{11}{6}} \qquad \text{Eq. 2.13}$$

where C_n^2 is the turbulence strength parameter for refractive index fluctuations and L is the path length. The expression to compute scintillation for strong turbulence regimes include more variables and are complicated.

Similar concerns have been raised for underwater light propagation. Small angle scattering ($<10^{-3}$rad) is known to be caused by suspended particles with the same refractive index of water and by refractive effects from large scale index of refraction variations [13]. In general this is a relatively unexplored area in literature.

Turbulent oceanic flows cause fluctuations in salinity, pressure and temperature [14]. These fluctuations can lead to changes in the density of the fluid and hence refractive inhomogeneities. Empirical equations for calculating the refractive index can be expressed as function of salinity, temperature and wavelength of operation [15]. Salinity variations are in the order of a few parts per thousand while the temperature fluctuations are in fractions of a degree. Variations in the refractive indices with fluctuations in water salinity, wavelength of light, temperature of water and pressure are shown in Figures 2-10 to 2-13 [1, 16].

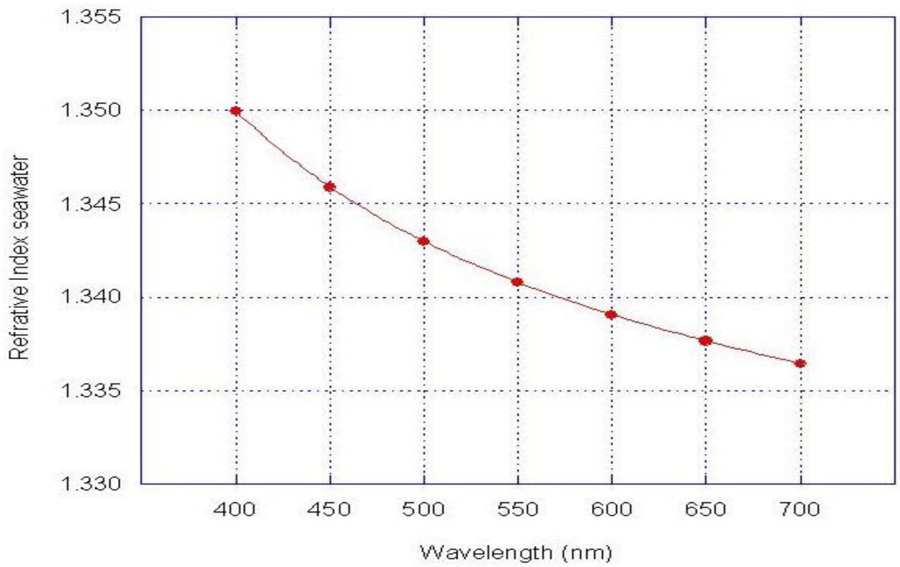

Figure 2-10 Variation in the refractive index of sea water with change in wavelength of light. Above data points are for seawater with Salinity=35‰ and Temperature=20 ^{o}C [1].

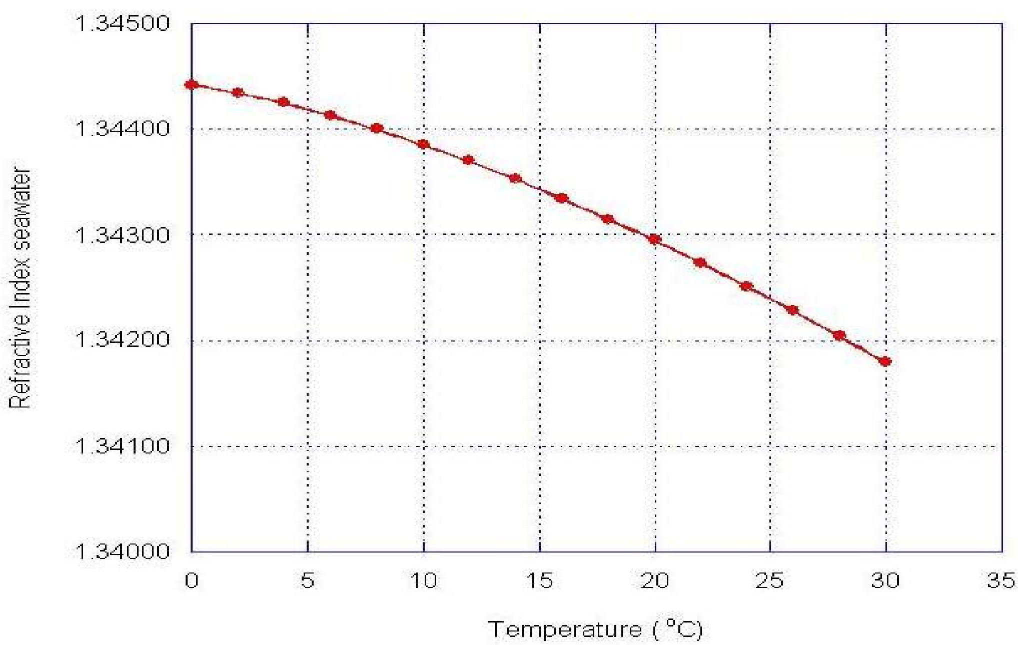

Figure 2-11 Variation in the refractive index of sea water with change in the temperature. Above measurements are for seawater with Salinity=35‰ and λ=500nm [16].

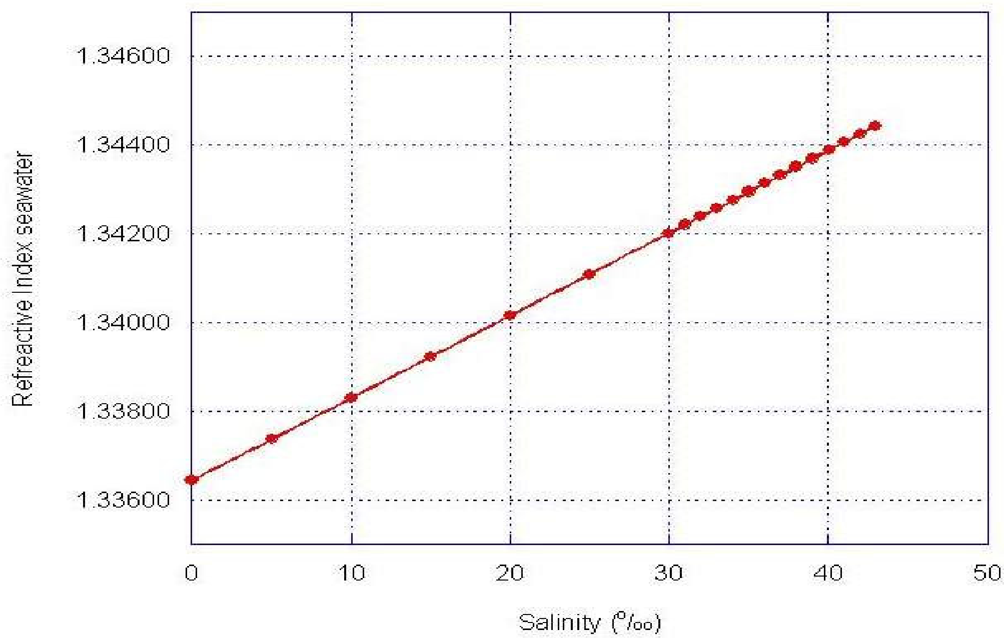

Figure 2-12 Variation in the refractive index of sea water with change in the salinity. Above measurements are for seawater with Temperature=20 °C and λ=500nm [16].

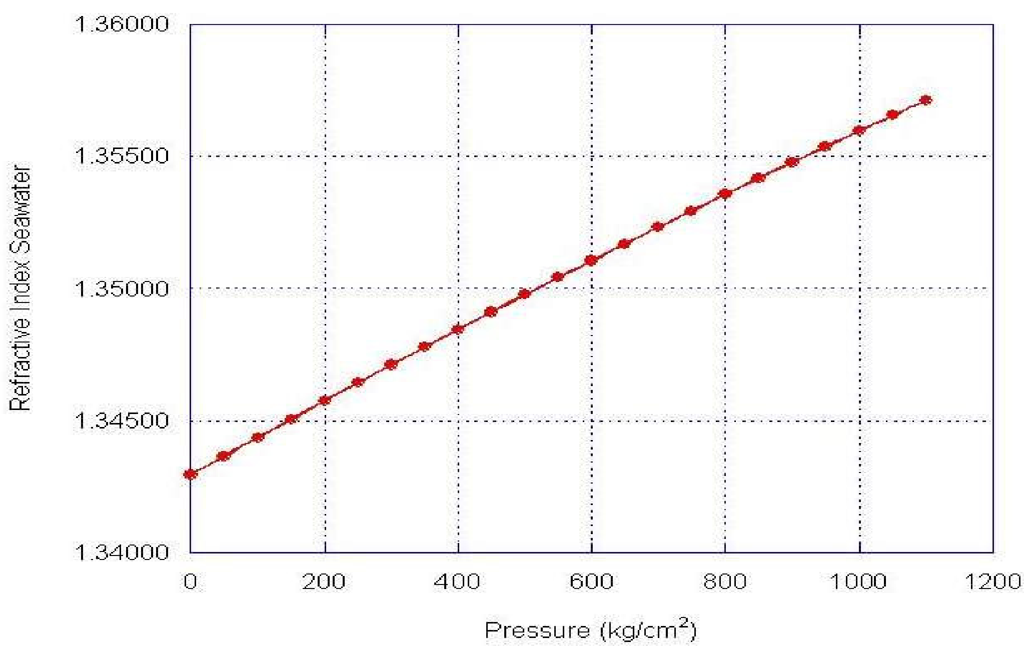

Figure 2-13 Variation in the refractive index of sea water with change in pressure. Above measurements are for seawater with Salinity=35‰ Temperature=20 °C and λ=500nm [16].

The electromagnetic beam experiences random distortion in intensity and phase when passed through a turbulent medium. The particle nature of light can used to explain this event, as the photons is deflected while traversing each turbulent cell. The length scales of turbulence cells in water are not well defined as compared to air.

Direct measurements of small angle scattering in the ocean suggest that the volume scattering function can be attributed to turbulence induced inhomogeneities. In laboratory experiments, scattering due to turbulence induced homogeneities is found to dominate over particle scattering for near-forward angles and for short distance (<0.25m) [17]. These experiments involve different turbulent flows with increasing value of temperature variance, which result in increase peaking in the near-forward angles.

Techniques such as aperture averaging are used to compensate for the effects of scintillation for terrestrial free space optical links. Approaches similar to these can be adopted to mitigate the losses in underwater applications [18]. Complexity of measurements and the dynamic nature of events have made it difficult to model this phenomenon in water. This study will not be included here in this work.

2.4 References

[1] C. D. Mobley, *Light and Water- Radiative Transfer in Natural Waters.* California: Academic Press Inc., 1994, pp. 60-144;300-303;487-488.

[2] R. C. Smith and K. S. Baker, "Optical properties of the clearest natural waters," *Applied Optics,* vol. 20, pp. 177-184, 1981.

[3] R. E. Walker, *Marine Light Field Statistics.* New York: John Wiley & Sons Inc., 1994, pp. 142-162;168-172.

[4] V. I. Haltrin and G. W. Kattawar, "Effects of Raman Scattering and Fluorescence Apparent Optical Properties of Sea Water," *Texas A&M University,* 1991.

[5] B. Woźniak, J. Dera, D. Ficek, R. Majchrowski, S. Kaczmarek, M. Ostrowska and M. O. Koblentz, "Modelling the influence of photo-and chromatic-acclimation on the absorption properties of marine phytoplankton," in *Ocean Optics Conference,* 1998, pp. 10-13.

[6] A. Morel and L. Prieur, "Analysis of variations in ocean color," *Limnology and Oceanography,* vol. 22, pp. 712-714, 1977.

[7] V. I. Haltrin, "Chlorophyll-based model of seawater optical properties," *Applied Optics,* vol. 38, 1999.

[8] C. L. Gallegos, D. L. Correll and J. W. Pierce, "Modeling Spectral diffuse attenuation, absorption and scattering coefficients in a turbid estuary," *Limnology and Oceanography,* vol. 35, pp. 1486-1502, 1990.

[9] A. Morel and B. Gentili, "Diffuse reflectance of oceanic waters: its dependence on Sun angle as influenced by the molecular scattering contribution," *Applied Optics,* vol. 30, 1991.

[10] O. V. Kopelevich, "Small –parametric model of the optical properties of seawater," *Ocean Optics,* pp. 208-234, 1983.

[11] L. C. Andrews and R. L. Phillips, "Impact of scintillation on laser communication systems: recent advances in modeling," *Free-Space Laser Communication and Laser Imaging, SPIE,* vol. 4489, 2001.

[12] L. C. Andrews, R. L. Phillips, C. Y. Hopen and M. A. Al-Habash, "Theory of optical scintillation ," *Journal of Optical Society of America,* vol. 16, 1999.

[13] H. T. Yura, "Small-angle scattering of light by ocean water," *Applied Optics,* vol. 10, 1971.

[14] D. J. Bogucki, J. A. Domaradzki, R. E. Ecke and R. C. Truman, "Light scattering on oceanic turbulence," *Applied Optics,* vol. 43, 2004.

[15] X. Quan and E. S. Fry, "Empirical equation for the index of refraction of seawater," *Applied Optics,* vol. 34, 1995.

[16] R. W. Austin and G. Halikas, "Index of refraction of seawater," *Scripps Institute of Oceanography,* vol. 76, 1976.

[17] D. J. Bogucki, J. A. Domaradzki, R. E. Ecke and R. C. Truman, "Near-forward light scattering on oceanic turbulence and particulates: An experimental comparison," in *XIV Ocean Optics Conference,*

[18] L. C. Andrews, R. L. Phillips and C. Y. Hopen, "Aperture averaging of optical scintillations: power fluctuations and the temporal spectrum," *Waves Random Media 10,* pp. 53-70, 2000.

CHAPTER 3 BIO-OPTICAL MODELS

3.1 INTRODUCTION

It is important to determine the absorption and scattering coefficients of the medium, in order to quantify the energy loss. The light energy that is absorbed or scattered in water is either transformed as heat or reemitted as Raman scattering and fluorescence. Oceanographic studies have often observed a significant cross correlation among the measured (*in situ*) inherent optical properties. This has led to the development of a one parameter model of the inherent optical properties for natural waters [1]. The model adopted for our study is based on the chlorophyll concentration in water for Case1 and some Case 2 waters [†] and couples the concentration of CDOM and Scattering Particles with the Chlorophyll concentration.

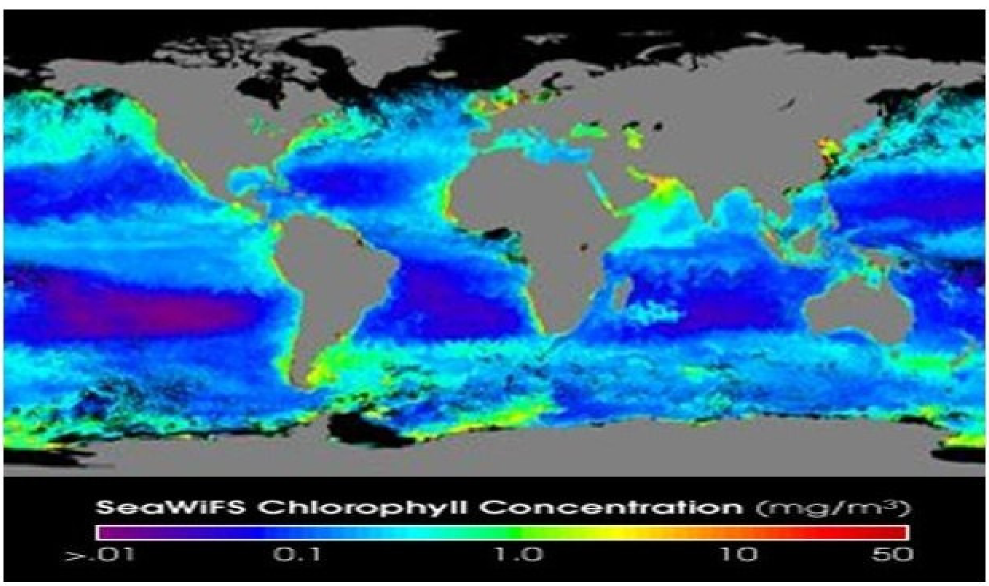

Figure 3-1 Satellite remote-sensing of Chlorophyll-a concentration [2].

[†] Case 1 is water type in which the concentration of phytoplankton is dominant as compared to several other inorganic particles. Case 2 water types have phytoplankton concentration lower than other organic and inorganic particles.

3.2 Model of Absorption

The absorption model is based on the chlorophyll concentration and two components of yellow substance (CDOM): fulvic acid and humic acid [1]. The model replies on *in situ* measurements of IOP's by various researchers. This model neglects the presence of detritus and inorganic particle like clay and quartz. The absorption coefficient $a(\lambda)$ (m^{-1}) is be defined as

$$a(\lambda) = a_w(\lambda) + a_c^0(\lambda)(C_c / C_c^0)^{0.602} + a_f^0 C_f(-k_f\lambda) + a_h^0 C_h(-k_h\lambda) \quad (m^{-1}) \qquad \text{Eq. 3.1}$$

where,

$a_w(\lambda)$ is the pure seawater absorption coefficient

$a_c^0(\lambda)$ is the spectral absorption coefficient of chlorophyll

a_f^0 is the specific absorption coefficient of fulvic acid with value 35.959 m^2/mg

a_h^0 is the specific absorption coefficient of humic acid with value 18.828 m^2/mg

C_c is the total concentration of chlorophyll in mg/m^3

C_c^0 is constant with a value equal to 1mg/m^3

k_f is constant with value 0.0189 nm^{-1}

k_h is constant with value 0.01105 nm^{-1}

C_f is the concentration of fulvic acid in mg/m^3

C_h is the concentration of humic acid in mg/m^3

The concentrations of humic acid and fulvic acid for chlorophyll concentrations in the range 0-12mg/m^3 is calculated using the relation as follows.

$$C_f = 1.74098 * C_c * \exp(0.12327(C_c/C_c^0)) \qquad \text{Eq. 3.2}$$

$$C_h = 0.19334 * C_c * \exp(0.12343(C_c/C_c^0)) \qquad \text{Eq. 3.3}$$

The values for spectral absorption coefficients of pure seawater and chlorophyll are calculated by interpolating the measured data [3, 4].

Table 3-1 Spectral absorption coefficients for pure seawater (left) and chlorophyll (right) [3, 4].

wavelength (nm)	$a_w(\lambda)$ (m^{-1})	$a_c^o(\lambda)$ (m^{-1})
200	3.07	0.013
250	0.559	0.026
300	0.141	0.051
350	0.0463	0.087
400	0.0171	0.06
450	0.0145	0.025
500	0.0257	0.012
550	0.0638	0.006
600	0.244	0.007
650	0.349	0.008
700	0.65	0.041
750	2.47	0.004

It is important to note that this model does not include the absorption due to detritus or the concentration of detritus. Below is the total spectral absorption coefficient $a(\lambda)$ of sea water having the chlorophyll concentration of $1 mg/m^3$

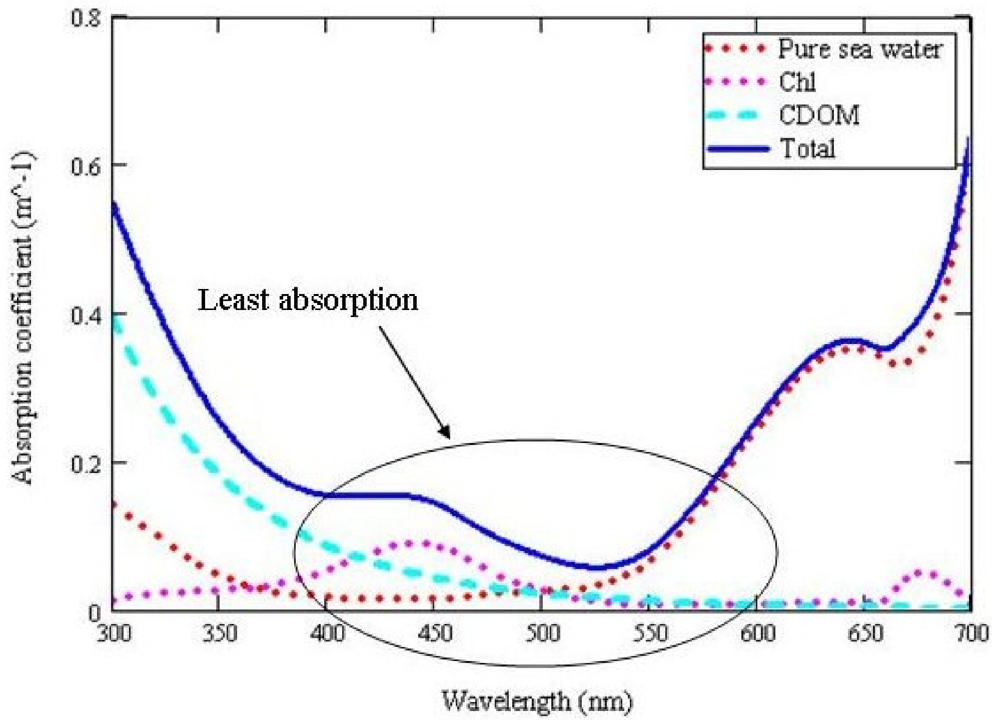

Figure 3-2 Absorption in sea water with 1mg/m^3 of Chlorophyll concentration [1, 4].

It can be noted from the graph in Figure 3-2 that the region between 475nm and 580nm has the least absorption indicating that this is the best window for wavelength of operation.

3.3 Model of Scattering

The model looks at scattering being caused by a combination of three events, that is scattering by pure seawater, large organic particles and small organic particles. The total scattering coefficient b(λ) is

$$b(\lambda) = b_w(\lambda) + b_s^0(\lambda) C_s + b_l^0 C_l \quad (\mathrm{m}^{-1}) \qquad \text{Eq. 3.4}$$

where $b_w(\lambda)$ is the scattering coefficient of pure seawater
$b_s^0(\lambda)$ is the spectral scattering coefficient of small particles
$b_l^0(\lambda)$ is the spectral scattering coefficient of large particles
C_s and C_l are the concentrations of the small and large particles

The equations for $b_w(\lambda)$, $b_s^0(\lambda)$ and $b_l^0(\lambda)$ are given as [1]

$$\mathrm{b_w}(\lambda) = 0.005826 * (400\mathrm{nm}/\lambda)^{4.322} \quad \mathrm{m^2/g} \qquad \text{Eq. 3.5}$$

$$\mathrm{b_s^0}(\lambda) = 1.151302 * (400\mathrm{nm}/\lambda)^{1.17} \quad \mathrm{m^2/g} \qquad \text{Eq. 3.6}$$

$$\mathrm{b_l^0}(\lambda) = 0.341074 * (400\mathrm{nm}/\lambda)^{0.3} \quad \mathrm{m^2/g} \qquad \text{Eq. 3.7}$$

As this is a single parameter model, the concentrations of small and large particles are dependent on the chlorophyll concentration. Their relation is given as

$$C_s = 0.01739(\mathrm{g}/\mathrm{mg}) * \mathrm{C_c} * \exp[0.11631(\mathrm{C_c}/\mathrm{C_c^0})] \quad \mathrm{mg/m^3} \qquad \text{Eq. 3.8}$$

$$C_l = 0.76284(\mathrm{g}/\mathrm{mg}) * \mathrm{C_c} * \exp[0.03092(\mathrm{C_c}/\mathrm{C_c^0})] \quad \mathrm{mg/m^3} \qquad \text{Eq. 3.9}$$

The total scattering coefficient over the visible spectrum obtained for a chlorophyll concentration of 1mg/m^3 is as shown in the Figure 3.3

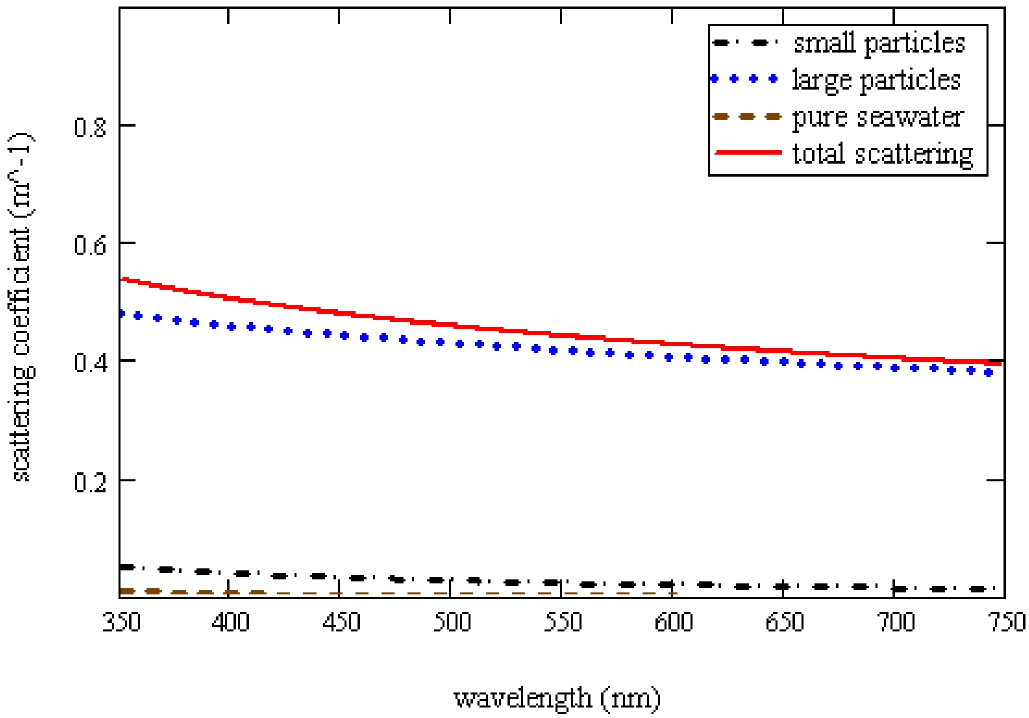

Figure 3-3 Various constituents of scattering coefficient with 1mg/m^3 of chlorophyll concentration.

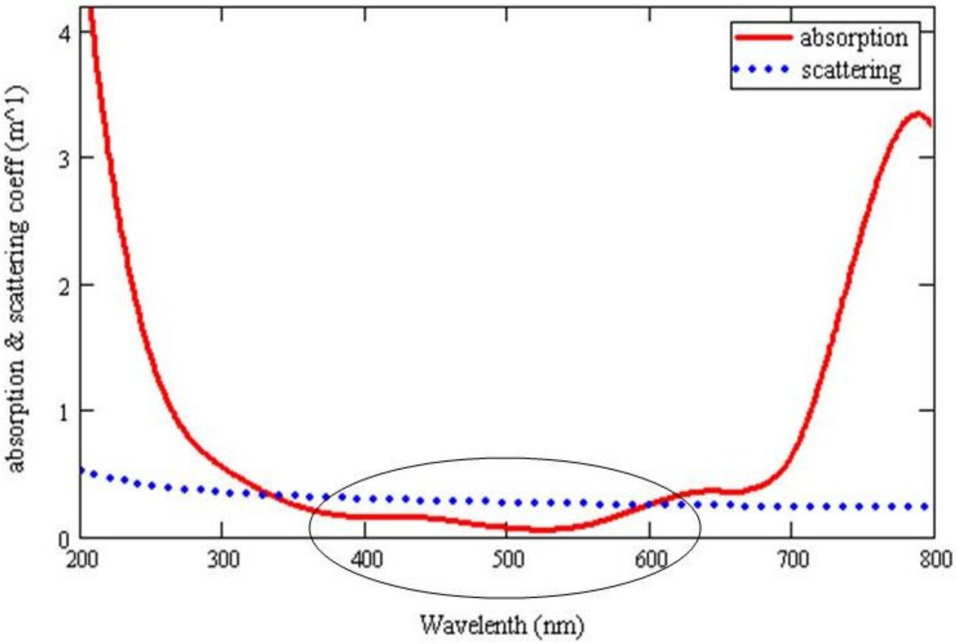

Figure 3-4 Total absorption and scattering coefficients of sea water with $1mg/m^3$ of chlorophyll concentration.

In the region of wavelengths (450nm – 600nm) the effect of scattering is more as compared to absorption.

3.4 Chlorophyll distribution

Chlorophyll is the principle pigment of phytoplankton biomass. The concentration of chlorophyll can be assumed to be proportional to the concentration of phytoplankton. Chlorophyll is present primarily in the well-lit surface layer of the lakes, sea and ocean. As shown in Figure 3-1, the amount of chlorophyll is not uniform throughout the water mass.

Phytoplankton is usually present in the top 50m to 200m below the surface of water. This region is the euphotic zone. There is also a variation observed in the concentration along the depth of a water column, i.e. the chlorophyll concentration is vertically distributed. Since the one-parameter model adopted is completely dependent on the chlorophyll concentration, it is important to understand the chlorophyll distribution.

3.4.1 Methods to determine the chlorophyll concentration

<u>Remote Reflectance:</u>

In the open ocean, the most important thing that influences color is phytoplankton. Different colors reveal to different concentrations of phytoplankton, and to different concentrations of sediments and dissolved organic materials [5, 6]. Ocean color sensors mounted on satellites scan the earth surface and records the upwelling radiance L (flux per unit area per unit solid angle) [7].

The spectral remote-sensing reflectance R_{rs} is defined as

$$R_{rs}(\theta,\phi,\lambda) \equiv \frac{L(z;\theta,\lambda)}{E_d(z;\lambda)} \qquad (sr^{-1}) \qquad \text{Eq. 3.10}$$

where $E_d(z;\lambda)$ is the downward irradiance.

An example of a passive ocean color sensor is the Coastal Zone Color Scanner (CZCS). Passive remote sensing is the method where the sensor observes the electromagnetic radiation that is naturally reflected by the water body [7]. There are various algorithms used to determine the concentration of chlorophyll pigments from remote-sensing. One of these that was used by the CZCS is

$$C = A[L(\lambda_1)/L(\lambda_2)]^B \qquad \text{Eq. 3.11}$$

where C is the concentration of chlorophyll

A and B are empirically determined constants

L is the irradiance

λ_1 and λ_2 are the two wavelengths used

In the case of CZCS the wavelengths used were 443nm and 550nm for low pigment concentration and 520nm and 550nm for high pigment concentrations [8].

<u>Fluorescence:</u>

Fluorescence is an inelastic process which occurs when a molecule absorbs a photon of a shorter wavelength and emits a photon of a higher wavelength [7]. Chlorophyll and other organic substances in natural waters fluoresce. Oceanographers use this property of substances to estimate the amount of chlorophyll present in water. For example, Chlorophyll *a* shows strong fluorescence with its wavelength centered on 685nm when excited with light of wavelength 450nm.

Fluorescence is measured using instruments called Fluorometers. Based on the above principle a chlorophyll fluorometer emits light around 450nm and detects the reflected light with wavelength 685nm [9]. In operation, fluorescence can be measured during vertical profiling of water by the instrument. This measured fluorescence value is equated to give the corresponding chlorophyll concentration.

3.4.2 Vertical Profile of Chlorophyll Concentration

As mentioned earlier, chlorophyll content varies along various parts of the water body as well as vertically. Our motivation to understand this distribution is to estimate the value of the total chlorophyll content between the source and receiver of our communication link. A Gaussian distribution pattern is observed vertical profile of chlorophyll concentration. The maximum chlorophyll concentration is not always near the surface of water, but sometimes lies at a subsurface depth. Below, are few chlorophyll vertical distribution profiles that taken around the Galapagos archipelago [10].

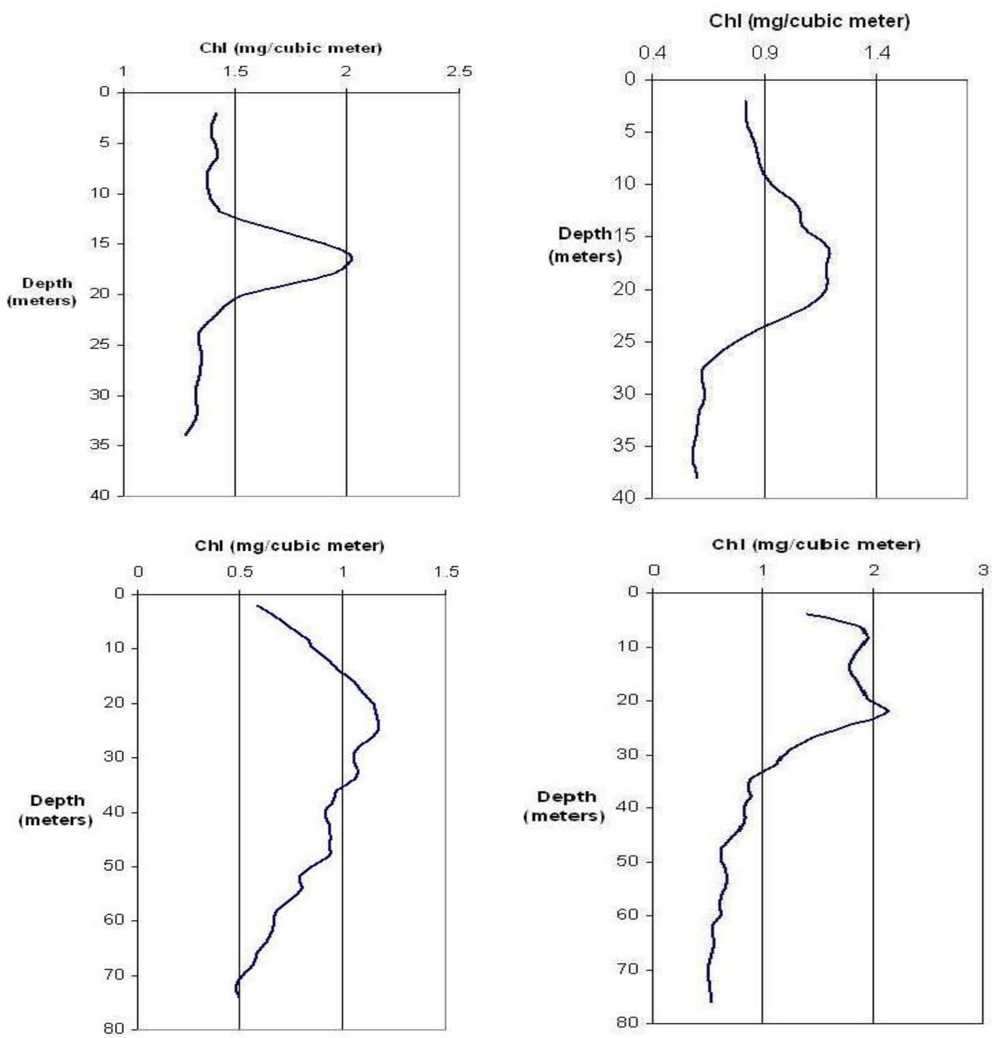

Figure 3-5 Vertical distribution profiles of chlorophyll [10].

In order to define the vertical distribution pattern of chlorophyll in a water column a five-parameter model is followed [11]. The empirical equation is based on large amount of field data that were collected in various oceanic regions throughout different seasons.

$$Chl(z) = B_o + S \times Z + \frac{h}{\sigma\sqrt{2\pi}} \exp\left[-\frac{(Z - Z_{\max})^2}{2\sigma^2}\right] \qquad \text{Eq. 3.12}$$

Chl(z) is the Chlorophyll concentration (mg/m^3) at the depth Z meters.

B_o is the Background chlorophyll concentration.

S is the vertical gradient ($mg/m^3/m$)

H is the total chlorophyll above background

Z_{max} is the Depth of maximum chlorophyll.

σ is the standard deviation of Gaussian distribution.

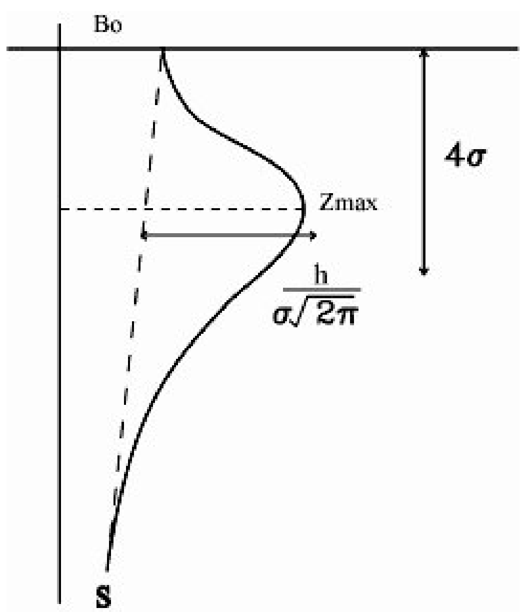

Figure 3-6 Vertical distribution model of chlorophyll [11].

These five parameters are obtained using regression as function of the surface chlorophyll ($Chl_{surface}$) as shown in Figure 3-7. Hence the accuracy of this data is largely dependent on the measured surface chlorophyll.

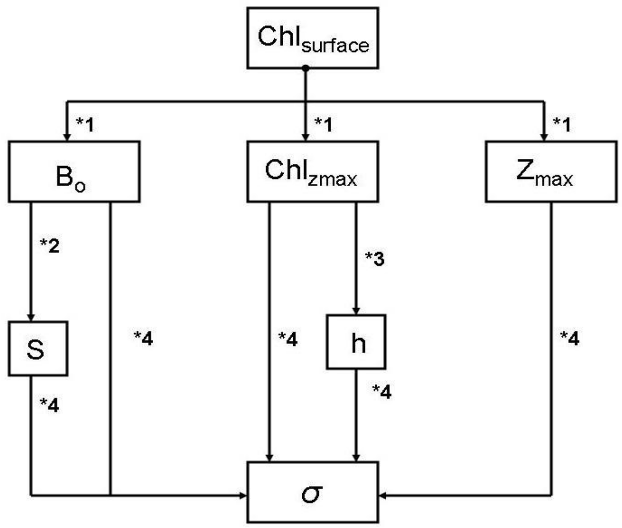

Figure 3-7 Procedure for estimating five parameters of the chlorophyll vertical profile from surface chlorophyll concentration [11].

3.4.3 Estimating chlorophyll concentration from vertical profile

Once the vertical distribution of chlorophyll is constructed, the value of chlorophyll concentration at every point along the depth is known using Equation 3.12. In order to apply the single parameter model for absorption and scattering, we have to determine the average chlorophyll concentration between the source and receiver.

With the assumption that the optical link has only one source and receiver we present a general scenario. The transmitter and receiver (or transmitter) are at a depth of z1 and z2 from the surface respectively. The line of sight path between the transmitter and receiver (or transmitter) makes an angle α with the vertical. Hence the total path length z_{total} can be calculated using Equation 3.13.

$$z_{total} = \frac{z2 - z1}{\cos(\alpha)} \qquad \text{Eq. 3.13}$$

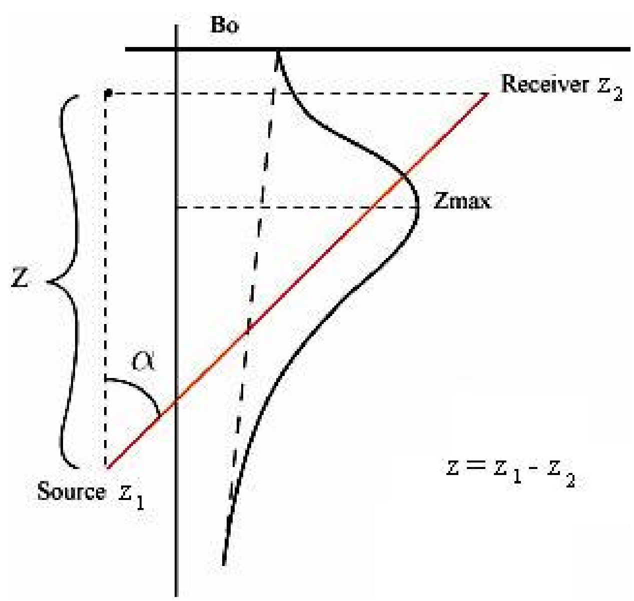

Figure 3-8 Calculating the chlorophyll concentration between the source and receiver

Total chlorophyll concentration between the transmitter and receiver is found by integrating Equation 3.12 over the limits z1 and z2. Further this is averaged by the vertical distance between them as shown in the Equation 3.14.

$$C_c = \frac{1}{\cos(\alpha)} * \left[\frac{1}{(z2 - z1)} . \int_{z1}^{z2} Chl(z).dz \right] \quad \text{mg/m}^3 \qquad \text{Eq. 3.14}$$

Further, the total path length can be divided into smaller intervals and then the absorption and scattering coefficient for each interval can be calculated. In the illustration shown below, L1, L2, L3,…Ln are the equal intervals between z_1 and z_2.

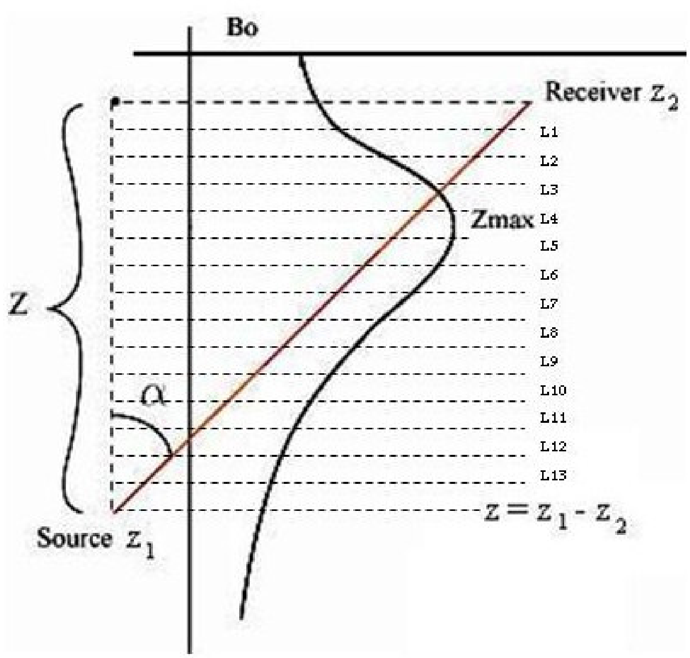

Figure 3-9 Dividing the path length into intervals to calculate the chlorophyll concentration

By reducing the size of the intervals to an infinitesimally small number, theoretically the absorption and scattering coefficient can be obtained across each chlorophyll cell. This method has been implemented in the MathCAD model‡. For various link lengths and chlorophyll profiles, it is found that the results of the model satisfactorily converge. The estimate of the chlorophyll concentration (mg/m^3) underlines the accuracy of the total attenuation model.

3.4.4 Jerlov Water Types

In a scenario where the chlorophyll concentration in the water mass is not accurately known, an alternate method is suggested. Though crude, this may provide a rough estimate of the chlorophyll content. Jerlov classified water types based on their spectral diffuse attenuation coefficient. He categorized ocean waters into JWT I, IA, IB, II and III and coastal waters into JWT 1-9. Here JWT stands for Jerlov Water Type.[12]

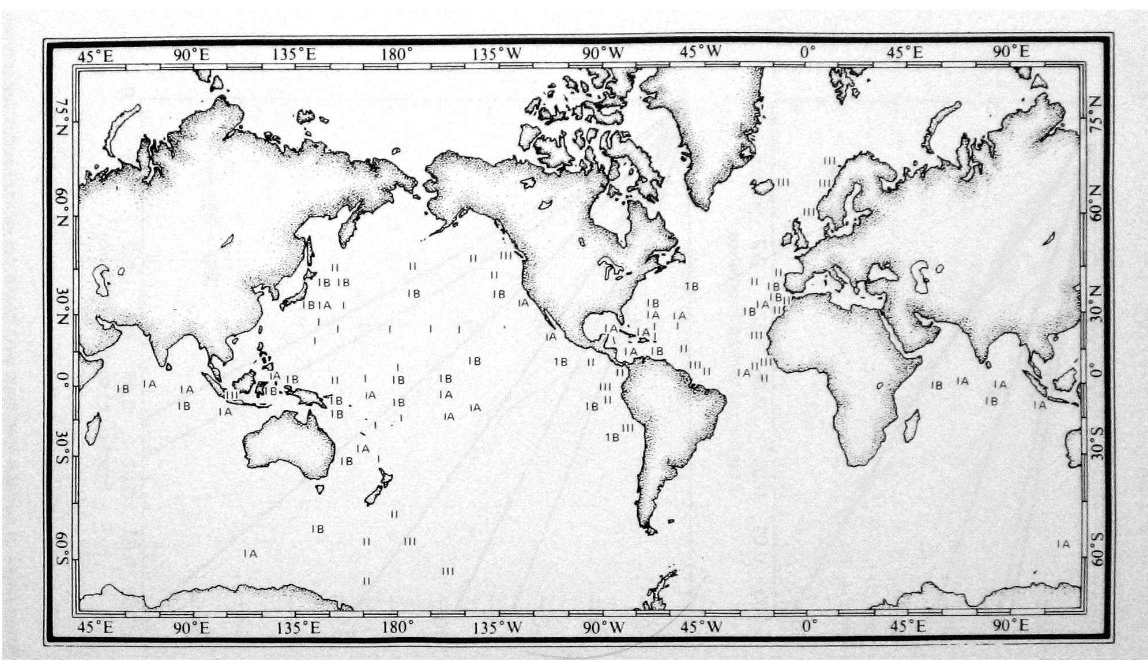

Figure 3-10 World plot of Jerlov water types for ocean waters[13, 14]

‡ Appendix A: MathCAD code

By overlapping the world plot of Jerlov Water types as in Figure 3-9 and the most recent satellite remote-sensed chlorophyll concentration like Figure 3-1, we can estimate approximate values of average chlorophyll concentrations over large areas. An example of this method is shown in Table 3-2.

Table 3-2 Average chlorophyll concentration for Jerlov Water Types estimated from ocean color sensor mounted on satellites [2, 13, 14].

Jerlov Water Types	Chlorophyll (mg/m3)
I	0.03
IA	0.1
IB	0.4
II	1.25
III	3

3.5 References

[1] V. I. Haltrin, "Chlorophyll-based model of seawater optical properties," *Applied Optics,* vol. 38, 1999.

[2] Global chlorophyll image (SeaWiFS), february 2006. *2006(08/08),* Available: http://earthobservatory.nasa.gov/Observatory/

[3] V. I. Haltrin and G. W. Kattawar, "Effects of Raman Scattering and Fluorescence Apparent Optical Properties of Sea Water," *Texas A&M University,* 1991.

[4] R. C. Smith and K. S. Baker, "Optical properties of the clearest natural waters," *Applied Optics,* vol. 20, pp. 177-184, 1981.

[5] "SeaWiFS Project," Available: http://oceancolor.gsfc.nasa.gov/SeaWiFS/

[6] A. Morel and L. Prieur, "Analysis of variations in ocean color," *Limnology and Oceanography,* vol. 22, pp. 712-714, 1977.

[7] C. D. Mobley, *Light and Water- Radiative Transfer in Natural Waters.* California: Academic Press Inc., 1994, pp.60-144; 300-303; 487-488.

[8] S. Sathyendranath and T. Platt, "Remote sensing of ocean chlorophyll: consequence of nonuniform pigment profile," *Applied Optics,* vol. 28, 1989.

[9] Seapoint chlorophyll fluorometer. *2006(06/05),* http://www.seapoint.com/scf.htm

[10] D. Kamykowski, "Galapagos Archipelago Cruise Expedition," North Carolina State University, 2005.

[11] T. Kameda and S. Matsumara, "Chlorophyll Biomass off Sanriku, Northwestern Pacific, Estimated by Ocean Color and Temperature Scanner (OCTS) and a Vertical Distribution Model," *Journal of Oceanography,* vol. 54, pp. 509-516, 1998.

[12] R. E. Walker, *Marine Light Field Statistics.* New York: John Wiley & Sons Inc., 1994, pp. 142-162;168-172.

[13] C. D. Mobley, D. Stramski, P. W. Bissett and E. Boss, "Optical Modeling of Ocean Water," *Oceanography,* vol. 17, 2004.

[14] J. R. Apel, *Principles of Ocean Physics.* London: Academic Press Inc., 1987, pp. 580-585.

CHAPTER 4 PATHLOSS

4.1 Understanding Scattering

Understanding the behavior of light in water is fundamentally knowing the absorption and scattering properties of water. The problem of radiative transfer in water has been well studied and documented [1-3]. Measuring and modeling the absorption is not as complex when compared to scattering, the random nature of scattering adds the technical difficulty of the complete characterization and its resulting contribution to the attenuation of light in natural waters. Theoretical approaches based on statistical approximations have been applied in order model these multiple scattering events [4-6].

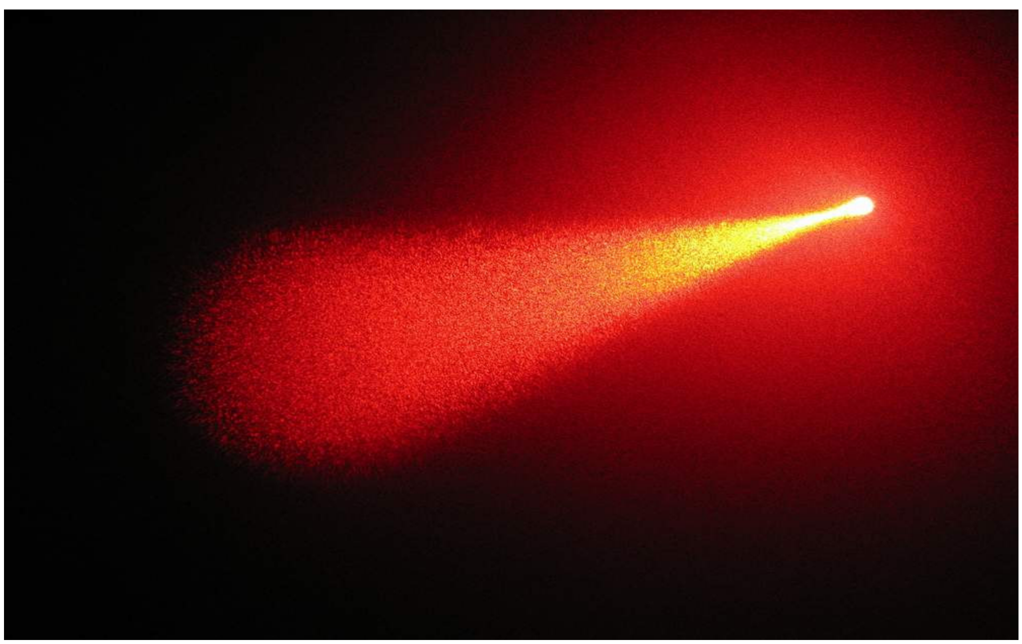

Figure 4-1 Scattering observed in sea water using a Red He-Ne Laser

The photons undergoing multiple scattering in the medium experience a change in the direction of propagation and eventually travel longer distance as compared to unscattered photons. Holistically, multiple scatterings cause the collimated light beam to spread. It can be subdivided into spatial, angular and temporal spread as shown in Figure 4-2. Spatial spread is the broadening of the pulse cross-section while the angular refers to the angular divergence of the beam. Temporal spread is attributed to addition time delay that the photon undergoes during multipath propagation.

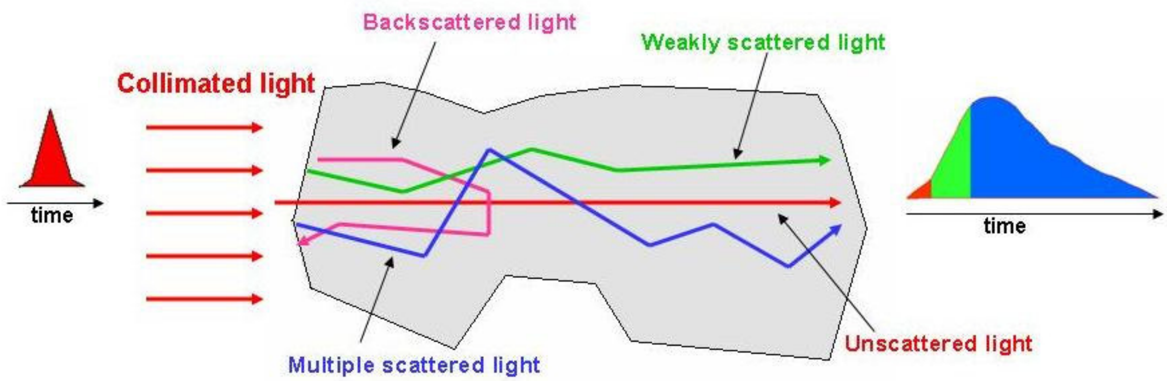

Figure 4-2 Beam spread due to multiple scattering in a medium [7].

The probability of scattering events increases with higher concentration of chlorophyll and dissolved organic material in natural water. As an analogy, images of the scattering of light can be seen when milk or Maalox® is added to water as shown in Figure 4-3 (from left to right) [8].

Figure 4-3 Images showing the effects of multiple scattering in water for increased concentrations of Maalox® (Left to Right)

It is difficult to experimentally measure the loss of intensity caused by scattering. Theoretical solutions to the problem of radiative transfer are very difficult. Monte Carlo techniques applied to provide uncompromised solutions, but are very computer intensive. An analytical method with simple approximations has to be approached to provide a meaningful result to the radiative transfer problem.

4.2 Empirical particulate scattering study

4.2.1 Motivation

Observing the beam spread for different water conditions can be considered important in understanding the effects of scattering. Unlike single scattering, multiple scattering is more deterministic, since the randomness of the interaction between particles and photons are averaged out over a large number of scattering events. To completely understand the scattering of light, we investigate the scattering of light in water containing different sized particles. From the definitions of Inherent optical properties of water, the scattering coefficient b, is defined as a function of the volume scattering function $\beta(\theta)$, where θ is the polar scattering angle [1]. Its relation is given as

$$b = \int_0^{\pi} \beta(\theta)\sin(\theta)d\theta \qquad \text{Eq. 4.1}$$

the volume scattering function $\beta(\theta)$ is the angular distribution of the scattered power, with units (m^{-1} sr^{-1}). The probability of a photon being scattering into a particular direction is obtained from the phase function given by

$$P = \int_{\theta 1}^{\theta 2} 2\pi\rho(\theta)\sin(\theta)d\theta \qquad \text{Eq. 4.2}$$

where $\rho(\theta)$ is the phase function. The phase function is obtained under single scattering conditions using the following relation

$$\rho(\theta) = \frac{\beta_{ss}(\theta)}{b} \qquad \text{Eq. 4.3}$$

where $\beta_{ss}(\theta)$ is the angular single-scattering function and b is the scattering coefficient.

From literature, it has been well observed that the scattering from particle size comparable or bigger than the wavelength of light, have a higher probability of being scattered in the forward direction [1,6,9]. This is applicable to atmospheric aerosols and natural waters and can be observed in the following experiments.

4.2.2 Experimental Setup

Optical power measurements were performed for the beam spread in tank of dimensions 1m x 0.4m x 0.3m filled with fresh tap water. A Si photodiode (Hamamatsu S2386-5K) was used to measure the received power. The photodiode was stationed on a translational stage driven by a lead screw. The photodetector was covered a black pipe of length 2.5cm and a aperture of 7mm to limit the field of view to less than 8^{o} (half angle).

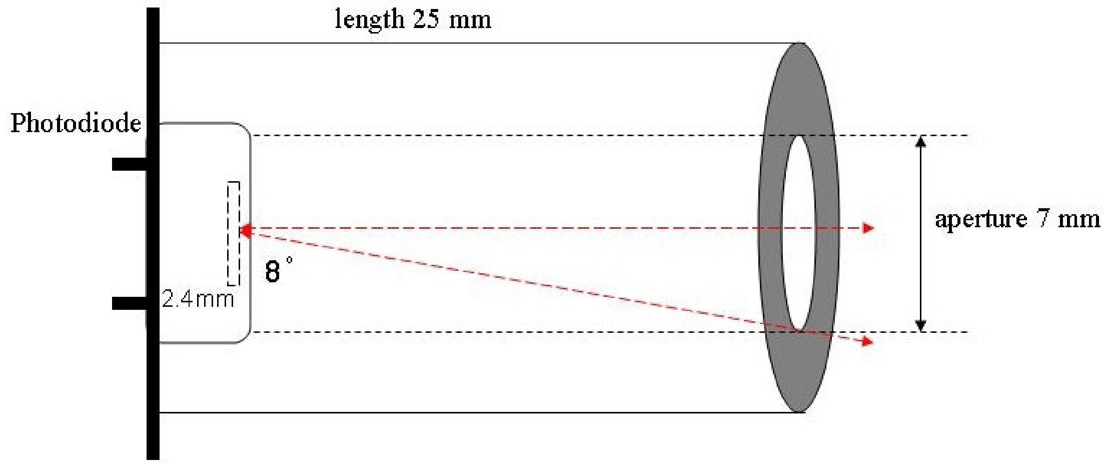

Figure 4-4 Schematic showing the tube and photodiode arrangement used for measurements.

A green laser pointer (532nm) and a red He-Ne laser (633nm) were used as two sources for the experiment. The lead screw translates the detector horizontally subtending a minimum angle of 0.076^{o} with the beam axis over a range of 0 to 8 degrees. The current from the photodiode was measured using a lock-in amplifier due to the high dynamic range of the instrument. An optical chopper was placed in between the tank and the laser and the reference frequency of the chopper was fed to the lock-in amplifier. The complete setup is shown in Figure 4-5.

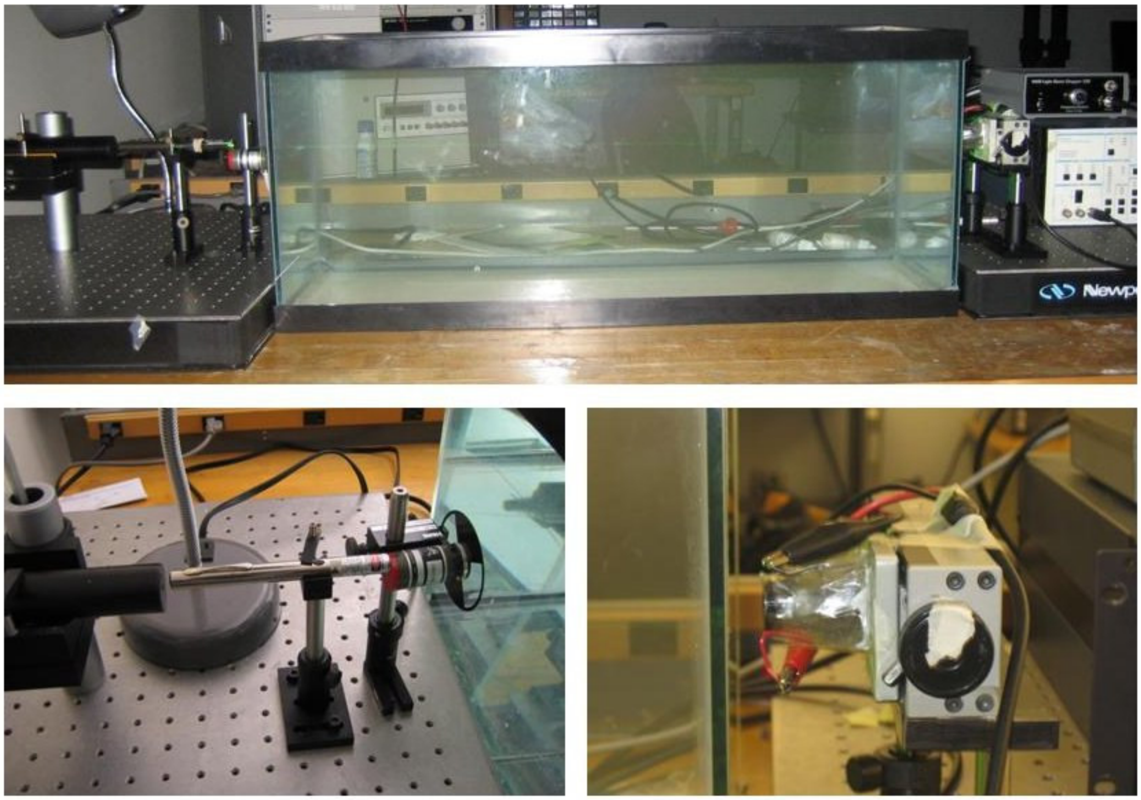

Figure 4-5 Experimental setup to measure the angular received power.

Uniform polystyrene latex spheres with refractive index 1.56 were used as scattering agents. Spheres of sizes 500nm and 6μm were added to water in measured quantities. Microscopic images of the two sphere samples are shown below.

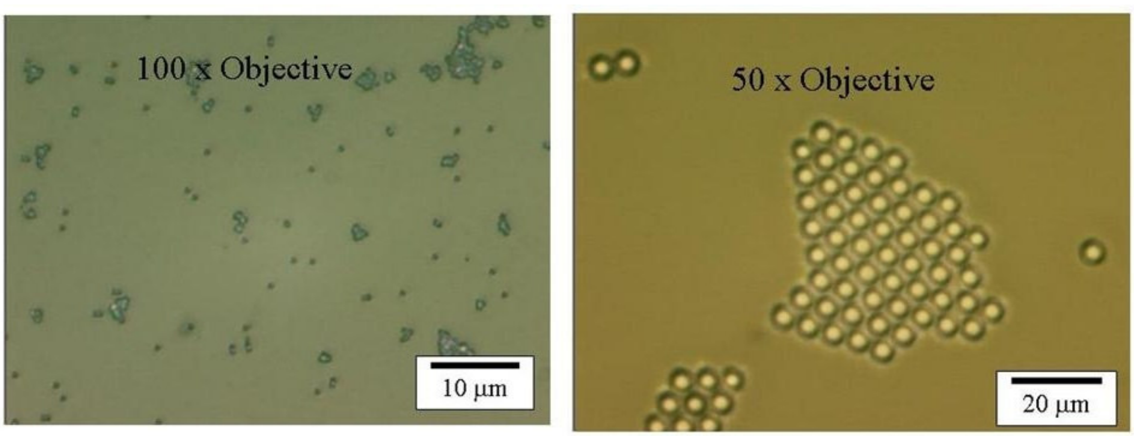

Figure 4-6 Microscopic images of the polystyrene sphere used as scattering agents.

4.2.3 Observation and Analysis

The received power was measured at every angle for different concentrations as shown in the graphs below. As seen from the graphs below the received power falls over four orders in magnitude for the first degree from the beam axis. A high forward scattering is prevalent over all water conditions and the similarity in their shapes is the striking feature of these graphs.

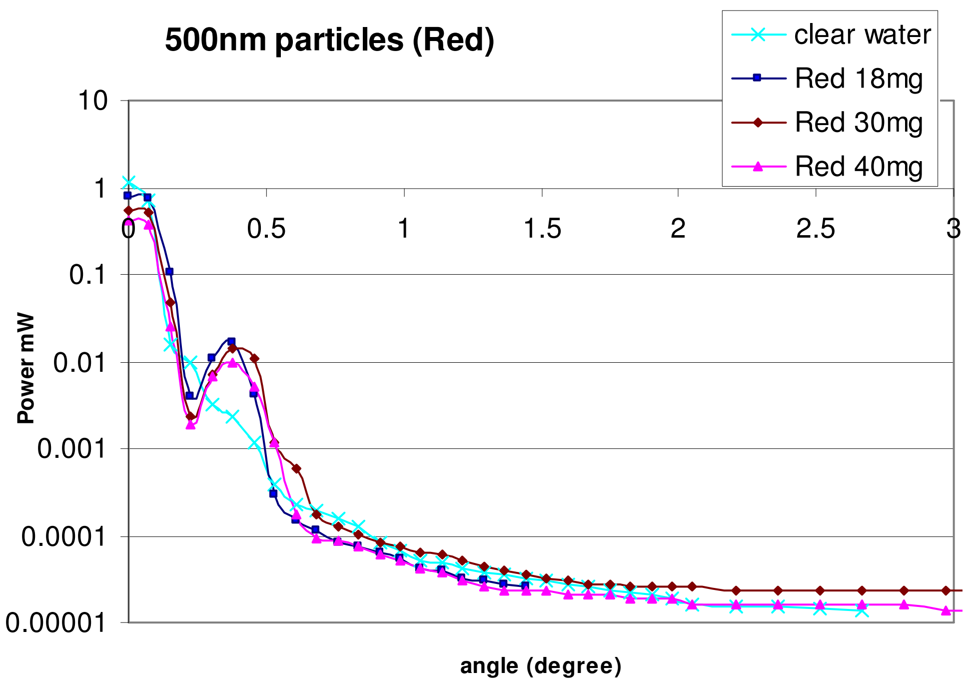

Figure 4-7 Measured received power of red laser over near forward angles for 500nm polystyrene latex sphere with different concentrations.

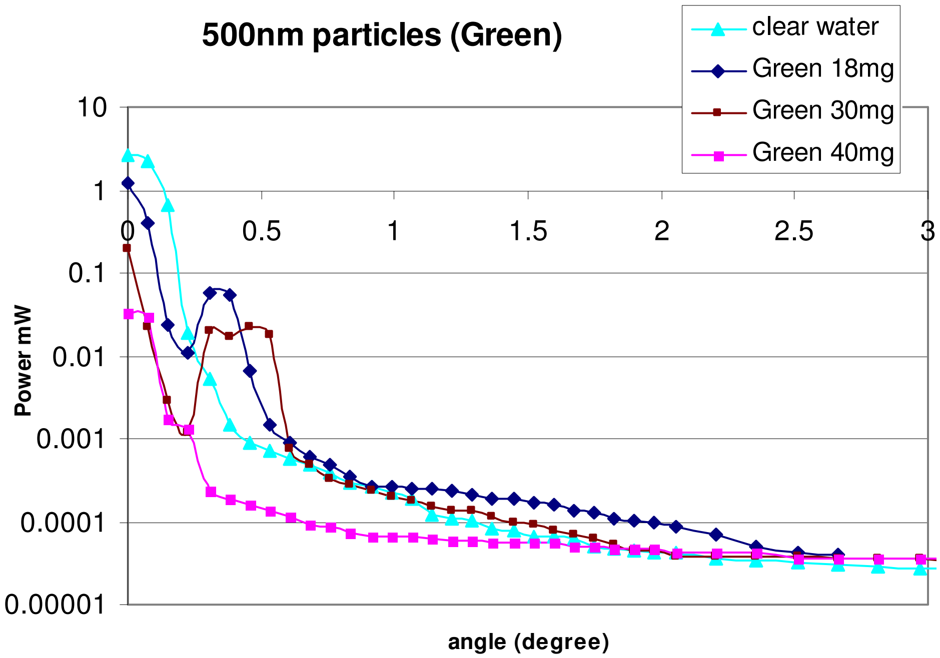

Figure 4-8 Measured received power of green laser over near forward angles for 500nm polystyrene latex sphere with different concentrations.

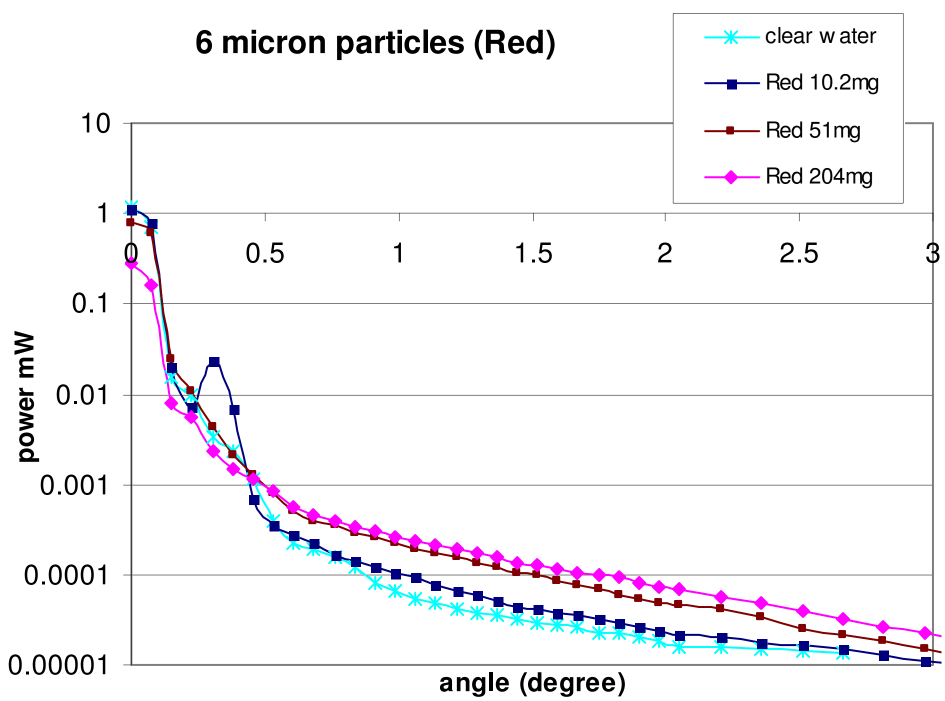

Figure 4-9 Measured received power of red laser over near forward angles for 6μm polystyrene latex sphere with different concentrations.

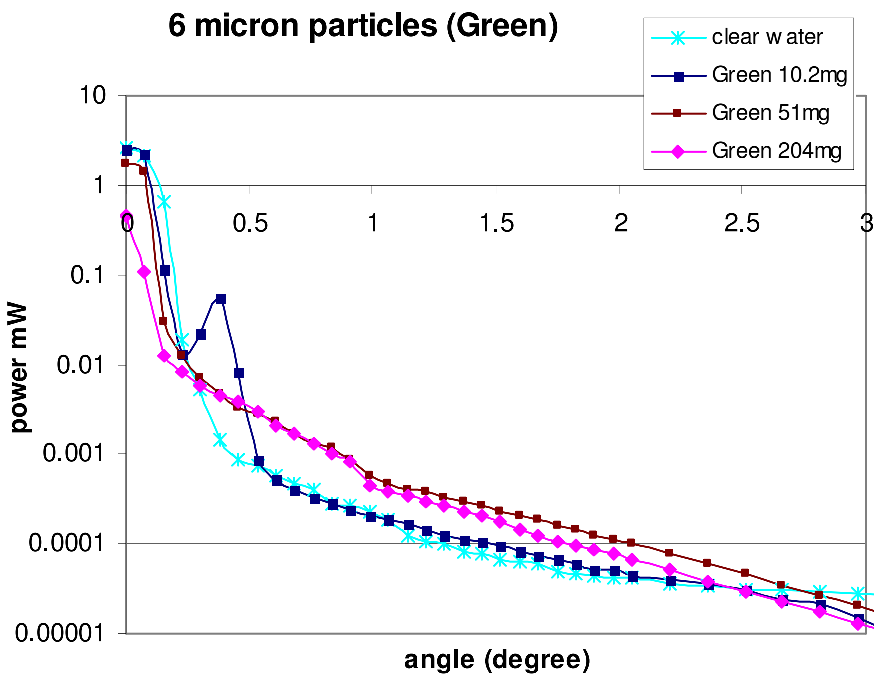

Figure 4-10 Measured received power of green laser over near forward angles for 6μm polystyrene latex sphere with different concentrations.

A strong second peak is observed for most concentrations of 500nm particles and lower concentrations of 6μm particles. These second or third order peaks are characteristic to Mie theory for large particle scattering. The primary reason to conduct experiments with 500nm and 6μm spheres is that these fall in the small particle and large particles range respectively as defined by the one parameter model. Equations 3.6 and 3.7 define the scattering by small and large particles. Small particle scattering is more wavelength dependent as compared to large particle scattering as shown in Figure 4-11. Small particle scattering decreases with the wavelength while large particle scattering is uniform over the range of 450nm to 800nm. Experimental observations are in agreement with these definitions and are shown in the graphs below.

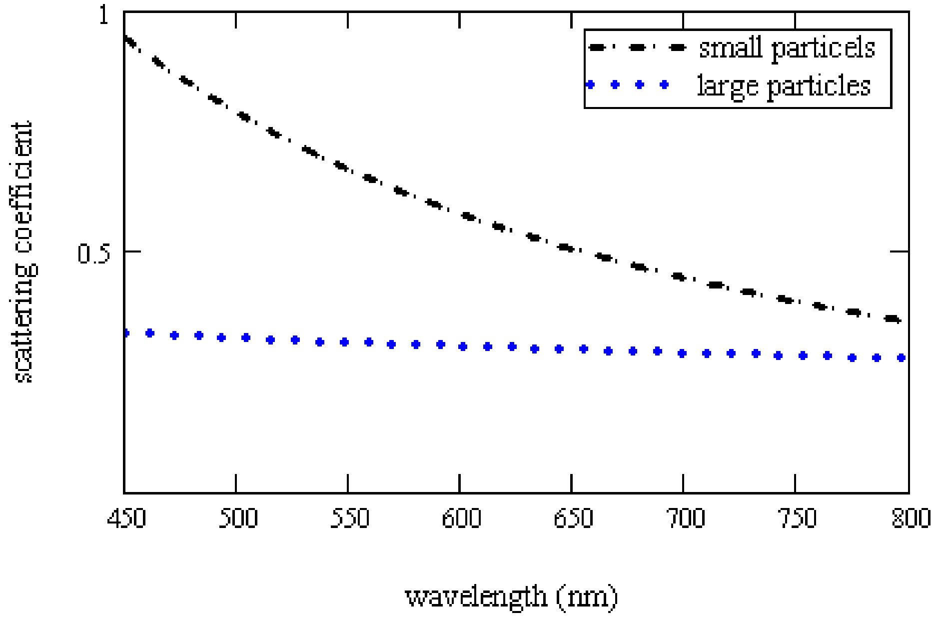

Figure 4-11 Wavelength dependence of small and large particle scattering

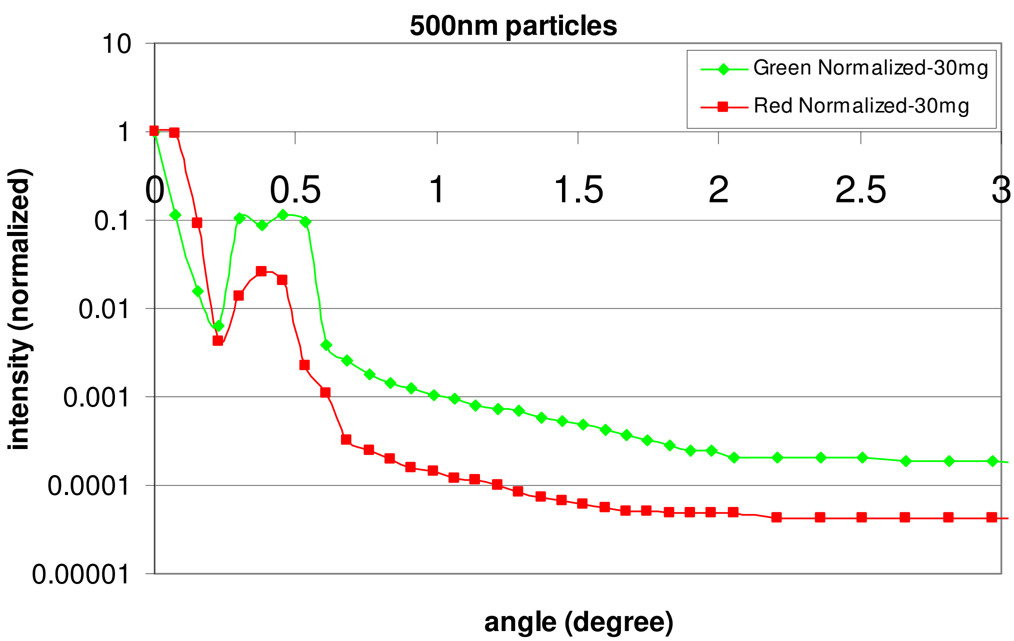

Figure 4-12 Measured received power over near forward angle for green and red wavelengths in water with 500nm polystyrene spheres.

There is more scattering observed for green wavelengths (532nm) as compared to red wavelength (633nm) for small particles (500nm polystyrene spheres); smaller wavelengths experience more scattering from 500nm sphere. Scattering by large particles (6μm polystyrene spheres) is similar for green and red wavelengths for uniform concentrations.

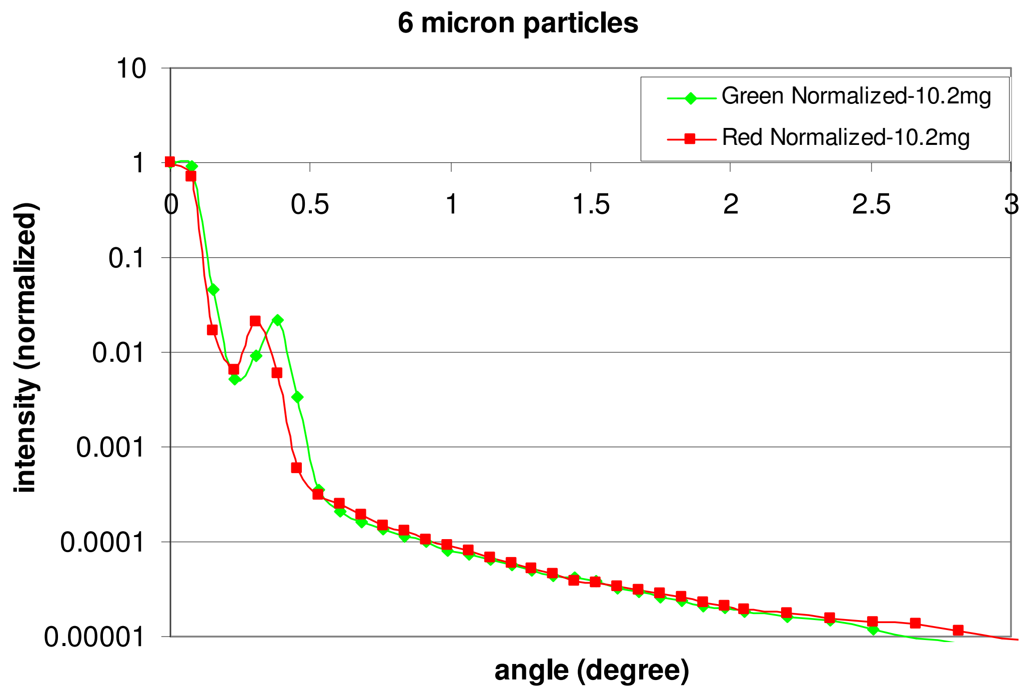

Figure 4-13 Measured received power over near forward angle for green and red wavelengths in water with 500nm polystyrene spheres.

Comparing the experimental data with *in situ* measured volume scattering function of natural waters would give us an insight on the similarities of scattering between the mediums. A very elaborate and careful study was conducted by Petzold (1972) for the volume scattering function for clear ocean waters, coastal waters and turbid waters [1]. These have been compared to experimental values. Since the experimental values are received power and not the scattering function, there is a difference in the intensity between the two, however a strong resemblance in the shape of the two curves suggest a similar phase function $\rho(\theta)$.

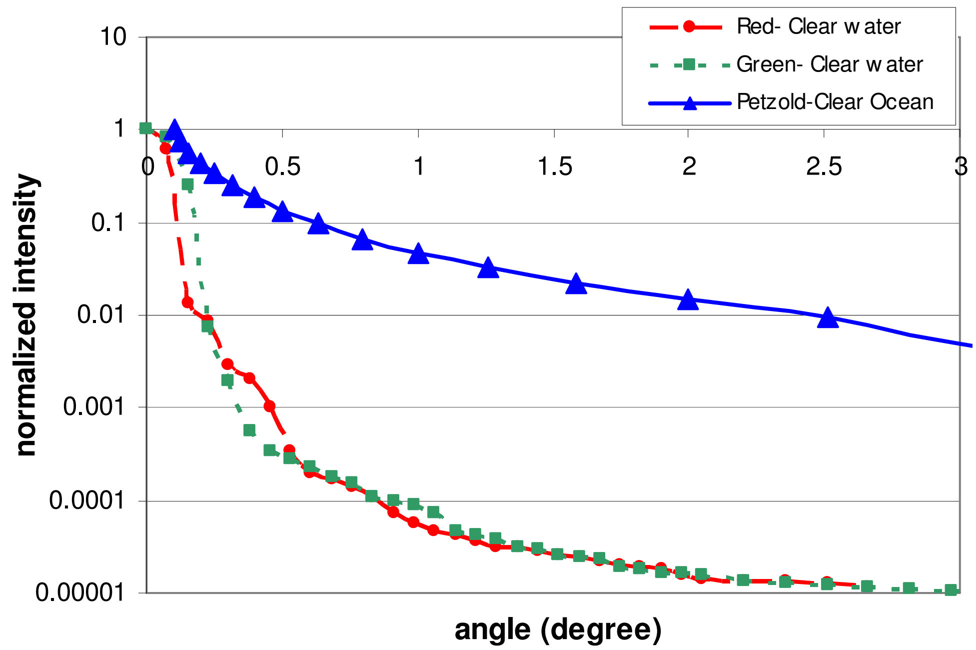

Figure 4-14 Comparison of experimental data of clear water and volume scattering function of natural clear waters [1].

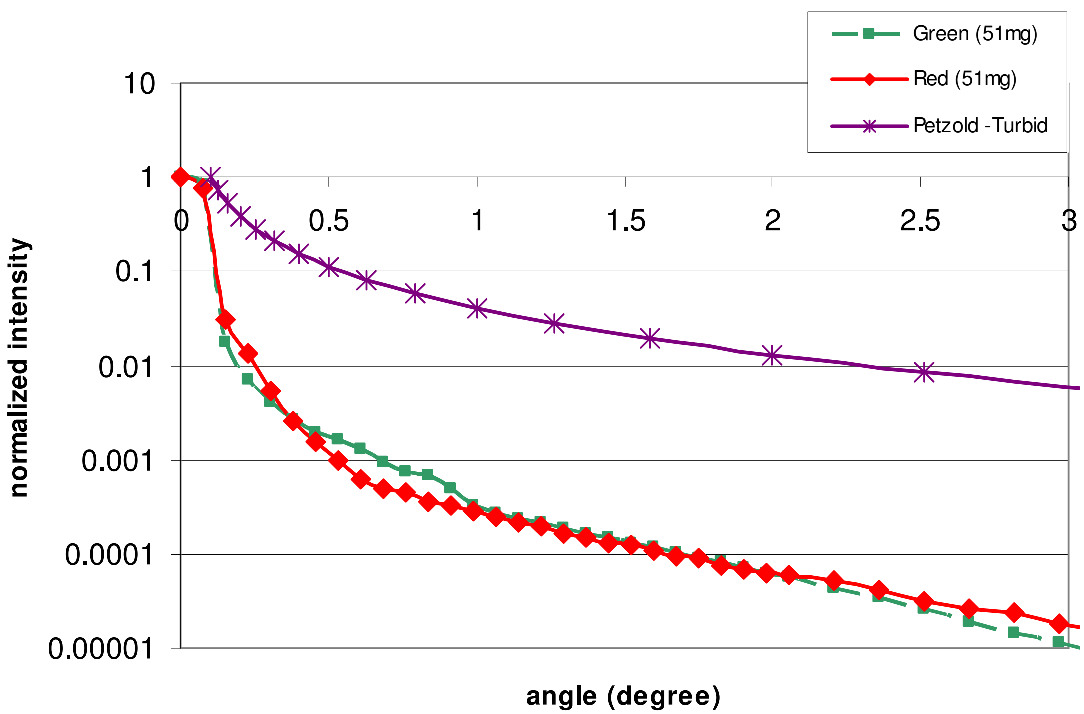

Figure 4-15 Comparison of experimental measurements with 6μm particles and volume scattering function of turbid waters [1].

Ideally VSF can be calculated using measuring instruments which can measure the attenuation and extinction separately and back calculate the scattering coefficient for every angle [10].

Mie theory simulations are satisfactorily be performed for the polystyrene spheres due to their spherical nature. The real part of the refractive index for is 1.56 while the complex part of the refractive index is considered negligible for simulations. The real and complex refractive index are directly associated with the scattering and absorption of the polystyrene spheres[§]. These simulations are carried out for the particles with diameter 500nm and 6μm. These results are compared with the experimental data for both operational wavelengths red and green. The normalized intensity is plotted for the near forward angles.

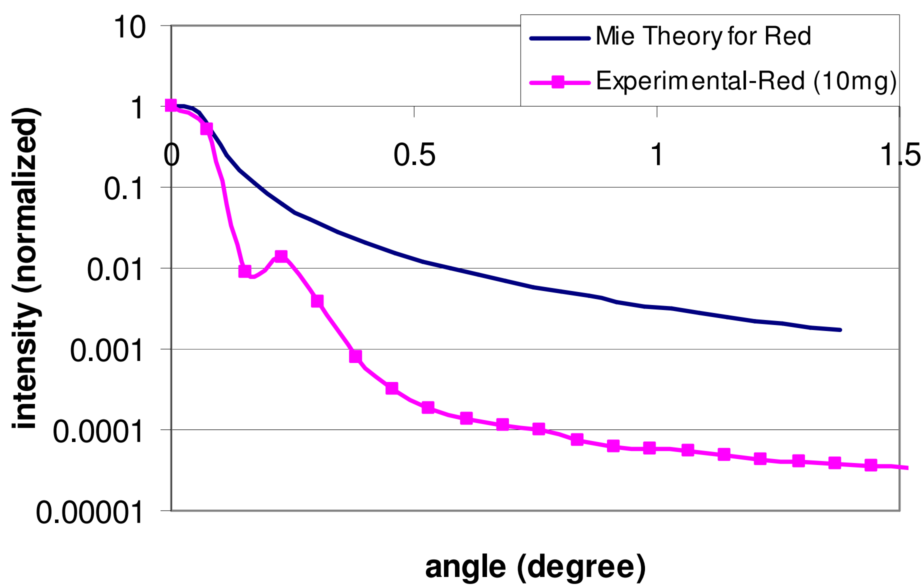

Figure 4-16 Comparison of experimental measurements and Mie Theory prediction for 500nm latex spheres.

§ Appendix D: Mie Theory (Maple Code)

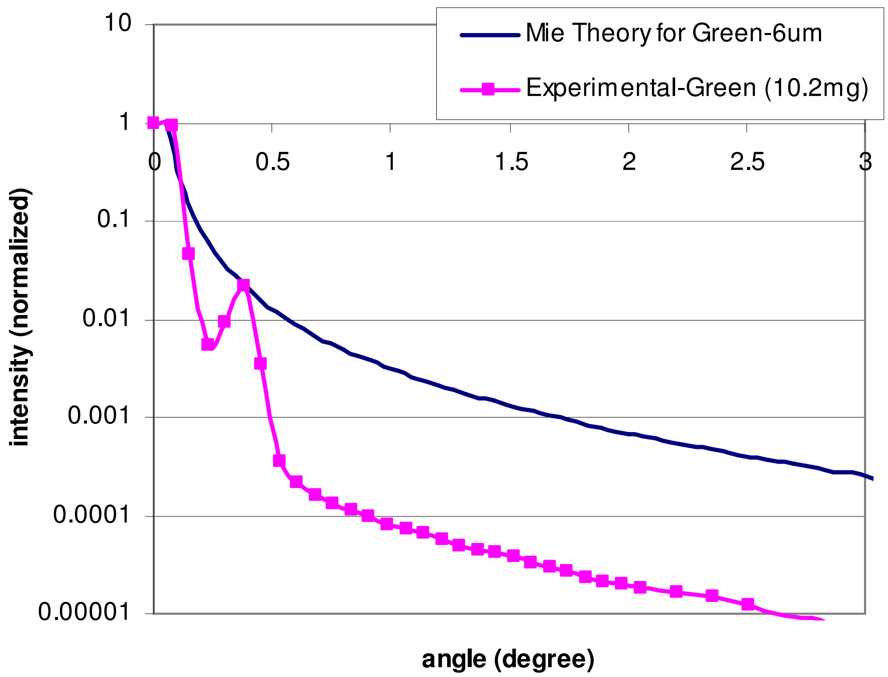

Figure 4-17 Comparison of normalized experimental measurements and Mie theory predictions of scattering from for 6μm latex spheres.

The Mie simulation results and experimental data are normalized to emphasize the strong agreement in the shape of the two curves.

The beam spread patterns of light beams show an exponential decay for most water conditions. With increasing link length the beam attenuation will increase exponentially, i.e. decrease in the intensity of light. When compared to Gaussian distribution of the beam at the source, the expanded beam would have a much larger radius. The intensity distribution for can be given as follows [11]:

$$I = I_o e^{-2r^2/w^2} \qquad \text{Eq. 4.4}$$

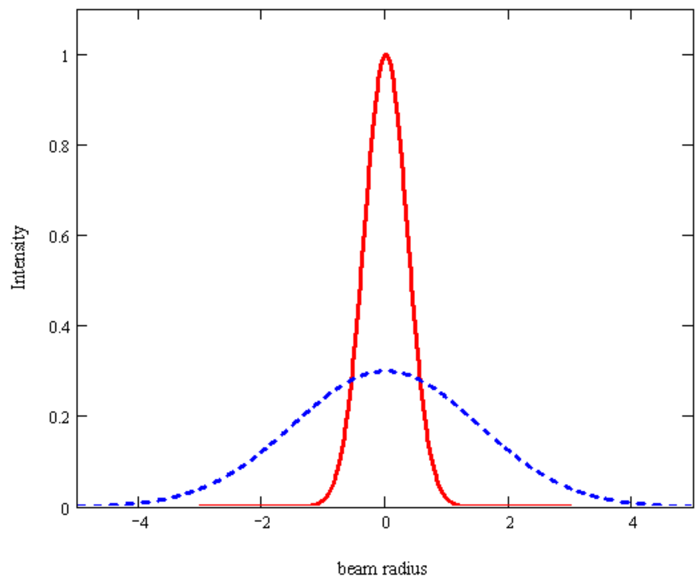

Figure 4-18 Normalized Gaussian intensity distribution[11].

The spot size of the beam is defined as the distance at which the beam intensity drops to $1/e^2$ of its peak value I_o. High absorption and scattering distorts the beam significantly and from a communication point of view this would decrease the signal to noise ratio ultimately falling below the minimum requirement for large link lengths. To present an example, front view images of the beam are analyzed as shown in Figure 4-19 (a) and (b). To increase the amount of scattering and absorption, solution of latex-acrylic paint was added to the tank of water. Volume of the latex-acrylic paint is denoted as χ ml [17]. Front view and side view images are taken using a digital camera equipped with a 8bit ADC. Further intensity profiles for the front view images were generated in an image editing software, ImageJ (1.36b). Qualitatively what can be seen is that the peak intensity of the beam decreases with the increase of paint concentration, this is due to the total attenuation of the beam. Paint particles cause the beam to scatter and spread during propagation through the medium.

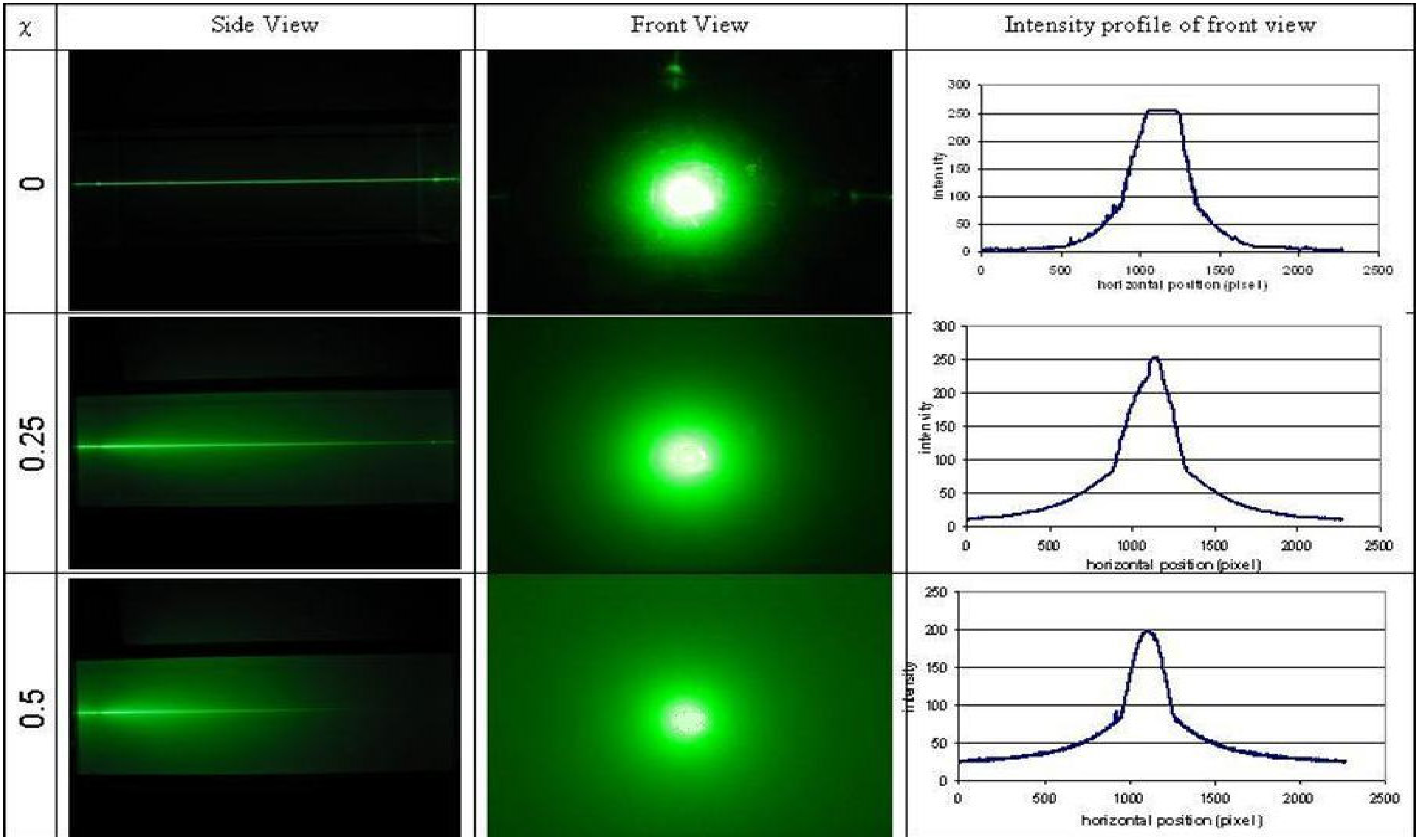

Figure 4-19(a) Side view and front view images of green laser beam spread for different latex-acrylic paint concentrations and the corresponding intensity profiles of the front view [17].

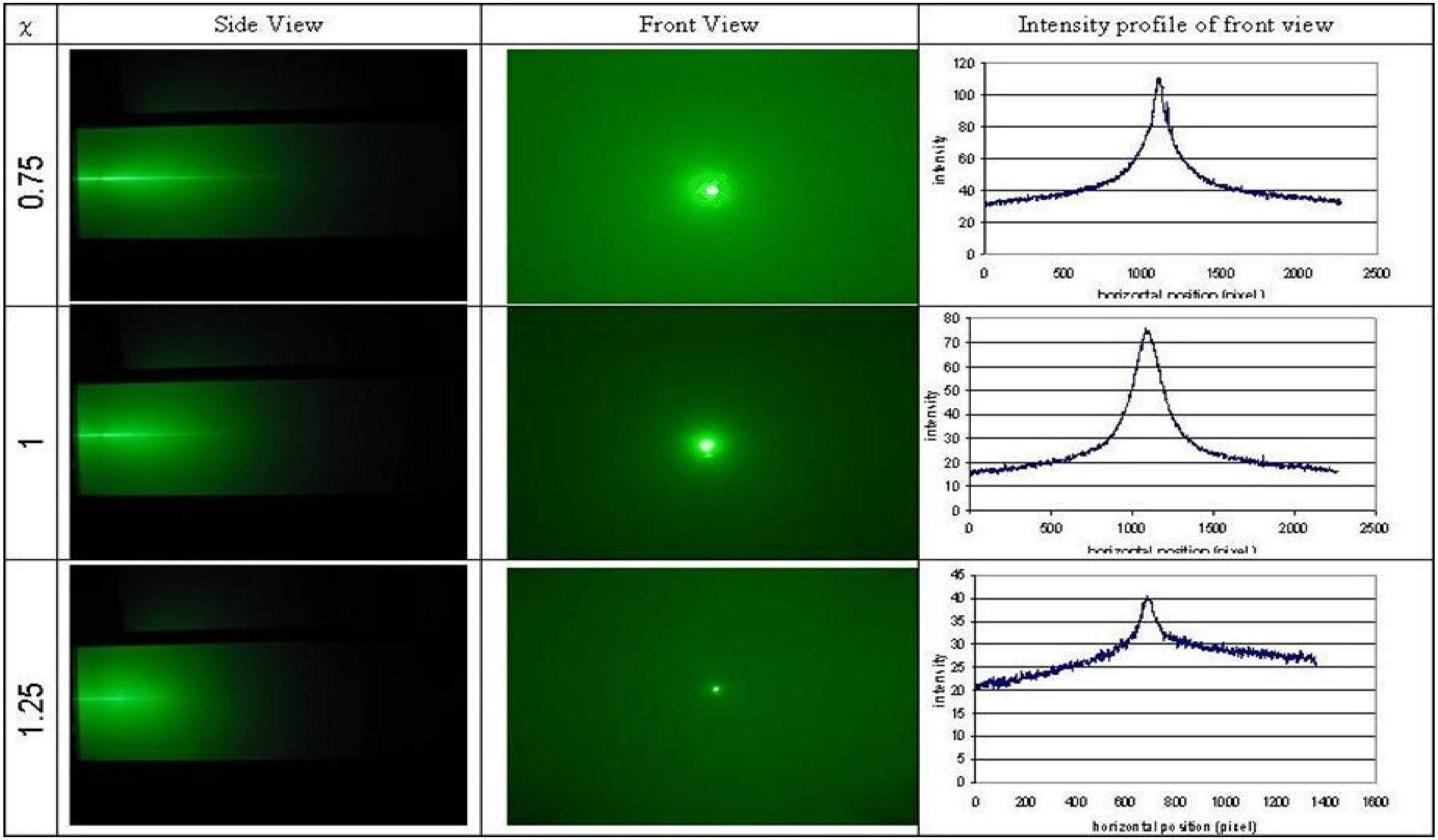

Figure 4-19(b) Side view and front view images of green laser beam spread for different latex- acrylic paint concentrations and the corresponding intensity profiles of the front view [17].

This gives us an insight into the beam dispersion, degradation in the spatial coherence and multipath time dispersion of the beam in the medium. From optical link standpoint, the multipath time spread is important, since it determines the maximum rate of communication [9]. Simulating each scenario using Monte Carlo method present fundamental difficulties, like defining the variables of the system accurately and sufficient computing power. Though Monte Carlo simulations have been used to support theories, but implementing it for all scenarios would be practically difficult. Hence, having an analytical model that would facilitate the evaluation of results would find great application in practical scenarios. Based on experimental results and *in situ* measurements we can extract useful information about the nature of scattering in a multiple scattering medium like ocean waters.

4.3 Beam Spread function

Beam spread function with time dispersion is an approach to quantify the contribution of scattering to the total attenuation of light [5]. This model relates the temporal spread of the light beam to the attenuation instead of the scattering coefficient itself. Each scattering event results in time delay, the average of multipath time delay is defined as the difference between the average transient time incurred from multiple scattering and the normal transient time in the absence of scattering. Since scattering can be treated as statically independent, the moments of multipath time dispersion can give a good idea of the scattering itself [4, 5].

The normalized radiative transfer equation can be presented as follows

$$k(z,\rho,s,\tau) = L(z,\rho,s,\tau)/Q \qquad \text{Equation 4.5}$$

where L(z,ρ,s,τ) is radiance as a function of distance z, position ρ, direction s, multipath time τ and Q is the energy.

Moments of the multipath time, displacement and directionality have been calculated with relation to scattering length (bz) [4]. The multipath time can be calculated using

$$\tau = (t - z/c) \qquad \text{Eq. 4.6}$$

c is the speed of light

z is the path length

The mean of the multipath time is found to be

$$\mu_\tau = 1/4\,(bz\langle\theta^2\rangle)(z/c) \qquad \text{Eq. 4.7}$$

Here b is the spectral scattering coefficient (b(λ)) of the medium.

$\langle\theta^2\rangle$ is the mean-square scattering angle

The variance of multipath time is found using

$$\sigma_\tau^2 = (z/c)^2\left[\left(1/12\right)bz\langle\theta^4\rangle + \left(1/24\right)(\mathrm{bz})^2\langle\theta^2\rangle^2\right] \qquad \text{Eq. 4.8}$$

Case 1 waters and parts of Case 2 waters observe forward scattering regime [1]. Our model assumes a characteristic scattering angle equal to 0.13 radians for calculations [5].

The analytical model suggests that the beam spread function with time dispersion is a product of a normalized temporal distribution function g(z,τ) and a normalized spatial-angular distribution function h(z,ρ,s,τ) [5].

$$k(z,\rho,s,\tau) = \exp(-act)\,g(z,\tau)\,h(z,\rho,s,\tau) \qquad \text{Eq. 4.9}$$

where a is the spectral absorption coefficient (a(λ)) of the medium. The temporal distribution function g(z,τ) is suggested to follow gamma distribution and is expressed as

$$g(z,\tau)=\frac{\mu_\tau}{{\sigma_\tau}^2\Gamma(\mu_\tau^2/\sigma_\tau^2)}\left(\frac{\mu_\tau\tau}{\sigma_\tau^2}\right)^{{\mu_\tau}^2/\,\sigma_\tau^2-1}\exp\left(-\frac{\mu_\tau\tau}{\sigma_\tau^2}\right) \qquad \text{Eq. 4.10}$$

where μ_τ and σ_τ are the mean and standard deviation of the multipath time dispersion obtained using Equation 4.7 and Equation 4.8

The normalized spatial-angular distribution is configured for a time dependent case as below

$$h(z,\rho,s,\tau)=\frac{3}{4\pi^2(c\tau)^2}\exp\left(-\frac{s^2-3s.\rho/z+3\rho^2/z^2}{\tau.c/z}\right) \qquad \text{Eq. 4.11}$$

If the average time t=$\langle\tau\rangle$ c/z is replaced by $\frac{1}{4}(bz\langle\theta^2\rangle)$ Equation 4.10 becomes time-independent. Equation 4.11 integrates over spatial and angular coordinates to yield Gaussian forms the enables the evaluation of the integrated beam spread function.

$$\int\ldots\int k(z,\rho,s,\tau)d\tau.d\rho.ds=\frac{\exp(-az)}{(1+ac\,\sigma_\tau^2/\mu_\tau)^{\mu_\tau^2/\sigma_\tau^2}} \qquad \text{Eq. 4.12}$$

Equation 4.12 can be treated as the total beam attenuation in the multiple scattering medium. The equation is fundamentally an exponential decay function proportional to the absorption coefficient of the medium and the denominator quantifies the additional attenuation associated with multipath time delay caused by scattering.

This model accounts for only scattered photons, while the probability of the unscattered photons decreases with increasing scattering lengths (bz). The integrated beam attenuation function can be directly used to determine the path loss between the source and receiver once the absorption and scattering coefficients are known. From an optical communication standpoint, it is important to know that this relation holds true for large field of view (FOV) receivers [18]

The beam attenuation given in Equation 4.12 and simulated by MathCAD** is shown in Figure 4-20. The simulation was done for a 1 W source operating at wavelength 532 nm. The beam attenuation versus depth is calculated for various chlorophyll concentrations. The spectral absorption and scattering coefficients are calculated using the one parameter model from Chapter 3.3 and 3.4.

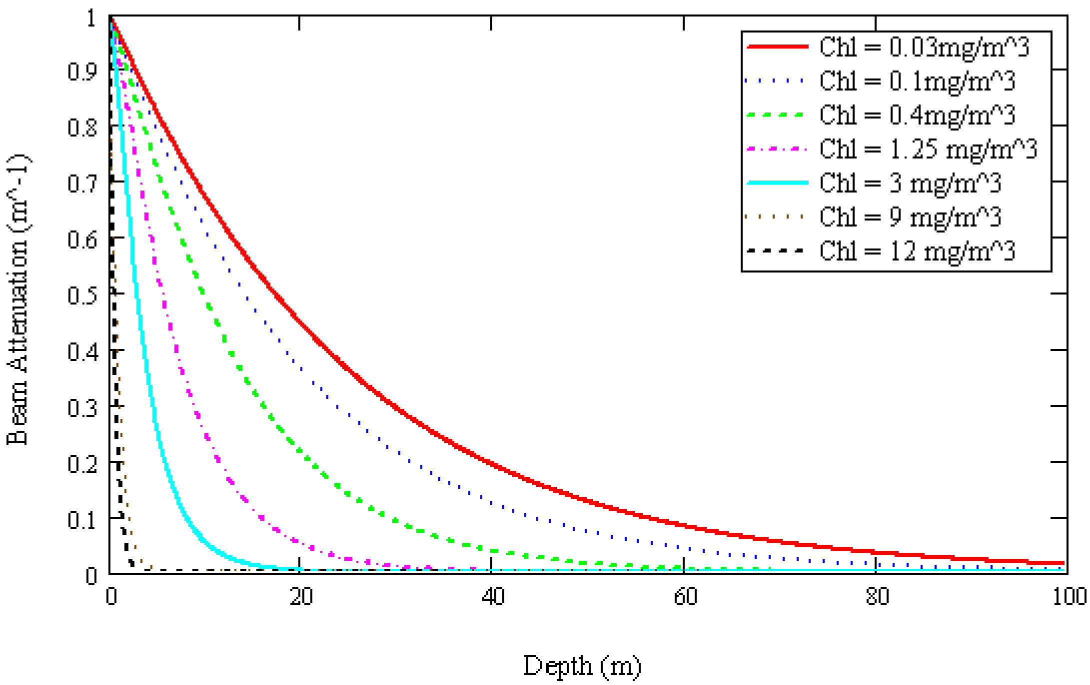

Figure 4-20 Beam attenuation vs. Depth for different chlorophyll concentrations using source operating at 532nm.

** Appendix A: MathCAD code

4.4 Spectral Attenuation

With the introduction of the complete attenuation model, it is worthwhile taking a second look at the beam attenuation k(λ) along the visible spectra. With the MathCAD model the wavelengths corresponding to minimum attenuation for various chlorophyll concentrations are found to shift to higher wavelengths and in shown Table 4-1

Table 4-1 Wavelengths corresponding to minimum attenuation for different chlorophyll-*a* concentrations

Jerlov Water Type	chlorophyll concentration (mg/m3)	wavelength of minimum attenuation (nm)
1	0.03	420
2	0.1	520
3	0.4	523
4	1.25	527
5	3	535
6	9	561
7	12	656

At higher concentrations of chlorophyll, the absorption by chlorophyll exceeds absorption by pure water. Also, scattering appears as a decreasing function of wavelength. The net effect brings about a shift in the wavelength corresponding to minimum attenuation, i.e. from the blue to the red region as seen in Figure 4-21 (a) and (b). It is thus concluded that the propagation medium determines the wavelength of the operation.

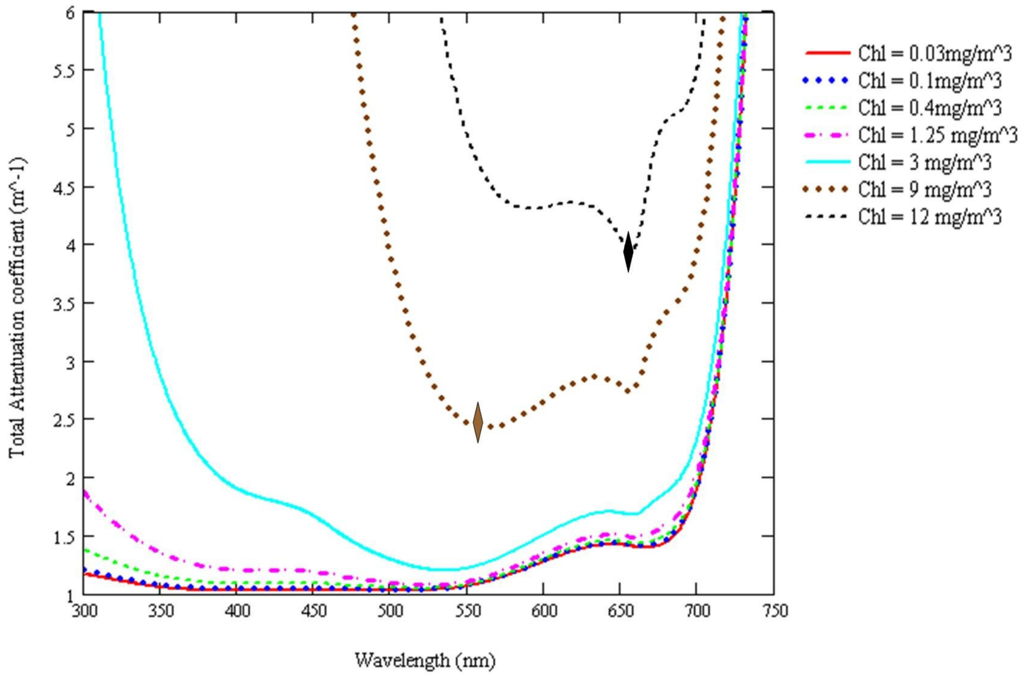

Figure 4-21(a) Wavelengths corresponding to minimum attenuation for different chlorophyll concentrations using MathCAD model.

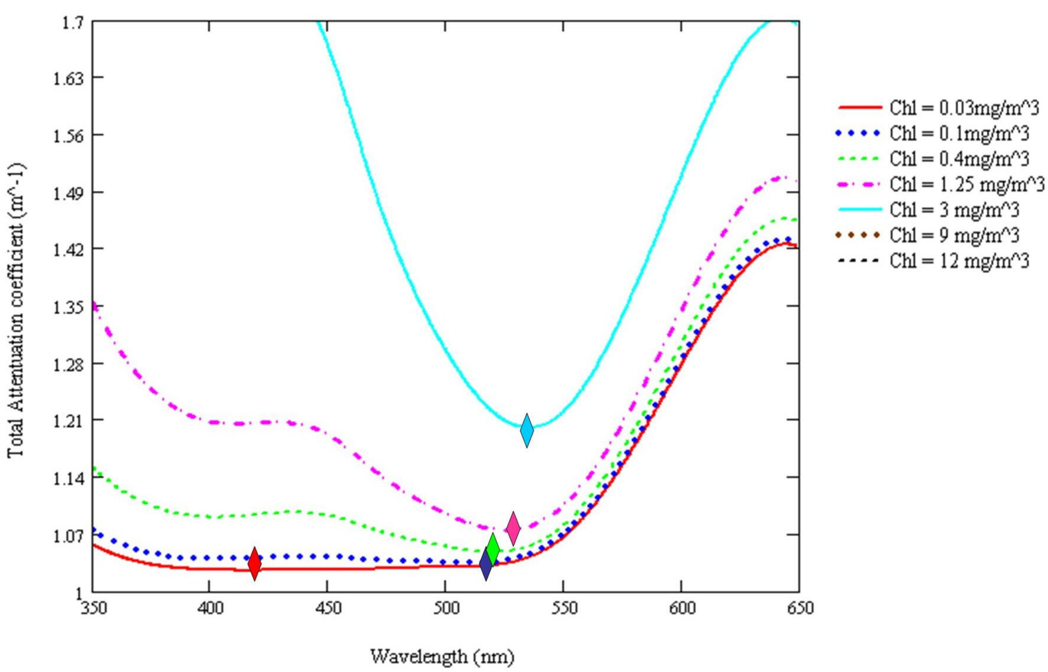

Figure 4-21(b) Wavelengths corresponding to minimum attenuation for different chlorophyll concentrations using MathCAD model (zoomed region 400nm-600nm).

4.5 Beer's law and beam spread function comparison

Traditionally the transmission losses between the source and receiver have been calculated using Beer's law [11, 12].

$$P_{Rx} = P_{Tx}.\exp^{-(c(\lambda).L)} \qquad \text{Eq. 4.13}$$

Where $c(\lambda)$ is the spectral attenuation coefficient and L is the distance between source and receiver. The spectral attenuation coefficient $c(\lambda)$ is the sum of the absorption coefficient and scattering coefficient [1, 2].

$$c(\lambda) = a(\lambda) + b(\lambda) \qquad \text{Eq. 4.14}$$

Equation 4.14 relates the attenuation directly proportional to the scattering coefficient. The beam spread function is not in agreement with this relation. A comparison is carried out between the beam spread function and Beer's law. For a given scenario of a 1 W source operating at 532 nm and receiver sensitivity of -30dBm, the maximum possible link length was calculated for the two approaches. These calculations were performed in MathCAD for different chlorophyll concentration. The maximum link lengths offered by the Beers law and the beam spread function are plotted in Figure 4-22. The difference between them with respect to the beam spread function is also shown in the figure.

The difference between the maximum link lengths offered by the beam spread function and Beer's law is greater than 70% for medium with chlorophyll concentration above 1.5 mg/m^3. In other words, Beer's law overestimates the attenuation when compared to the beam spread function. To corroborate this, a laboratory experiment was planned and is described in the next subsection.

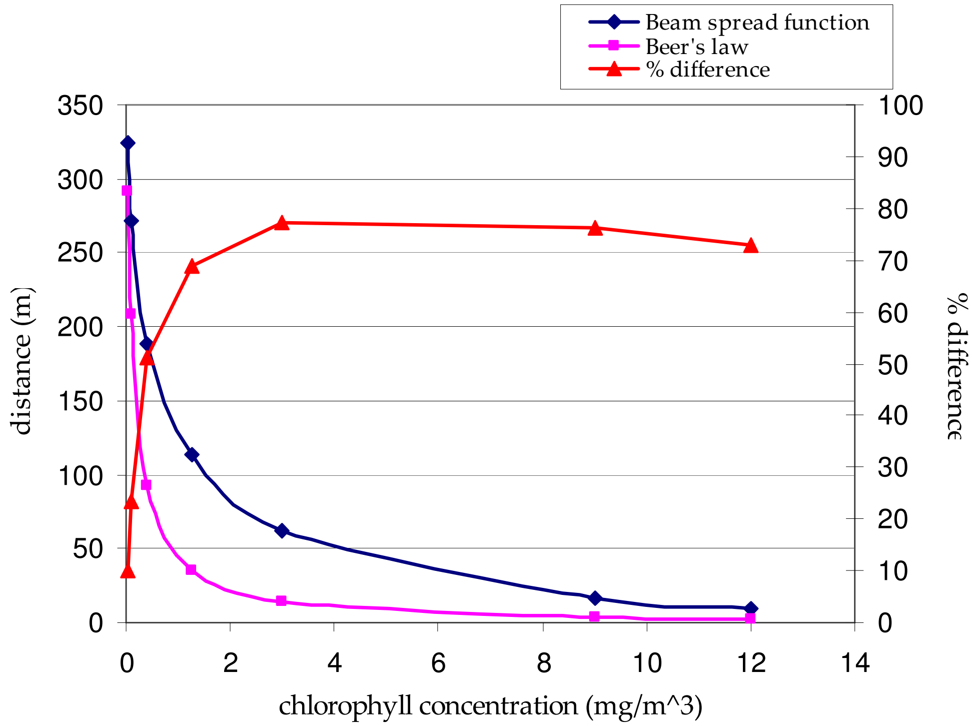

Figure 4-22 Percentage difference between Beer's law and beam spread function for different concentrations of chlorophyll calculated using MathCAD.

4.6 Seawater Experiment

4.6.1 Introduction

Experimental evidence should be important to corroborate the beam spread function as the beam attenuation. An experiment is conducted with a scattering medium like seawater and the additional attenuation caused by chlorophyll when compared to pure seawater is observed. A comparison between the calculated values given by Beer's law and beam spread function is necessary to support our claim.

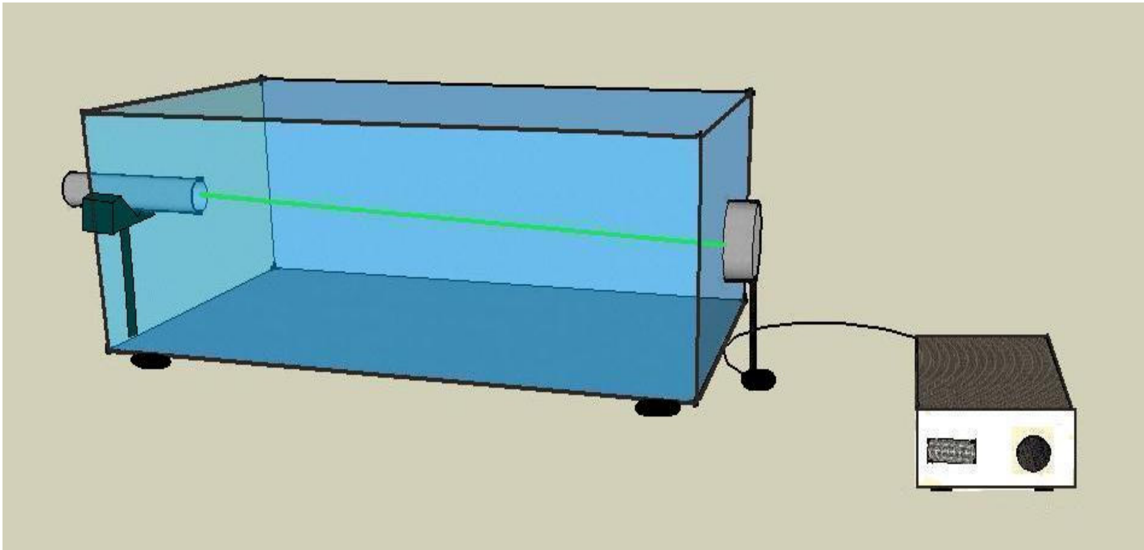

Figure 4-23: Experimental setup for measuring attenuation in seawater

4.6.2 Experimental Setup

As the source of attenuation seawater was filled in an isolated water tank of dimensions 1m x 0.4m x 0.3m. Two runs of direct power measurements were carried out to exhibit attenuation by pure sea water and by chlorophyll added to sea water.
Two light sources: Green Laser (<5mW) and Red He-Ne Laser (1mW) were used for the experiment. The received radiant power is measured using a broadband power meter as depicted in the Figure 4-23 [13, 14].

4.6.3 Observations and Results

Power measurements for the pure seawater and chlorophyll added to seawater were taken using both sources. The average size of phytoplankton added to water was 17.3 µm. The concentration of phytoplankton in seawater was measured as 6.2 mg/m^3, which predominantly contained chlorophyll-*a*. The average no of phytoplankton cells in the medium were 12060 cells/ml with majority of the particles in the size range of <5µm.

Simulations are carried out for the exact values of the two scenarios neglecting any gains or losses.

Table 4-2 Measured received power of green laser (532nm) propagating through seawater and the corresponding calculated values using the beam spread function and Beer's law

Observed Values	seawater with no chlorophyll	seawater with 6.2 mg/m^3 chlorophyll
Transmitted Power (in water)	3.17 mW	3.17 mW
Received Power	2.14 mW	1.767 mW
Calculated values		
Beam spread function Eqn. 4.11	2.445 mW	1.996 mW
Beer's Law, PRx=Ptx.exp{-$\alpha(\lambda)$z}; $\alpha(\lambda)$=a(λ)+b(λ)	2.44 mW	0.2852 mW

Table 4-3 Measured received power of red laser(633nm) propagating through seawater and the corresponding calculated values using the beam spread function and Beer's law

Observed Values	Seawater with no chlorophyll	Seawater with 6.2 mg/m3 chlorophyll
Transmitted Power (in water)	0.55 mW	0.55 mW
Received Power	0.31 mW	0.2457 mW
Calculated values		
Beam spread function Eqn. 4.11	0.3123 mW	0.2992 mW
Beer's Law, PRx=Ptx.exp{-$\alpha(\lambda)$z}; $\alpha(\lambda)$=a(λ)+b(λ)	0.312 mW	0.04895 mW

The simulated results obtained from the beam spread function model using MathCAD model are in close agreement with the experimental ("observed") results as shown in the tables 4-2 and 4-3. Difference between the two can be attributed to the losses due to receiver efficiency, space between the glass surface and the photodetector.

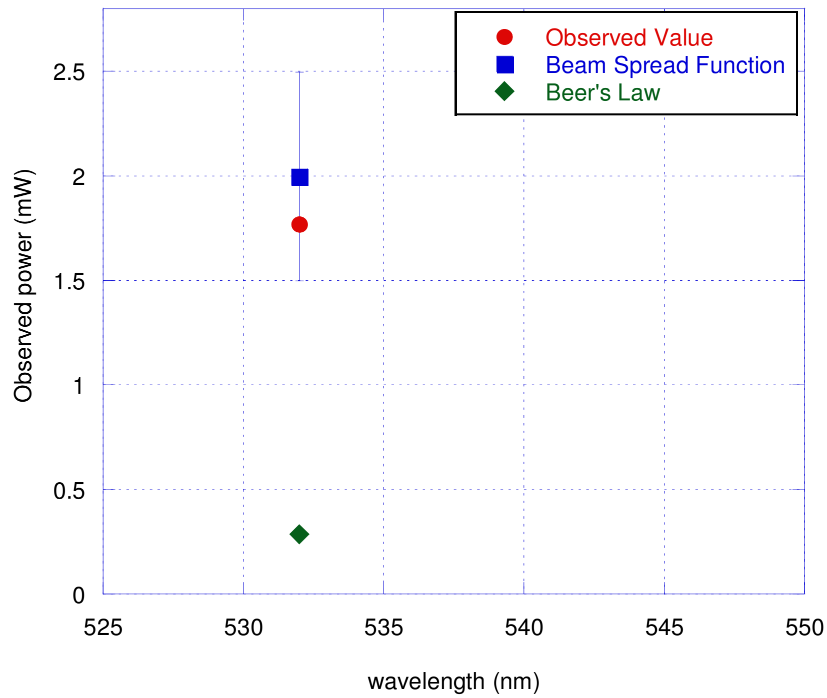

Figure 4-24 (a) Comparison between the observed values and calculated values of beam attenuation for green laser (<5 mW)

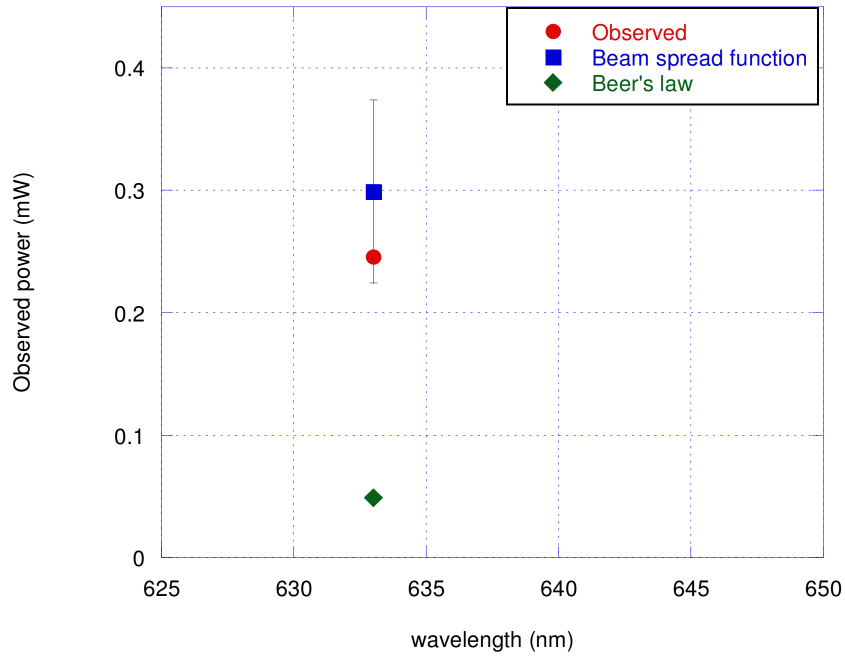

Figure 4-24 (b) Comparison between the observed values and calculated values of beam attenuation for red laser (1 mW)

Overall, the observed values of the received power falls within 25% error margin of the calculated received power from the beam spread function model for both the green laser and red laser as seen in Figure 4-24. The received power calculated using Beer's law is over 80% lower than the observed values of the received power. We conclude that the figures for attenuation obtained by Beer's law are an over-estimate of the actual attenuation.

4.6 Link equation using beam spread function

Power budget analysis are always useful to determine the maximum possible link length for a given receiver sensitivity. Using MathCAD simulations, the maximum link lengths available are calculated for 1 W and 100 mW sources. The minimum received sensitivity is assumed to be 10^{-6} W or -30 dBm. The equation that is used to compute the received power is as

$$P_{Rx}(\lambda, z) = P_{Tx}.k(\lambda, z) \qquad \text{Eq. 4.15}$$

This example does not consider any losses or gains from the system components. Graphs for Equation 4.15 are plotted for different chlorophyll concentrations.

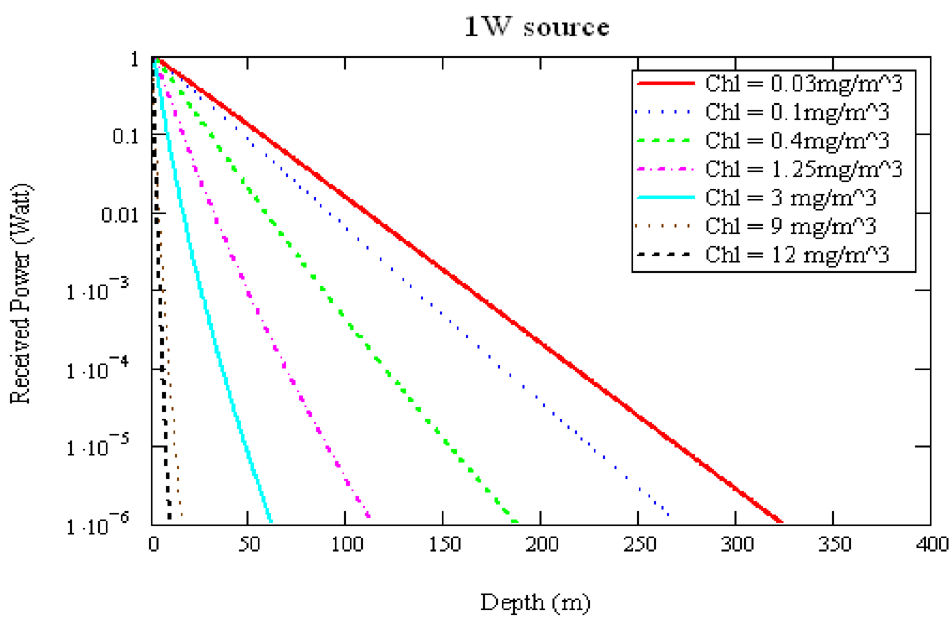

Figure 4-25 Received power calculated using beam spread function for different concentrations of chlorophyll with 1 W source.

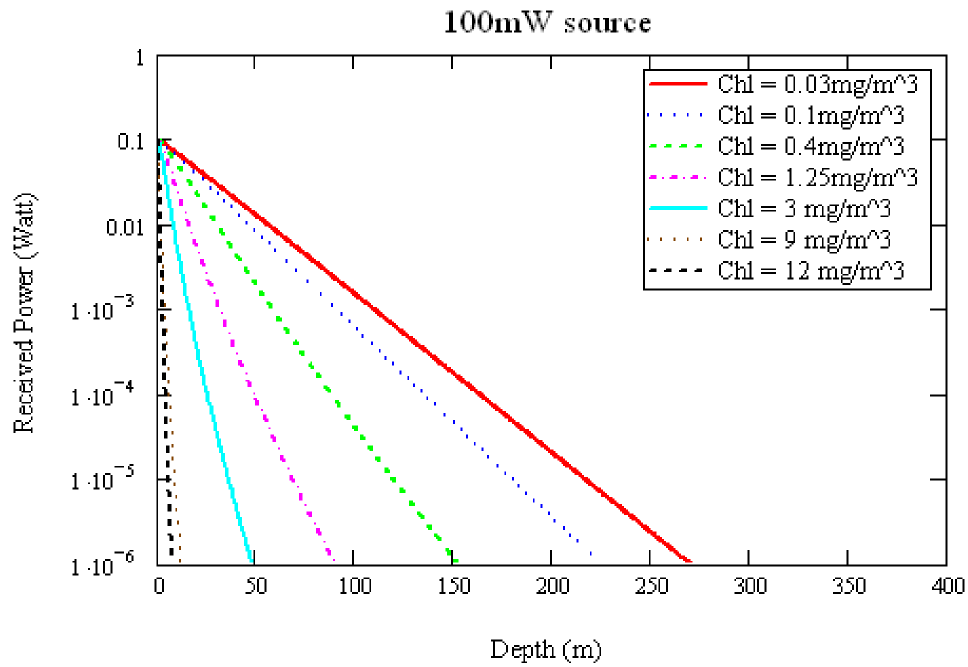

Figure 4-26 Received power calculated using beam spread function for different concentrations of chlorophyll with 100 mW source.

4.7 Link budget examples

From the available *in situ* measured chlorophyll concentration for waters around Galapagos islands, the vertical variations are observed [20]. In order to reconstruct the vertical profiles from the five parameter model [19], the variables of the model are adjusted to fit each of the three distribution profiles. Our aim is to calculate the link budgets for each of the regions. After reconstruction of the vertical profiles, we incorporate the variables in the MathCAD model and calculate the average chlorophyll concentration between the receiver and source. We consider four cases to calculate the effective average chlorophyll concentration and further what is the maximum available link lengths possible using the Equation 4.11.

Transmit optical power is assumed as a 100mW source operating at 532nm wavelength and the receiver sensitivity is -30dBm.

Table 4-4 System parameters considered for calculating link budget

Optical Power	20 dBm
Receiver Sensitivity	-30 dBm
Available Power	50 dB

The corresponding maximum available link lengths are calculated for the following four cases

Case 1: Average chlorophyll calculated along the vertical depth of the water column.

Case 2: Average chlorophyll calculated along an inclined path (45°) from the vertical.

Case 3: Maximum chlorophyll concentration corresponding to the horizontal max

Case 4: Minimum chlorophyll concentration corresponding to the horizontal min

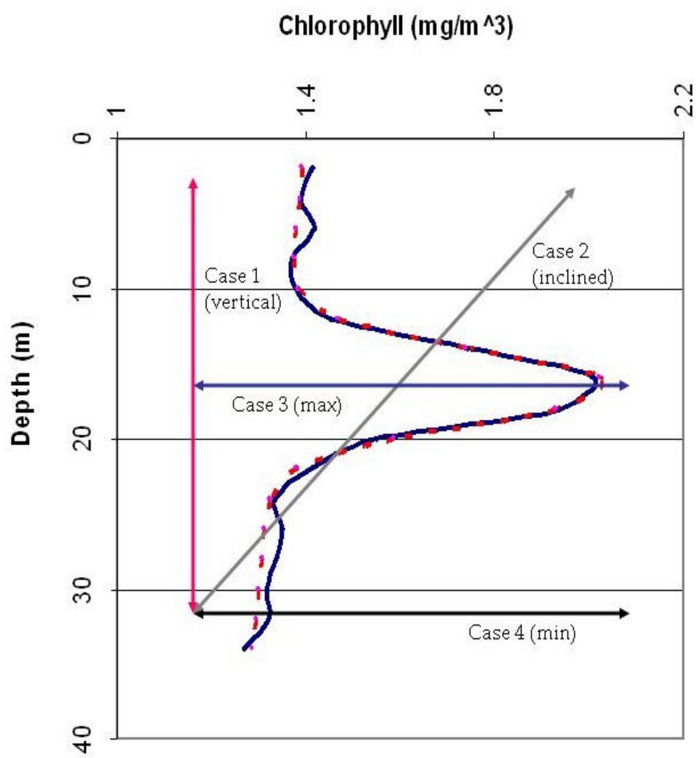

Figure 4-27 Four cases considered for link budget calculations

Region 1: The three vertical distribution profiles are as shown in the Figures below. The variable of the equation 4.16 are obtained for each profile.

$$Chl(z) = B_o + S \times Z + \frac{h}{\sigma\sqrt{2\pi}} \exp\left[-\frac{(Z - Z_{\max})^2}{2\sigma^2} \right] \qquad \text{Eq. 4.16}$$

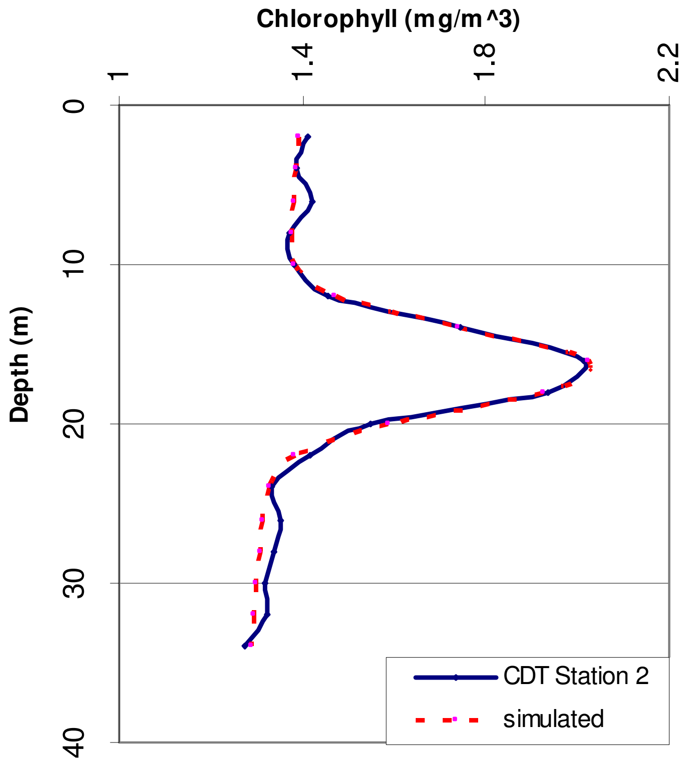

Figure 4-28 Vertical chlorophyll distribution and five parameter curve fit for region 1.

The value of the variables of the model obtained for this case are given in Table 4-5

Table 4-5 Five parameters to define the vertical chlorophyll profile of region 1

Bo	1.4
Z_{max}	16.6
h	4.19
σ	2.4
S	$-3.316 * 10^{-3}$

Maximum available link length and the loss for each of afore mentioned cases are calculated.

Table 4-6 Chlorophyll concentrations and corresponding maximum available length calculated from MathCAD model for region 1

	Chlorophyll concentration (mg/m³)	Loss dB/m	Maximum length (m)
Case 1 (vertical)	1.467	0.38	131
Case 2 (inclined)	2.063	0.47	106
Case 3 (horizontal max)	2.22	0.48	104
Case 4 (horizontal min)	1.287	0.35	141

<u>Region 2:</u>

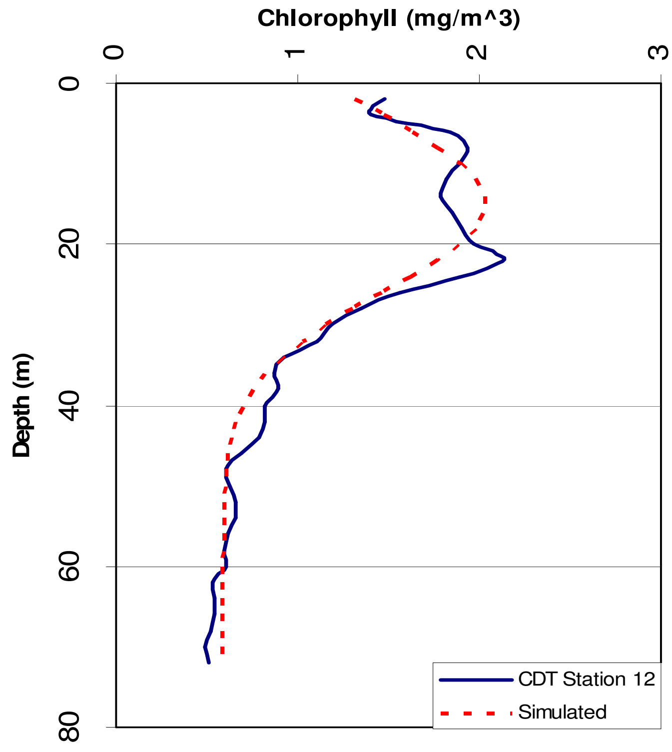

Figure 4-29 Vertical chlorophyll distribution and five parameter curve fit for region 2.

Table 4-7 Five parameters to define the vertical chlorophyll profile of region 2

Bo	0.61
Z_{max}	15
h	39
σ	10.9
S	-37.24

Maximum link lengths and loss for the above chlorophyll distribution profiles are calculated for each of the cases.

Table 4-8 Chlorophyll concentrations and corresponding maximum available length calculated from MathCAD model for region 2

	Chlorophyll concentration (mg/m^3)	Loss dB/m	Maximum length (m)
Case 1 (vertical)	1.094	0.32	152
Case 2 (inclined)	1.539	0.39	128
Case 3 (horizontal max)	2.027	0.46	108
Case 4 (horizontal min)	0.492	0.24	206

Region 3:

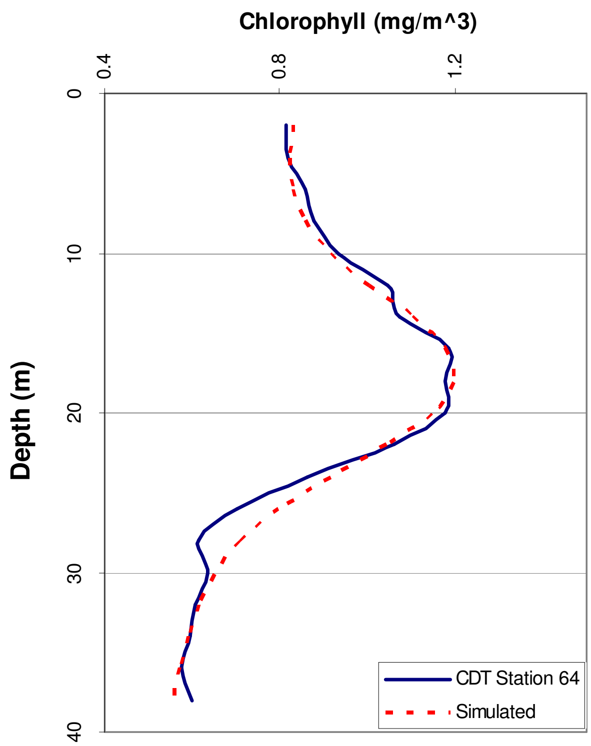

Figure 4-30 Vertical chlorophyll distribution and five parameter curve fit for region 2.

Table 4-7 Five parameters to define the vertical chlorophyll profile of region 3

Bo	0.84
Z_{max}	18
h	6.4
σ	5.2
S	$-7.458*10^{-3}$

The maximum available link lengths and the loss (dB/m) are calculated from the MathCAD model and are shown below.

Table 4-10 Chlorophyll concentrations and corresponding maximum available length calculated from MathCAD model for region 3

	Chlorophyll concentration (mg/m^3)	Loss dB/m	Maximum length (m)
Case 1 (vertical)	0.867	0.29	169
Case 2 (inclined)	1.219	0.34	145
Case 3 (horizontal max)	1.842	0.43	115
Case 4 (horizontal min)	0.576	0.254	195

Based on the above calculated results, the performance of the system is largely influenced by the region of operation within the vertical distribution profile. One can suggest that the optical power should be adaptively adjusted during the operation for successful reception.

4.8 Graphical User Interface

A graphical user interface (GUI) is developed using Visual Basic® for computation of parameter of the link equation (Equation 4.15). The interface designed is characterized by its ease of operation as compared to using the MathCAD program itself.

The GUI is linked to MathCAD that is operational in the background. The input variables assigned by the user are transferred to the MathCAD routine and the results are fed back to the program. Simple modifications to the program can be made to achieve results for different unknowns' of a link equation, *viz.* maximum available link length, minimum transmit power required, received power at a specific link length etc.

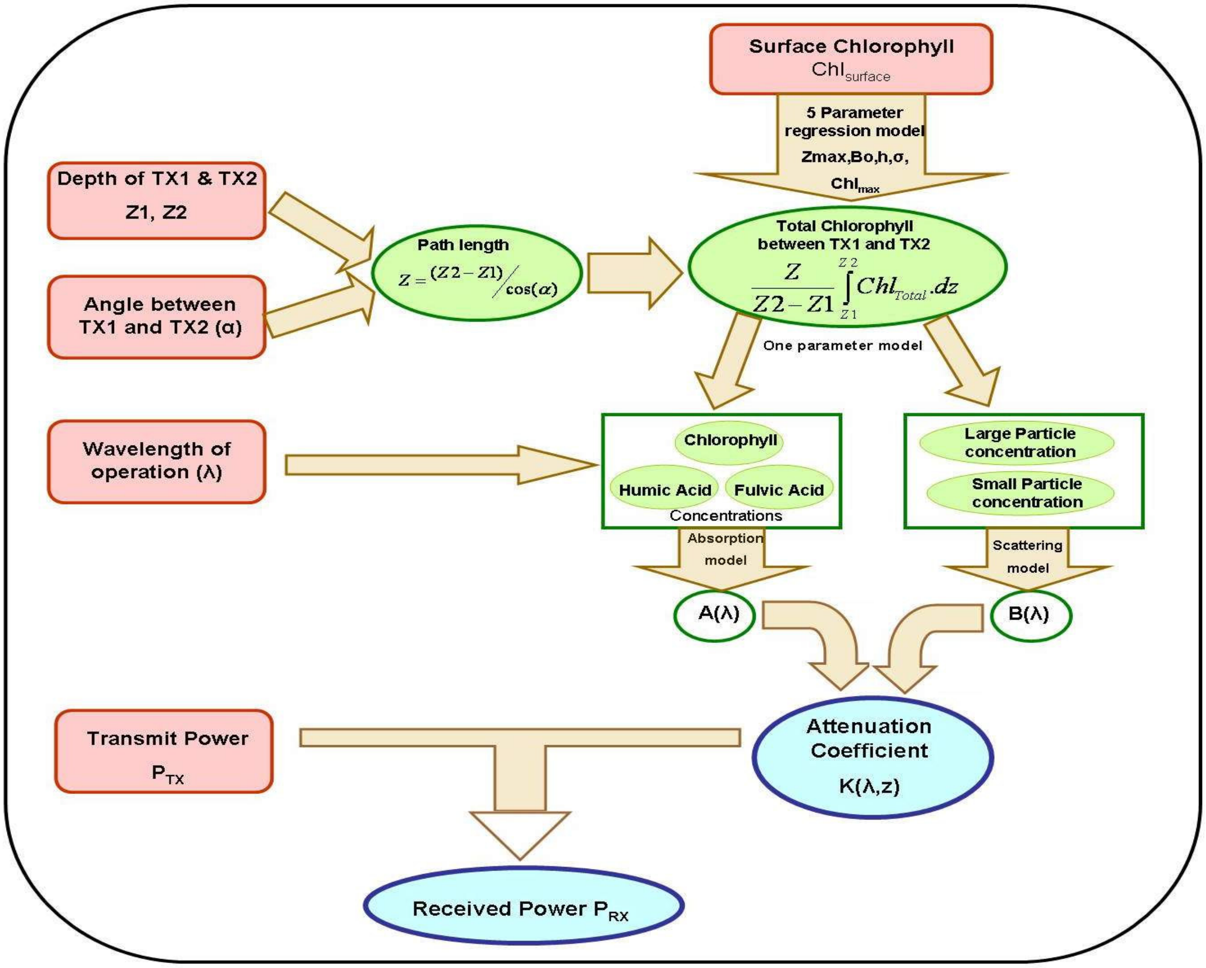

Figure 4-31 Block diagram to calculate beam attenuation and the received power

The approach adopted for our GUI is represented in Figure 4-31. The user is expected to enter 3 sets of inputs to completely define the underwater optical link. Source power and wavelength of operation are the variables available for the transmitter. To define the medium of propagation the Surface Chlorophyll is the known parameter. Using the five parameter model defined in Section 3.4.2 the regression relations between the surface chlorophyll and the other parameters (*viz*. background chlorophyll, standard deviation, depth of chlorophyll peak, width of chlorophyll peak and maximum chlorophyll content) should be known to construct the vertical distribution profile of chlorophyll [15]. Further the chlorophyll is used to calculate the absorption coefficient and scattering coefficient [16].

Finally the positions of the transmitter and receiver are used to determine the total link length. Depth of the two nodes from the surface and the angle of the path with respect to the vertical are to be known. The MathCAD model[††] calculates the attenuation and received power of the link defined by the input parameters, which are displayed on the right hand side of the screen as shown in Figure 4-32.

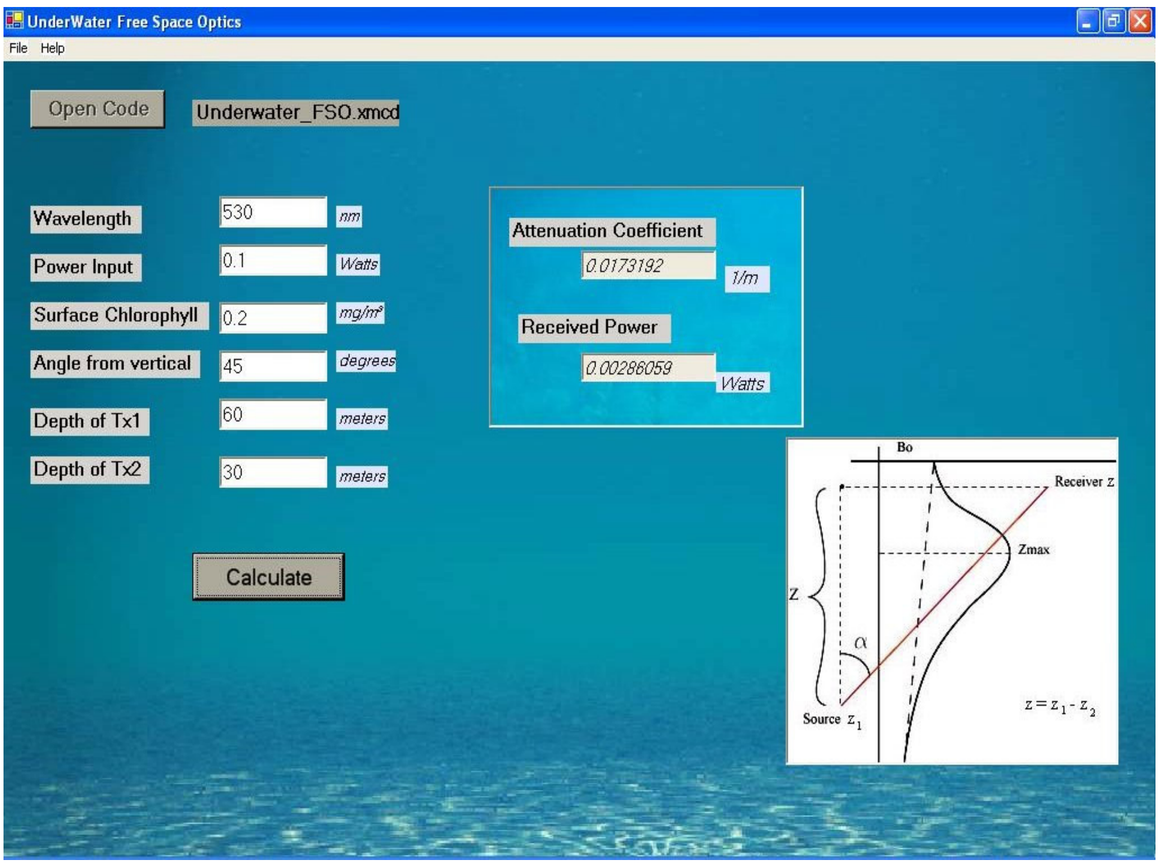

Figure 4-32 Graphical user interface to calculate the link equation

[††] Appendix A: MathCAD code

4.8 References:

[1] C. D. Mobley, *Light and Water- Radiative Transfer in Natural Waters.* California: Academic Press Inc., 1994, pp.60-144; 300-303; 487-488.

[2] R. E. Walker, *Marine Light Field Statistics.* New York: John Wiley & Sons Inc., 1994, pp.142-162; 168-172.

[3] V. I. Haltrin and G. W. Kattawar, "Effects of Raman Scattering and Fluorescence Apparent Optical Properties of Sea Water," *Texas A&M University,* 1991.

[4] R. F. Lutomirski, A. P. Ciervo and G. J. Hall, "Moments of multiple scattering," *Applied Optics,* vol. 34, 1995.

[5] J. W. McLean, J. D. Freeman and R. E. Walker, "Beam spread function with time dispersion," *Applied Optics,* vol. 37, 1998.

[6] L. B. Stotts, "Closed form expression for optical pulse broadening in multiple scattering media," *Applied Optics,* vol. 17, 1978.

[7] S. Premože, M. Ashikhmin, J. Tessendorf, R. Ramamorrthi and S. Nayar, "Practical rendering of multiple scattering effects in participating media," in *Eurographic Symposium on Rendering,* 2004,

[8] *Liquid Maalox*®. Parsippany NJ-07054-0622 ©2005: Novartis Consumer Health Inc.,

[9] Edward A. Bucher, "Computer simulation of light pulse propagation for communication through thick clouds", *Applied Optics, Vol. 12, 10, 1973*

[10] A. Laux, R. Billmers, l. Mullens, B. Concannons, J. Davis, J. Prentice and V. Contarino, "The a,b,cs of oceanographic lidar predictions: a significant step forward towards closing the loop between theory and experiment." *Journal of Modern Optics, Vol.49, No.3/4, 2002*

[11] J. C. Palais, *Fiber Optic Communication.* ,5th ed. New Jersey: Pearson Prentice Hall, 2005, pp. 40-61.

[12] I. I. Kim, B. McArthur and E. Korevaar. Comparison of laser beam propagation at 785nm and 1550nm in fog and haze for optical wireless communication. Available: http://www.systemsupportsolutions.com/WhitePapers/

[13] *Model 1815-C Optical Power Meter.* Newport Corporation,

[14] *Self Contained (1500 Series) He-Ne Laser (1mW).* JDS Uniphase Corporation,

[15] T. Kameda and S. Matsumara, "Chlorophyll Biomass off Sanriku, Northwestern Pacific, Estimated by Ocean Color and Temperature Scanner (OCTS) and a Vertical Distribution Model," *Journal of Oceanography,* vol. 54, pp. 509-516, 1998.

[16] V. I. Haltrin, "Chlorophyll-based model of seawater optical properties," *Applied Optics,* vol. 38, 1999.

[17] *Painter's Touch® Multi-Purpose Latex Paint (Flat White):* 11 Hawthorn Pkway, Vermon Hills, IL 60061: Rust-Oleum® Corporation.

[18] J. W. McLean and R. E. Walker, "Lidar equations for turbid media with pulse stretching," *Applied Optics,* vol. 38, 1999.

[19] T. Kameda and S. Matsumara, "Chlorophyll Biomass off Sanriku, Northwestern Pacific, Estimated by Ocean Color and Temperature Scanner (OCTS) and a Vertical Distribution Model," *Journal of Oceanography,* vol. 54, pp. 509-516, 1998.

[20] D. Kamykowski, "Galapagos Archipelago Cruise Expedition," North Carolina State University, 2005.

Chapter 5 LINK BUDGET

5.1 Geometric Loss

The beam attenuation model presented in chapter 4 is independent of the type of source used. It is purely estimates the loss of signal intensity. However in practice the source and receiver apertures are finite which enforces limitations on the received beam spot size. In cases such as a LED source, where the beam full angle divergence is of the order of tens of milli radians, the beam spreading is much larger than the receiver aperture. The signal power not captured by the receiver is considered as Geometric loss. Illustration of this scenario is as shown in Figure 5-1. For longer link ranges the large spot size is a serious concern. Geometric loss is a function of the path length, aperture sizes of the transmitter and receiver aperture [1].

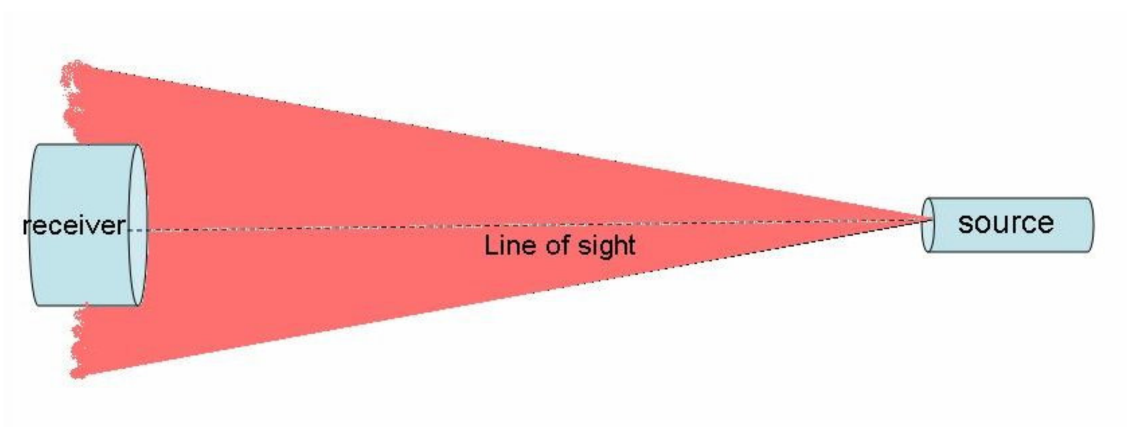

Figure 5-1 Diagram showing the larger spot than the field of view of the detector.

$$GL(Range) = \left\{ \frac{D_{RX}}{D_{TX} + (Range \times DivAngle)} \right\}^2 \qquad \text{Equation 5.1}$$

where D_{RX} and D_{TX} are the aperture diameters (m) of the receiver and transmitters respectively. The range of the link is expressed in km while the divergence angle is in mrad.

With the beam divergence angle and the aperture size of the transmitter and receiver as constant, the range of the link is the only variable that influences geometric loss. For directional links where the long link ranges are sought, using large receiver apertures and sources with small divergence angles is the best way to mitigate the geometric losses. The spot diameter v/s. link length for sources with beam divergence angles of 1.6 mrad, 3 mrad, and 5 mrad are calculated.

$$diameter_{Spot} = 2 \times Dist \times \tan(\tfrac{1}{2}\theta_{divergence}) \qquad \text{Equation 5.2}$$

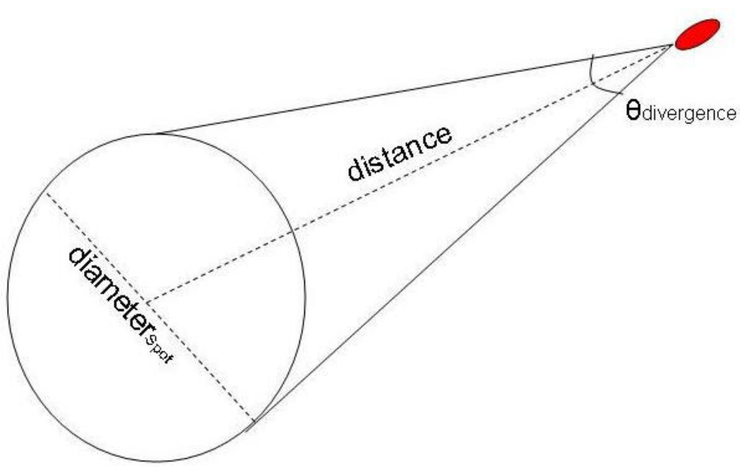

Figure 5-2 Geometry used to calculate the diameter of the spot size v/s. distance.

The beam full angle of divergence can be calculated from the wavelength of operation (λ) and the near field spot radius (w) [2].

$$\theta_{divergence} = \frac{2\lambda}{\pi w} \qquad \text{Eq. 5.3}$$

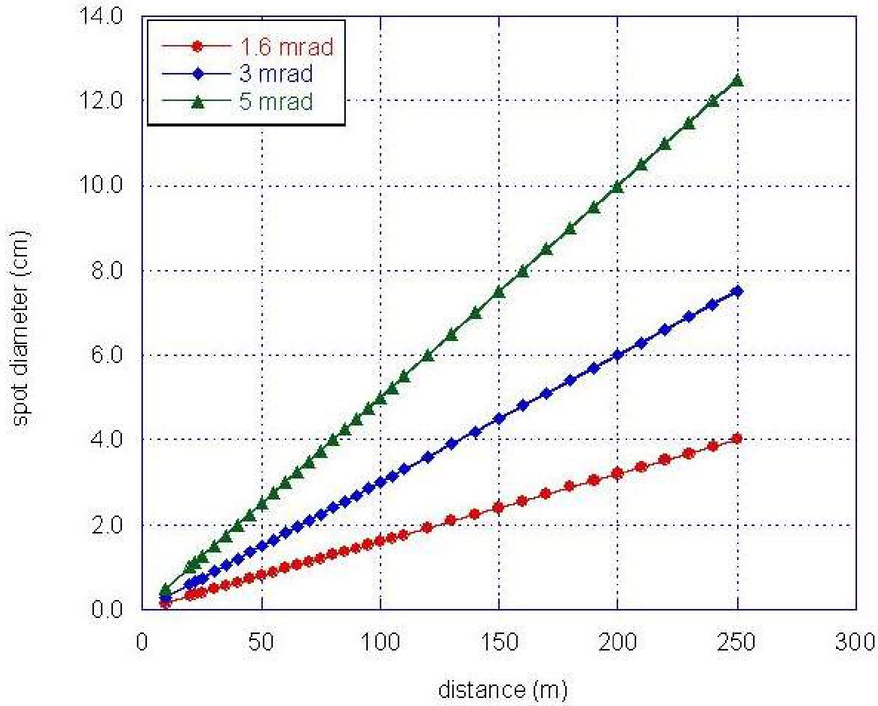

Figure 5-3 Spot sizes v/s. link range for lasers with divergence angles 1.6mrad, 3mrad and 5mrad.

The modified equation for a perfectly aligned optical link that includes the geometric loss can be stated as Equation 5.4.

$$P_{Rx}(\lambda, z) = P_{Tx} \cdot k(\lambda, z) \cdot GL(z) \qquad \text{Eq. 5.4}$$

where λ is the operating wavelength of the source and z is the link range.

In multiple scattering medium like ocean waters, scattering can have cascading effects on the geometric loss as well. Monte Carlo calculations for multiple scattering events could be useful to simulate these effects; however this is not included in this work. Scattering effects are ignored for the above calculations. The geometric losses increase exponentially with the link distance. Larger beam divergence angles for sources such as LEDs the possible link distances are much lower.

5.2 Optical Link Budget

In the process of engineering an optical link, it is important to gather accurate information about the losses that the optical signal undergoes between the source and receiver. The key building blocks of an optical link equation are analogous to that of a microwave point to point link which involves variable like free space loss, isotropic antenna gain, receiver sensitivity etc.. However the ultimate goal remains in determining the maximum possible link length for a given transmit power. Bandwidth and Power budgets are usual practices employed in designing an optical communication link. Power budget analyses establish a reliable signal to noise ratio for required Bit Error Rate performance. Power Budget is simply stated as the total received power (dB) which is the difference between the transmitted power (dB) and sum of all the losses (dB).

A link equation accounts for all of the gains and losses from the transmitter, through the medium to the receiver in a telecommunication system. The general link equation is:

$$P_{Rx} = P_{Tx} \cdot Gain_{Tx} \cdot Loss_{Transmitter} \cdot Loss_{Path.}\ Loss_{Rx} \cdot Gain_{Rx} \qquad \text{Eq. 5.5}$$

The gain and loss terms are usually expressed in decibels to facilitate computation of the received power.

5.2.1 Building an Underwater Optical Link Budget

A typical wireless optical system would include a semiconductor light source with collimating optics and a photoreceiver with focusing lenses. The losses for the water medium are calculated using the Beam Spread Function model. Detailed understanding of the other elements in Equation 5.5 is presented below.

Starting with the transmit source power, available power and costs determine choice of the appropriate source. Light Emitting Diodes (LED) and Laser Diode (LD) are common light sources used in optical communications. Additional information about the source are important in the selection process like wavelength of operation, pulsewidth, divergence angle, peak power etc [3, 4].

Transmitter losses are the multiplicative losses observed at each the optical surface of the telescope. The quality of the optical energy out of the telescope can be improved by using good design techniques and superior optical coatings [1]. The optical components of the telescope or the optical antenna are responsible for an effective isotropic transmit gain. They are the efficiencies of directing power into a beam as compared to an isotropic radiator. The far-field optical antenna gain is calculated using the relation in Equation 5.6 [5].

$$\text{Gain}_{\text{Tx}}(dB) = 10\log_{10}\left(\frac{2\pi a}{\lambda}\right)^2 \qquad \text{Eq. 5.6}$$

where a is the radius of the source aperture radius.

Operating at smaller wavelengths, optical antennas offer higher directional gains as compared to RF or Microwave antennas. However with small beamwidths and divergence angles they require better pointing and tracking techniques. We have not considered the optical antenna gain factor for our MathCAD simulations and strictly observe these gains as, relative to isotropic antennas.

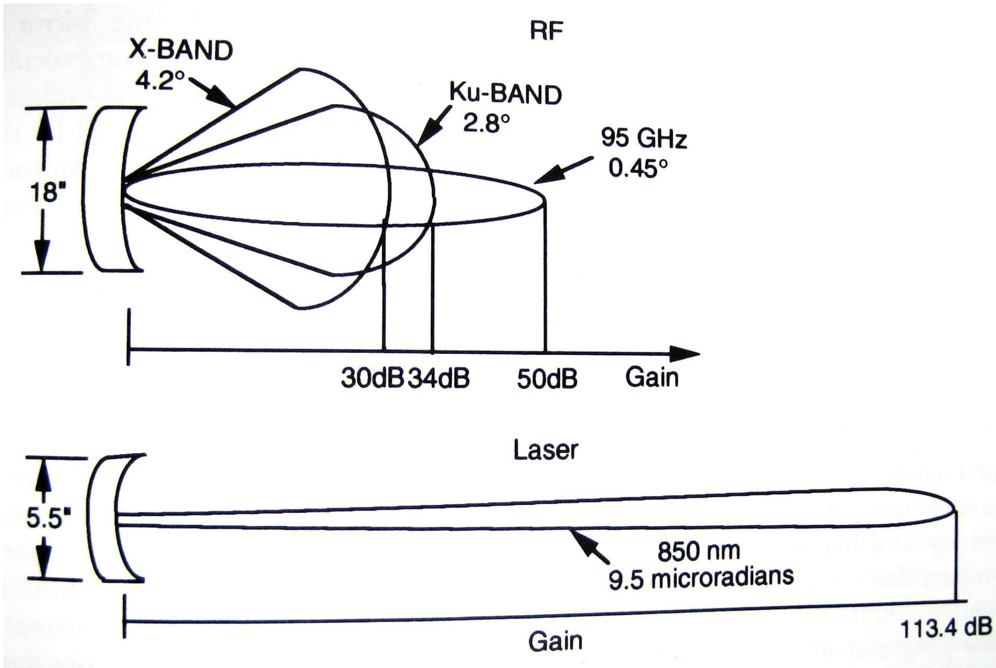

Figure 5-4 Beam Divergence and Antenna Gain comparison [3].

The Pathloss component of the Equation 5.5 is the total signal attenuation between the transmitter and receiver. The beam spread function with time dispersion model presented represents the attenuation offered by the natural waters in its entirety. For an unfixed optical link the medium of propagation is biggest unknown and a major source of signal degradation. The beam spread function offers a simple solution to this problem.

Finally, a photoreceiver either PIN diode or APD (Avalanche Photo diode) along with the focusing lens form the receiver part of the system. Akin to the transmitter gain, the optical elements of the receiver offer directional gain and wavefront losses. The receiver optical antenna gain is calculated using [6].

$$\text{Gain}_{\text{Rx}}(dB) = 10\log_{10}\left(\frac{2\pi a}{\lambda}\right)^2 \qquad \text{Eq. 5.7}$$

where a is the radius of the antenna aperture radius.

Link Margin is observed in calculating the power budget, and is the margin set above the minimum receiver sensitivity to ensure reliability of the link under any circumstances. Overall a comprehensive knowledge of each component of the system improves the accuracy of calculating the power budget.

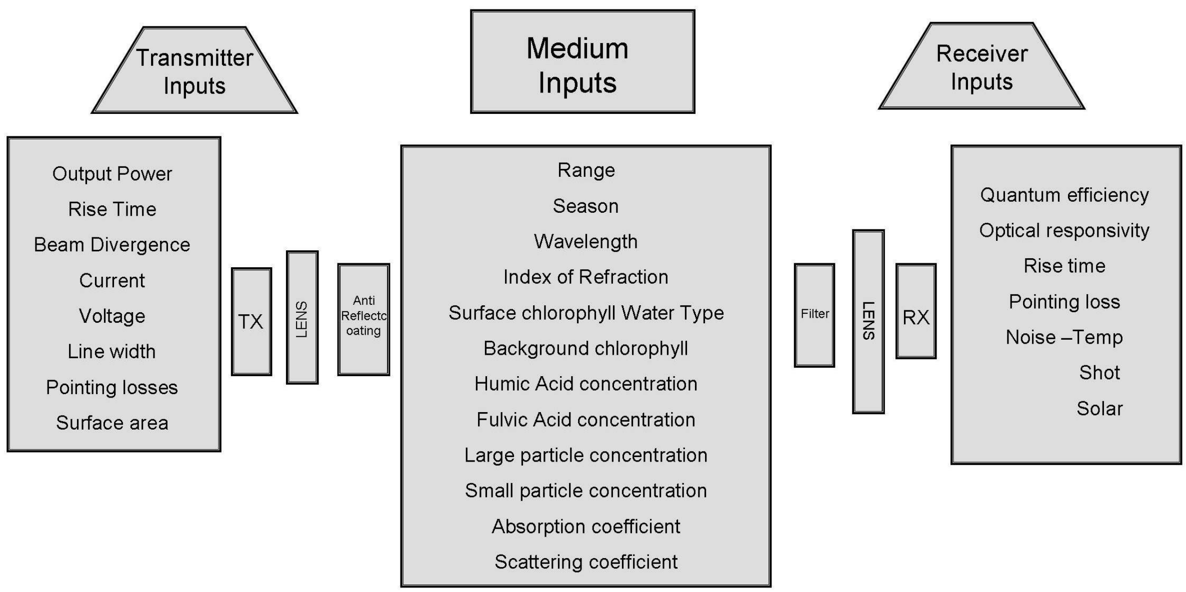

Figure 5-5 Block Diagram summarizing all the variable needing consideration in the link budget [7].

5.2.2 *Example of an optical link budget*

As an example, we develop a link budget for the simple laboratory setup of a free space optical link as shown in Figure 5-6. Typically, a FSO link budget includes inputs for transmit power; receive sensitivity, optical system losses and geometric losses. The link budget predicts the margin or the extra power available for propagation loss.

Optical system loss is considered since the measurements of transmit and received power are taken at the lasers and detectors; it is assumed to be 6 dB [1]. Optical system losses include scatter, surface reflections and absorption. Geometric losses are those losses that occur due to the spreading of the transmitted beam between the transmitter and the receiver. Typically, the beam spreads to a size larger than the receive aperture, and this “overfill” energy is lost. In general, larger receive apertures or smaller transmit divergences result in less geometric loss for a given range.

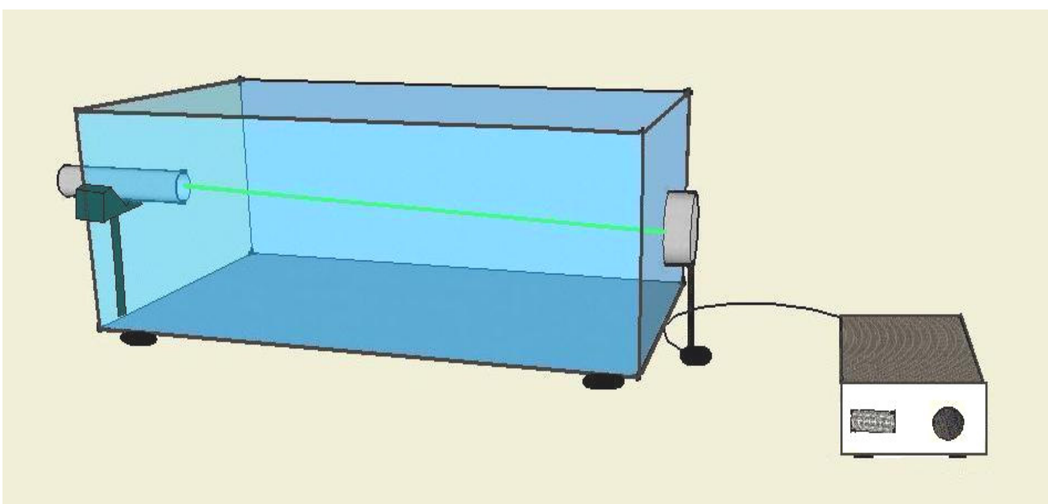

Figure 5-6 Experimental setup for an optical link budget

Average Transmit Power = +4.3306 dBm

Minimum Receiver Sensitivity = -33 dBm

Available Power = +37.33 dB

2 Glass surfaces x -0.466 dB = -0.932 dB

System loss (combined Tx and Rx losses) = -6 dB

Geometric Loss = 0 dB

Total setup losses = (-.0932 db) + (-6 dB)

Available margin for pathloss = Available Power – Total Setup losses

= +31.57 dB

The beam divergence of the laser source is of the order of 1mrad and for a path length of 1 m the beam spread is totally captured by the receiver aperture, hence it does not contribute to any losses. The available link margin for the setup is 31.57dB. The received power is measured for various water conditions. Known quantities of liquid Maalox® is added to water and are presented in the following example. A tank of dimensions 1m x 0.4m x 0.3m contains 45.2 l of water. From the calculations below it is seen that for clear water conditions maximum link lengths are close to 29.66m and 2m for turbid waters (20ml of liquid Maalox®).

Table 5.1 Pathloss for different Maalox® concentrations

Liquid Maalox® concentration in 45.2 l of water (ml)	Loss (dB/m)	Maximum path length possible (m)
0	-1.06	29.66
1	-1.33	23.65
5	-2.25	14.03
10	-7.37	4.28
20	-15.3	2.06

5.3 Pointing and Tracking

Directional optical wireless links with full angle beam divergence of a few milliradians would require active pointing and tracking systems to maintain line of sight [8]. Much goes into the planning of free space optical links against the underwater disturbances like water currents, vibrations, pressure, etc.

Existence of pointing and tracking systems for free space optical networks has been around for quite some time. Use of mechanical gimbals for coarse steering and beam steering mirrors for fine-pointing have been the common in practice [4]. Closed loop techniques such as feed-forward tracking, coherent tracking, tone tracking systems are used to control the beam steering mirrors for accuracy in pointing and tracking [3].

For mobile environments such as oceans, employing spherical optical antenna provide 3-dimensional line of sight. By tessellating multiple transceivers on the surface of a sphere and using auto-alignment circuit would reduce the limitations of single directional line of sight [9]. This geometry of a sphere provides spatial and angular diversity.

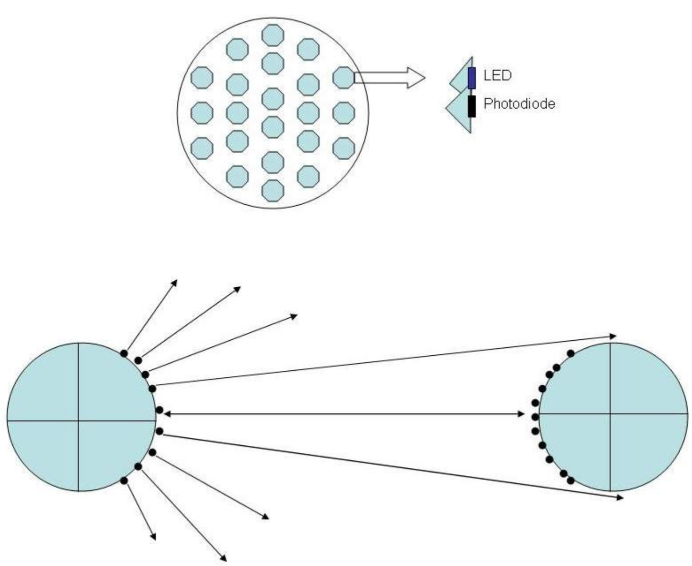

Figure 5-7 Sphere tessellated with LED and photodiodes transceivers (top). Line of sight for the tessellated sphere (bottom) [9].

Alternate methods to optically aimed systems are using acoustics to provide the tracking information of the receiver. Information about the azimuth and elevation can be provided to the optical pointing system. Limitation of low speeds of acoustic lead to slower update rate which impact the transmission [10]. For short range communication links between fixed node and mobile vehicle where pointing and tracking is a priority, following transmitter-receiver configurations could be considered for underwater applications [10].

Case 1: A directional optical transmitter and omnidirectional receiver on the mobile and fixed platforms. Omnidirectional receiver with a spherical geometry is able to provide a 4π steradians of field of view. Alignment circuits can detect the direction of the incoming signal and realign the transmitter for better line of sight. The configuration is illustrated in Figure 5-8.

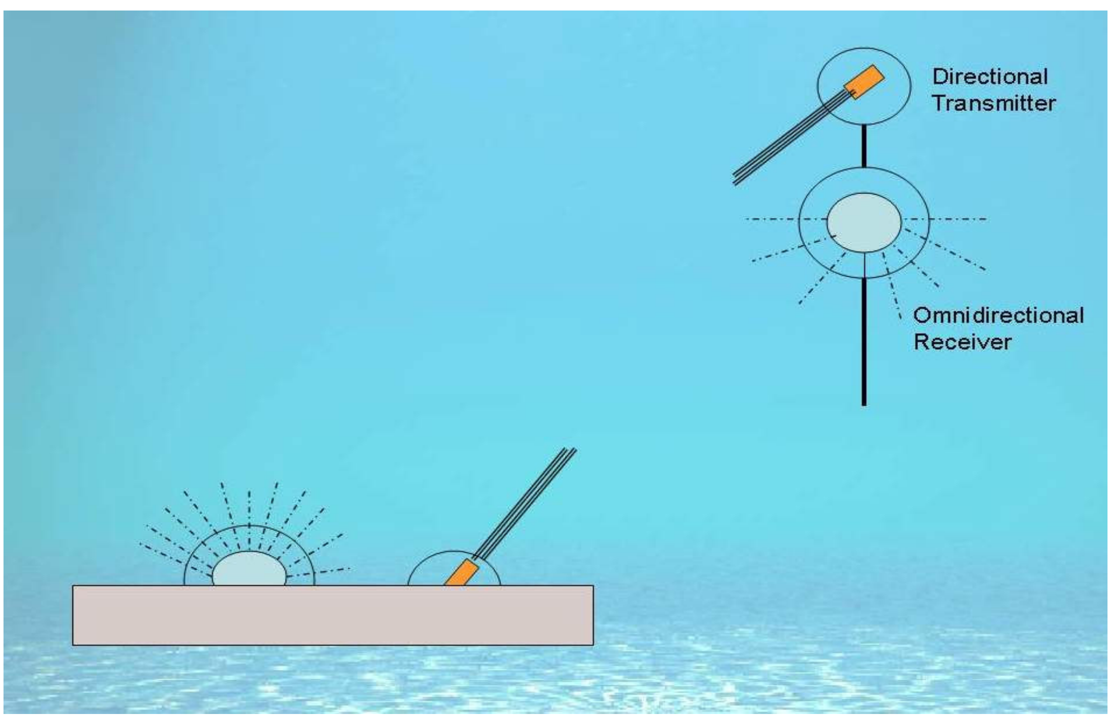

Figure 5-8 Configuration of directional transmitter and omnidirectional receiver [10].

Case 2: The simplest approach to counter pointing and tracking issue is to use omnidirectional transmitter and receivers. Ideal for ad-hoc applications and sensor networks, this configuration can be achieved using an array of broad divergent sources like LEDs and complemented by beam diverging optics [8].

The tradeoffs of these alternate configurations are increased power consumption and low data rate performance.

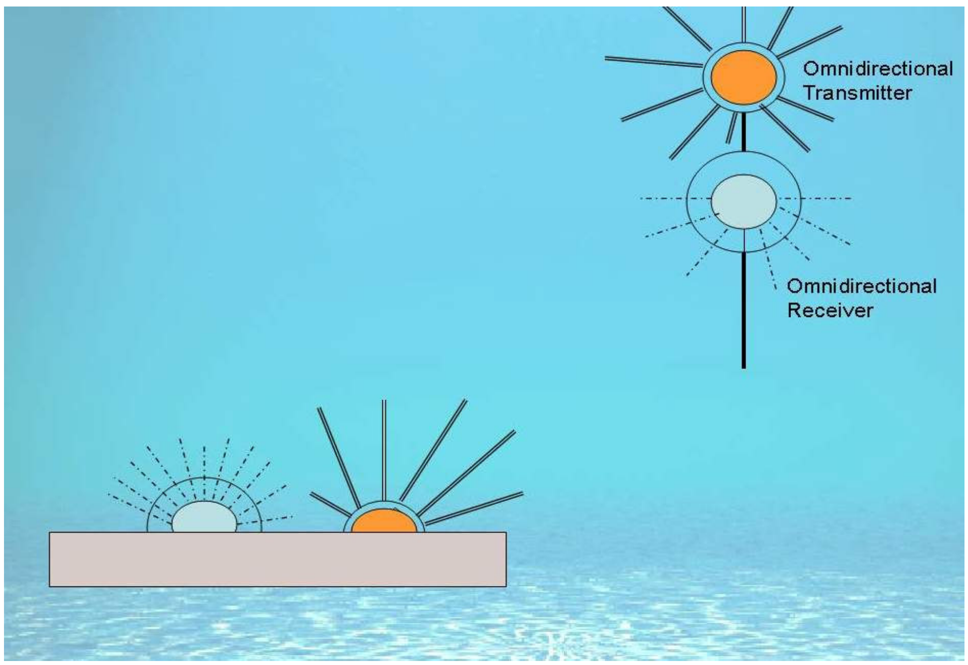

Figure 5-9 Configuration of omnidirectional transmitter and omnidirectional receiver [10].

5.4 References

[1] S. Bloom, E. Korevaar, J. Schuster and H. Willebrand, "Understanding the performance of free-space optics," *Journal of Optical Networking,* vol. 2, 2003.

[2] J. C. Palais, *Fiber Optic Communication.* ,5th ed.New Jersey: Pearson Prentice Hall, 2005, pp. 40-61.

[3] S. G. Lambert and W. Casey, *Laser Communication in Space.* MA: Artech House Inc., 1995, pp. 94-119.

[4] M. E. Katzman, *Laser Satellite Communications.* New Jersey: Prentice Hall Inc., 1987, pp. 1-30.

[5] B. J. Klein and J. J. Degnan, "Optical Antenna Gain. 1: Transmitting Antennas," *Applied Optics,* vol. 13, 1974.

[6] B. J. Klein and J. J. Degnan, "Optical Antenna Gain. 2: Receiving Antennas," *Applied Optics,* vol. 13, 1974.

[7] M. Chancey, "Short range underwater optical communication links," *North Carolina State University,* 2005.

[8] S. Trisno, T. Ho, S. D. Milner and C. C. Davis, "Theoretical and expreimental characterization of omnidirectional optical links for free space optical communications," in *IEEE Military Communications Conference 3,* 2004, pp. 1151-1157.

[9] J. Akella, L. Chang, D. Partyka, M. Yuksel, S. Kalyanaraman and P. Dutta, "Building blocks for mobile free-space-optical networks," *Wireless and Optical Communications Networks,* pp. 164-168, 2005.

[10] N. Farr, A. Chave, L. Freitag, J. Preisig, S. White and D. Yoerger, "Optical modem technology for seafloor observatories," *IEEE,* 2005.

CHAPTER 6 CONCLUSIONS AND RECOMMENDATIONS FOR FUTURE WORK

This research is a building block for future Underwater Free Space Optics. With this study and analysis of the optical properties of water we have tried to explain the nature of attenuation of light in water. Combining chlorophyll estimating techniques and the single parameter model we have presented a systematic framework to define the losses in the medium. Giving the scattering of light more importance, we have explained empirically as well as theoretical how scattering influences the total attenuation of light. Adopting the theory of beam spread function with multipath time dispersion, we have also tried to validate these efforts with a controlled sea water experiment. A method to evaluate the power budget for an underwater free space optical link is detailed that would prove helpful in completing the problem from in context to link engineering.

Simulation results from MathCAD have suggested that sources with 1W of optical power can achieve link lengths of over 50m for a majority of ocean waters. Under clear ocean conditions a 1W optical source can surpass link lengths of 300m. These promising results suggest Free Space Optical underwater communications are promising for short range high band width applications. Suggested future work includes:.

- Careful experimentation of signal attenuation in natural seawaters. Power measurements for seawater with different quantities of phytoplankton. By using sources of varying wavelengths a systematic study would further validate the attenuation model presented in this research.
- Experiments to measure angular deviation and scattering using wavefront sensors such as an array of apertures like Hartmann array.
- To build a complete digital communication link and perform BER measurements for different water conditions.
- Study of turbulence induced effects on radiative transfer in water. Using localized heaters in water tanks, the effect turbulence can be analyzed qualitatively and to

develop a scattering model that includes the effects of large scale turbulence in water.

- Addressing the issue of pointing and tracking. Exploring options like beam steering, adaptive optics and optical antenna topologies as possible solutions.

APPENDICES

APPENDIX A: MathCAD CODE

Units

$nm := 10^{-9} m$

$um := 10^{-6} m$

$pW := 10^{-12} watt$

$nW := 10^{-9} watt$

$uW := 10^{-6} watt$

$mW := 10^{-3} watt$

$dBm := mW$

$g := 1 \cdot 10^{-3} kg$

Constants

$h := 6.626178 10^{-34} joule \cdot sec$ Planck's constant

$eV := 1.6 \cdot 10^{-19} joule$

$c = 2.998 \times 10^{8} \frac{m}{s}$ Speed of light

Transmitter Parameters

$\lambda := 500nm$ Laser Wavelength

$f(\lambda) := \frac{c}{\lambda}$ Optical Frequency

$Pt := 1 \cdot W$ Transmitter Power

$Div := 1 \cdot 10^{-3}$ Beam Divergence (rad)

$Dt := 5 \cdot 10^{-2}$ Transmitter Lens Diameter

$\theta div(\lambda) := 4 \frac{\lambda}{\pi Dt}$ Transmitter Divergence

$Gt(\lambda) := \frac{32}{\theta div(\lambda)^2}$ Transmitter Gain

$Lt := 0.77$ Losses due to transmitter

Receiver Parameters

$\eta := 0.8$	Quantum Efficiency
$Rp := \frac{\eta \cdot eV \cdot \lambda}{h \cdot c}$	Optical responstivity as a function of wavelength
$D_r := 10 \cdot 10^{-2}$	Receiver lens diameter
$Ar := 0.000064 m^2$	Physical Area of photodetector junction
$Gr(\lambda) := \left(\pi \cdot \frac{D_r}{\lambda}\right)^2$	Receiver Gain
$Lr := 0.77$	Losses due to receiver

Ocean Parameters

$n := 1.34$	Index of Refraction for medium (Constant)
$c_o := \frac{\frac{c}{n}}{\frac{m}{sec}}$ $\quad c_o = 2.237 \times 10^8$	Speed of light in water

Chlorophyll Distribution

(Vertical Distribution Profile- Example)

$B_o := 0.8$	Background Chlorophyll (mg/m^3)
$z_{max} := 37.5$	Depth of Max Chlorophyll (m)
$h_{chl} := 25$	Chlorophyll above background mg/m^3
$\sigma := 7$	Standard Deviation (decides the thickness of the peak)
$R1 := 0.79$	Regression Coefficient (specific to this example)
$grad := 0.00035 - 0.0055 \cdot B_o \cdot R1^2$	Slope of the vertical profile

$$\mathrm{Chl}_{depth}(z) := B_o + grad\cdot z + \frac{h_{chl}}{\sigma\cdot\sqrt{2\pi}}\cdot e^{\frac{-(z-z_{max})^2}{2\cdot\sigma^2}}$$

Chlorophyll concentration at depth z (mg/m^3)

Optical Link Parameters

$z1 := 2($ Depth of Transmitter 1

$z2 := 7($ Depth of Transmitter 2

$\alpha := 0.7\&$ α is the angle between the vertical and the optical path between the transmitters (radians)

Model of Absorption

$$\lambda s := \begin{pmatrix} 200\cdot 10^{-9} \\ 250\cdot 10^{-9} \\ 300\cdot 10^{-9} \\ 350\cdot 10^{-9} \\ 400\cdot 10^{-9} \\ 450\cdot 10^{-9} \\ 500\cdot 10^{-9} \\ 550\cdot 10^{-9} \\ 600\cdot 10^{-9} \\ 650\cdot 10^{-9} \\ 700\cdot 10^{-9} \\ 750\cdot 10^{-9} \\ 800\cdot 10^{-9} \end{pmatrix} \qquad as := \begin{pmatrix} 3.07 \\ .559 \\ .141 \\ 0.0463 \\ .0171 \\ .0145 \\ .0257 \\ .0638 \\ .244 \\ .349 \\ .650 \\ 2.47 \\ 2.07 \end{pmatrix}$$

$a_s(\lambda) := \mathrm{interp}(\mathrm{cspline}(\lambda s, as), \lambda s, as, \lambda)$

Cubic spline interpolation for absorption of pure seawater

$$a_o(\lambda) := a_s\left(\frac{\lambda}{m}\right)\cdot\frac{1}{m}$$

Pure water Absorption Coefficient function of λ

$$\lambda_c := \begin{pmatrix} 300\cdot 10^{-9} \\ 350\cdot 10^{-9} \\ 400\cdot 10^{-9} \\ 450\cdot 10^{-9} \\ 470\cdot 10^{-9} \\ 500\cdot 10^{-9} \\ 520\cdot 10^{-9} \\ 550\cdot 10^{-9} \\ 600\cdot 10^{-9} \\ 650\cdot 10^{-9} \\ 660\cdot 10^{-9} \\ 670\cdot 10^{-9} \\ 700\cdot 10^{-9} \\ 750\cdot 10^{-9} \end{pmatrix} \qquad a_c := \begin{pmatrix} 0.013 \\ 0.026 \\ 0.051 \\ 0.087 \\ 0.06 \\ 0.025 \\ 0.012 \\ 0.006 \\ 0.007 \\ 0.008 \\ 0.014 \\ 0.041 \\ 0.004 \\ 0.002 \end{pmatrix}$$

$$a_{clo}(\lambda) := \mathrm{interp}\left(\mathrm{cspline}\left(\lambda_c, a_c\right), \lambda_c, a_c, \lambda\right)$$

Cubic spline interpolation for specific absorption coefficient of chlorophyll

$$a_{co}(\lambda) := \frac{a_{clo}\left(\frac{\lambda}{m}\right)}{m}$$

Specific Absorption coefficient of chlorophyll function of λ

$$k_f := \frac{0.0189}{nm}$$

constant

$$k_h := \frac{0.01105}{nm}$$

constant

$$a_f := 35.959\frac{m^2}{mg}$$

Specific Absorption Coefficient of fulvic acid 1st component of CDOM

$$a_h := 18.828\frac{m^2}{mg}$$

Specific Absorption Coefficient of humic acid 2nd component of CDOM

Model of Scattering

$$b_o(\lambda) := 5.826 \cdot 10^{-3} \cdot \left(\frac{400nm}{\lambda}\right)^{4.322} \frac{1}{m}$$ Scattering Coefficient of pure water

$$b_s(\lambda) := 1.1513 \cdot \left(\frac{400nm}{\lambda}\right)^{1.7} \frac{m^2}{g}$$ Scattering Coefficient of small particles

$$b_l(\lambda) := 0.3411 \cdot \left(\frac{400nm}{\lambda}\right)^{.3} \frac{m^2}{g}$$ Scattering Coefficient of large particles

Scattering Angle

Scattering is random event. We generate random numbers for scattering angle θ.
mean considered is 0.13 radians

$n := 1 \times 10^3$ $\mu := 0.122$ $\sigma := 0.05$

$$\theta(n, \mu, \sigma i) := \left| \begin{array}{l} \text{for } i \in 0..5 \\ \quad \left| \begin{array}{l} \text{Seed}(1) \\ \text{nums} \leftarrow \text{rnorm}(n, \mu, \sigma) \\ M^{\langle i \rangle} \leftarrow \text{nums} \end{array} \right. \\ M \end{array} \right.$$

$$\Theta(n, \mu, \sigma i) := \left| \begin{array}{l} \text{for } i \in 0..5 \\ \quad \left| \begin{array}{l} \text{Seed}(1) \\ \text{nums} \leftarrow \text{rnorm}(n, \mu, \sigma) \\ M^{\langle i \rangle} \leftarrow \text{nums} \end{array} \right. \\ M^2 \end{array} \right.$$

$\theta(n, \mu, \sigma) =$

	0
0	0.101
1	0.089
2	0.099

$\Theta(n, \mu, \sigma) =$

	0
0	0.053
1	0.047
2	0.052

$\theta_{mean} := \text{mean}\left(\theta(n, \mu, \sigma)^2\right)$

$\theta_{mean} = 0.063$

$\theta_{mean1} := \text{mean}\left(\Theta(n, \mu, \sigma)^2\right)$

$\theta_{mean1} = 0.017$

The chlorophyll content is different along the depth. Hence the absorption and scattering coefficient corresponding to the chlorophyll content will also vary along the depth. The link length is divided into smaller intervals and the attenuation for each interval is calculated.

$divisions := 3$ Number of intervals

$$
\begin{aligned}
K_{attenuation} := \; & K_{tot} \leftarrow 1 \\
& \text{for } i \in 1 .. \text{divisions} \\
& \quad HU \leftarrow z1 + \frac{(z2 - z1)\cdot(i-1)}{\text{divisions}} \\
& \quad HL \leftarrow z1 + (z2 - z1)\frac{i}{\text{divisions}} \\
& \quad Lm1 \leftarrow \frac{HL - HU}{\cos(\alpha)} \\
& \quad C_{c1} \leftarrow \frac{1}{(HL - HU)\cdot\cos(\alpha)}\cdot\left(\int_{HU}^{HL} Chl_{depth}(z)\, dz\cdot\frac{mg}{m^3}\right) \\
& \quad C_{co} \leftarrow 1\,\frac{mg}{m^3} \\
& \quad C_{f1} \leftarrow 1.74098 C_{c1}\cdot e^{0.12327\cdot\frac{C_{c1}}{C_{co}}} \\
& \quad C_{h1} \leftarrow 0.19334 C_{c1}\cdot e^{0.12343\cdot\frac{C_{c1}}{C_{co}}} \\
& \quad C_{sp1} \leftarrow 0.01739\left(\frac{g}{mg}\right)\cdot C_{c1}\cdot e^{0.11631\cdot\frac{C_{c1}}{C_{co}}} \\
& \quad C_{lp1} \leftarrow 0.76284\left(\frac{g}{mg}\right)\cdot C_{c1}\cdot e^{0.03092\cdot\frac{C_{c1}}{C_{co}}} \\
& \quad a_{y1} \leftarrow a_f\cdot C_{f1}\cdot e^{-(k_f\cdot\lambda)} + a_h\cdot C_{h1}\cdot e^{-(k_h\cdot\lambda)} \\
& \quad a_{cl1} \leftarrow a_{co}\cdot\left(\frac{C_{c1}}{C_{co}}\right)^{.602} \\
& \quad A1 \leftarrow a_o + a_{cl1} + a_{y1} \\
& \quad b_{part1} \leftarrow b_s\cdot C_{sp1} + b_l\cdot C_{lp1} \\
& \quad B1 \leftarrow b_o + b_{part1} \\
& \quad a1 \leftarrow A1\cdot m \\
& \quad b1 \leftarrow B1\cdot m \\
& \quad \mu_\tau \leftarrow \frac{1}{4}\cdot b1\,\frac{Lm1^2}{c_o}\cdot\theta_{mean} \\
& \quad var_\tau \leftarrow \left[\left(\frac{1}{12}\right)\cdot b1\cdot Lm1\cdot\theta_{mean1} + \left(\frac{1}{24}\right)\cdot(b1\cdot Lm1)^2\cdot\theta_{mean}{}^2\right]\cdot\left(\frac{Lm1}{c_o}\right)^2 \\
& \quad k \leftarrow \frac{\exp(-a1\cdot Lm1)}{\left(1 + a1\cdot c_o\cdot\frac{var_\tau}{\mu_\tau}\right)^{\frac{\mu_\tau{}^2}{var_\tau}}} \\
& \quad K_{tot} \leftarrow K_{tot}\cdot k \\
& \text{return } K_{tot}
\end{aligned}
$$

Received Power

$$Pr := Pt \cdot (Lt) \cdot K_{attenuation} \cdot (Lr)$$

Total Recieved power calculated considering the loss at the transmitter and receiver.

$$Pr = 4.274 \times 10^{-3}\ W$$

Logarithimic Converstion

(Link Budget Equation)

$$LogPt := 10\log\left(\frac{Pt}{1W}\right) \qquad LogPt = 0$$

$$LogGt(\lambda) := 10\log(Gt(\lambda)) \qquad LogGt(\lambda) = 112.953$$

$$LogGr(\lambda) := 10\log(Gr(\lambda)) \qquad LogGr(\lambda) = 115.964$$

$$LogLt := 10\log(Lt) \qquad LogLt = -1.135$$

$$LogLr := 10\log(Lr) \qquad LogLr = -1.135$$

$$LogK_{attenuation} := 10\log\left(K_{attenuation}\right) \qquad LogK_{attenuation} = -21.422$$

$$LogPr := 10\log\left(\frac{Pr}{1W}\right) \qquad LogPr = -23.692$$

$$dBPr := LogPt + LogK_{attenuation} + LogGt(\lambda) + LogGr(\lambda) + LogLt + LogL$$

APPENDIX B: MathCAD RESULTS

A consolidated table for the MathCAD model is presented in this section. For the three common wavelength sources, i.e. blue (450nm), green (532nm) and red (633nm), the absorption, scattering coefficients, total beam attenuation and the maximum link length is calculated. These results are obtained by calculations from the MathCAD model.

These results are calculated for seven chlorophyll concentrations. The total beam attenuation is calculated for a link length of 50m. The maximum length is calculated for a source of 10mW and receiver sensitivity of -30dBm. This calculation neglects the gain and losses associated with the different optical link components.

This table can serve as an easy look-up table to gain information about the beam attenuation for different chlorophyll concentrations.

Source	Chlorophyll concentration (mg/m^3)	Absorption coefficient a(λ) (m^-1)	Scattering coefficient b(λ) (m^-1)	Total beam attenuation (m^-1)	Maximum link length (m)
Blue	0.03	0.026	0.012	0.224	290
	0.1	0.04	0.03	0.078	175
	0.4	0.081	0.112	2.458 x 10^-3	77
	1.25	0.169	0.354	1.711 x 10^-6	33
	3	0.348	0.9	9.682 x 10^-12	15.5
	9	1.376	3.409	0	4
	12	2.401	5.166	0	2.5
Green	0.03	0.038	0.009242	0.127	216
	0.1	0.04	0.027	0.084	180
	0.4	0.047	0.104	0.019	120
	1.25	0.065	0.33	8.8 x 10^-4	68
	3	0.108	0.84	7.177 x 10^-6	36
	9	0.419	3.157	1.616 x 10^-14	9.3
	12	0.752	4.753	0	5.5
Red	0.03	0.344	0.007886	2.623 x 10^-8	26.5
	0.1	0.345	0.024	1.5 x 10^-8	25.5
	0.4	0.349	0.096	2.341 x 10^-9	23
	1.25	0.358	0.309	1.006 x 10^-10	19
	3	0.375	0.786	3.161 x 10^-12	15
	9	0.476	2.931	0	9
	12	0.577	4.388	0	7

APPENDIX C: SYSTEM PERFORMANCE OVER DIFFERENT WATER CONDITIONS

A useful experiment to illustrate the prominent effects of the medium on a communication link is presented in this section. A Free Space Optical transmitter and receiver are tested for underwater applications. The setup is as shown in figure below, consists of a modulated retroreflector using a Liquid Crystal Polarized Grating (LCPG). The retroreflector and LCPG are encased in a fish eyed lens that enhances the field of view of the device. The ideal field of view (FOV) of the retroreflector setup is ~±60°. For varying water conditions the field of view of the system is tested.

Maalox a commercial antacid medication is added to water to increase the turbidity. These increased concentrations of Maalox® can be assumed as different regions in the water mass, like the most turbid medium as harbor waters and clearest medium as open ocean waters. Below are the observations for modulated signals with water as the medium. The setup includes a glass water tank of dimensions 1m x 0.3m x 0.4m completely filled with 60L of clear tap water. The laser transceiver (15mW operating at 633nm) was placed in line-of-sight with the retroreflector device at either ends of the tank, as shown.

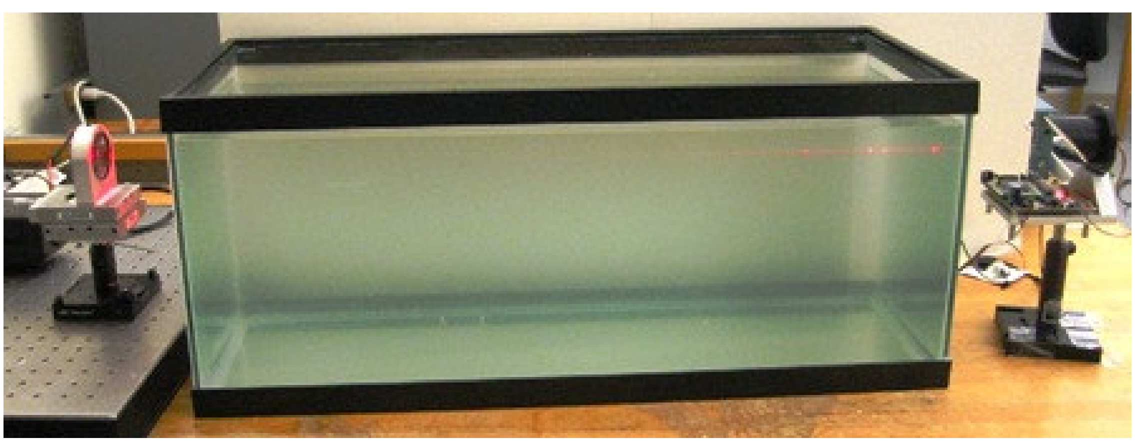

Figure C-1 Underwater experiment tank filled with 5mL of Maalox® liquid (side view)

Maalox® containing aluminum and magnesium hydroxides acts as a scattering agent of light. Greater effects are observed since the measured voltage is from the reflected light signal which travels 2x (twice the length) of the tank and propagates through different glass surfaces and air. Figure below shows these effects in decreasing intensity of the laser beam at the retroreflector side.

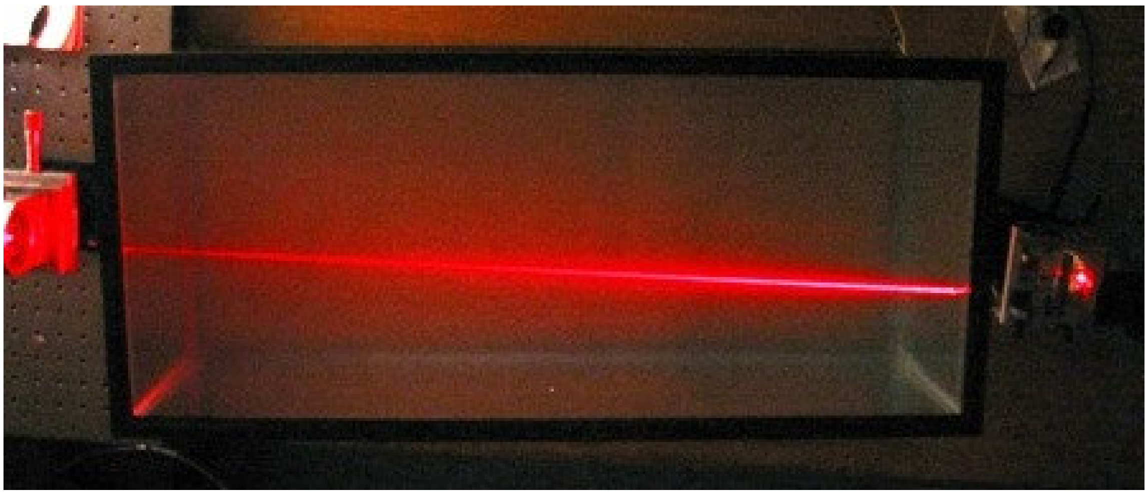

Figure C-2 Red laser propagating in water with 5mL of Maalox® liquid (Top view)

It is however hard to accurate relate this to natural water conditions, but for a loose comparison we can relate the water conditions with Maalox® as follows.

Table C-1 Maalox concentrations compared to natural water

Concentration of Maalox® (mL) in 60 l of water	Natural Waters
0 mL	Clear water
2 mL	Costal water
3 mL	Harbor water
5mL	Turbid water

Voltage readings of the photodiode were noted for various water conditions. Liquid Maalox® was added to water in measured quantities and the received voltage power was measured from the photo-detector circuit. The detector circuit has 1000 amplification gain, thus it is very sensitive to low signals strength. On the other hand, high laser intensity produces strong signals that reach the amplifier maximum rails and thus the received voltage was clipped.

The FOV of the retroreflector device was tested under different water conditions. Figure below show the curves of the received power, of 1kHz modulated signals, at different Maalox concentrations. It is obvious that there is inverse relation between retroreflector FOV and water turbidity. Thus, when this device is to be used for underwater communications, the more the water is turbid the more the two transceivers should be aligned.

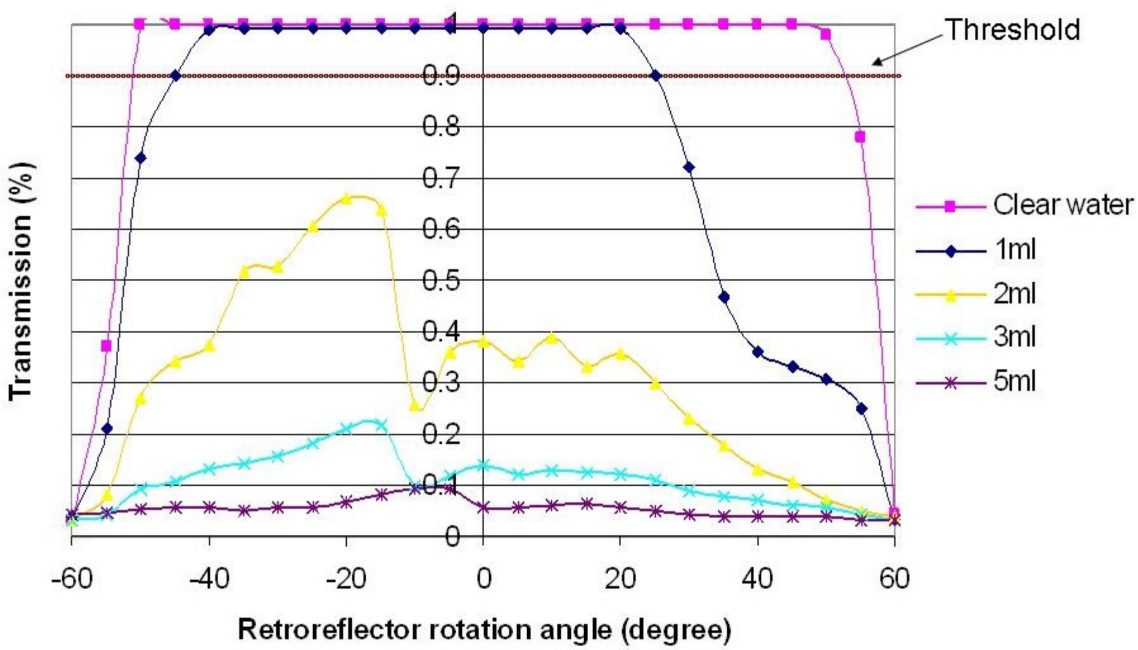

Figure C-3 Received modulated voltage at (1kHz) with increased Liquid Maalox® concentrations

First, it looks that the peeks of the curves are skewed toward -20 degrees rotation angle. This is due to imperfection in retroreflector's lenses and coating surface. It is important for the received voltages to cross the receiver threshold level for a reliable digital communication. The receiver circuit Schmitt trigger considers voltages greater than 3V as logical ‘1’ and logical ‘0’for voltages less than 0.7V. The curves in the figure indicate that digital signals can not be detected, with this system, in turbid water with Maalox concentration more than 1mL. At 5mL concentration, the attenuation was severe that it was hard to detect any changes in the received signal. Hence the system could not have successful performance only for water containing greater than 1ml of Maalox®.

In conclusion, the system performance is significantly altered with the medium of light propagation. For high scattering or absorbing media like in the cases above, a systematic link budget needs to be calculated for successful and reliable digital communication links. The link budget can also be treated as preliminary tool to decide system parameter if the region of operation is decided.

APPENDIX D: MIE THEORY (MAPLE CODE)

```
L:=633;
lambda:= L*(10^(-9));                                            (Wavelength)
pi:= evalf(Pi);
n2:=1.33;                                (Real refractive index of medium-water)
k2:=0;                                 (imaginary refractive index of the medium)
epsilon:= 8.85*0.000000000001;
k0:= ((2*pi)/lambda);                                            (wave number)
R:= 300*(10e-6);                                 (distance of the observation)
k01:= ((2*pi)/lambda)*n2;
n10:=1.56;             (Real part of refractive index of the polystyrene latex spheres)
k10:= 0.022;        (imaginary part of the refractive index of polystyrene latex spheres)
n1:=n10+i*k10;
e2:=n2^2;
e1:=n1^2;
        Mo:= 4*Pi*0.0000001;                           (The permeability constant)
        mu:= evalf(Mo);
        nn:= sqrt(mu/epsilon);           (ratio of the permeability and permittivity
                                                                      constants)
r1:= 3e-6;                                              (radius of the particle)
B:=35;                              (No of terms to be considered for evaluation)
```

```
For D1 from 1 by 1 while D1<= B do

    xx:= k0*r1*n2;

    mm:= n1/n2;

    MM:= mm*xx;

    J0:= r-> BesselJ(0,r);                        (Bessel function of the first kind
                                                  and order 0, r just being a
                                                  variable which will assume
                                                  values)
    Y0:= r-> BesselY(0,r);                        (Bessel function of the second
                                                  kind and order 0)
    jjn:= sqrt(pi/(2*r))*(BesselJ(n  + 0.5,r));   (BesselJ(n  + 0.5,r) is the Bessel
                                                  function of the first kind of order
                                                  {n  + ½} )
    yyn:= sqrt(pi/(2*r))*(BesselY(n + 0.5,r));    (BesselY(n  + 0.5,r) is the Bessel
                                                  function of the second kind of
                                                  order {n  + ½} )
    zzn:= jjn + I*yyn;                            (The spherical Hankel function of
                                                  the  first kind: It is a linear
                                                  combinations of jjn and yyn)
    Un:= r*jjn;                                   (Riccati-Bessel function of the
                                                  first kind)
    UUn:= diff(Un,r);

    Sn:= r*(jjn- I*yyn);               (Riccati-Bessel function of the second kind)


    SSn:= diff(Sn,r);
```

```
        an:= (mm*(eval(Un,r=MM))*(eval(UUn,r=xx)) -
(eval(Un,r=xx))*(eval(UUn,r=MM)))/(mm*(eval(Un,r=MM))*(eval(SSn,r=xx)) -
(eval(Sn,r=xx))*(eval(UUn,r=MM)));                              (Mie Coefficients)

        bn:= (-mm*(eval(Un,r=xx))*(eval(UUn,r=MM)) +
(eval(Un,r=MM))*(eval(UUn,r=xx)))/(-mm*(eval(UUn,r=MM))*(eval(Sn,r=xx)) +
(eval(SSn,r=xx))*(eval(Un,r=MM)));                              (Mie Coefficients)

        aan[D]:= eval(an, n = D);

        bbn[D]:= eval(bn, n=D);

end do;

For D2 from 1 by 1 while D2<=  B do  with(orthopoly):
        ppn1[D2]:= (P(D2,cos(theta1)))/(sin(theta1));
        ppn1[D2]:= (P(D2,cos(theta1)))/(sin(theta1));
        ppn10[D2]:= (P(D2,cos(theta1)))/(1);
        pppn1[D2]:= diff(ppn10[D2], theta1);
end do;

For D3 from 1 by 1 while D3<=  B do
        i1[D3]:= (aan[D3]*ppn1[D3]+bbn[D3]*pppn1[D3]*(2*D3+1)*(1/(D3*(D3+1)));
```

```
    i2[D3]:=(aan[D3]*pppn1[D3]+bbn[D3]*ppn1[D3]*(2*D3+1)*(1/(D3*(D3+1)));
end do;

thetazero:= 0.001;
deltheta1:=0.001;
thetafinal:= 0.1;
c1:=0;

i22:= evalf(Sum ( i2[D], D=1..B));                (Scattered parameter  – S1(θ))
i11:= evalf(Sum ( i1[D], D=1..B));                (Scattered parameter – S2(θ))

i111:= abs(i11);
i222:= abs(i22);

 For theta1 from thetazero by deltheta1 while theta1<= thetafinal do
    c1:=c1+1;
    Iext[c1]:= ((i111^2 + i222^2)/(2*(k0^2)*(R^2)));
            (Overall scattered intensity at a distance R from the scattering element)
end do;

for c1 from 1 by 1 while c1<=100 do Iext[c1]; end do;
for c1 from 1 by 1 while c1<=100 do Iext[c1]/Iext[1]; end do;         (normalizing)
```